EFFECTS OF COOLING SYSTEM PARAMETERS ON HEAT TRANSFER IN PAFC STACK

Ali A. Abdul-Aziz

Master of Sicence in Mechanical Engineering
Cleveland State University
1981
Bachelor of Science in Mechanical Engineering
Cleveland State University
1980

Submitted in partial fullfillment of requirements
for the degree
DOCTOR OF ENGINEERING
at
THE CLEVELAND STATE UNIVERSITY
August, 1985

This dissertation has been approved for the Department of Mechanical Engineering and the College of Graduate Studies by

K. G. Alkasab

Dr.K. Alkasab (Dissertation Committee Chairperson)

Mechanical Engineering / 8-16-1985
(Department/Date)

Dr.A. Presler,

NASA LEWIS RESEARCH CENTER / 8-16-1985
(Department/Date)

Dr.E. Turker,

Industrial Engineering 8/16/1985
(Department/Date)

Dr.J. Frater,

Mechanical Engineering 8-16-85
(Department/Date)

Dr. W. Atherton

Mechanical Engineering 8/16/85
(Department/Date)

ACKNOWLEDGEMENTS

The author wishes to express his sincere gratitude to his advisor Dr. K.A. Alkasab, Committee Chairman and Dissertation Advisor. His constructive advice and encouragement during the supervision of this research project is highly appreciated. I would also like to extend my appreciation to the members of the doctoral committe.

The author would like to especially thank Dr. A. Presler for his confidence, advice, and help, both as a committee member and a friend.

The author would like to acknowledge the financial support of NASA Lewis Research Center (Fuel Cell Office).

Last, and not least, I am grateful for my wife Mona, for her confidence and infinite patience.

ABSTRACT

Analytical and experimental study for the effects of cooling system parameters on the heat transfer and temperature distribution in the electrode plates of a phosphoric acid fuel-cell has been conducted.

An experimental set-up that simulates the operating conditions prevailing in a phosphoric-acid fuel-cell stack was designed and constructed. The set-up was then used to measure the overall heat transfer coefficient, the thermal contact resistance, and the electrode temperature distribution for two different cooling plate configurations.

Two types of cooling plate configurations, serpentine and straight, were tested. Air, water, and oil were used as coolants. Measurements for the heat transfer coefficient and the thermal contact resistance were made for various flow rates ranging from 16 to 88 Kg/hr, and stack clamping pressure ranging from 0 to 3448 Kpa.

The experimental results for the overall heat transfer coefficient were utilized to derive mathematical relations for the overall heat transfer coefficient as a function of stack clamping pressure and Reynolds number for the three coolants.

The empirically derived formulas were incorporated in a previously developed computer program to predict electrodes temperature distribution and the performance of the stack cooling system. The results obtained were then compared with those available in the literature. The comparison showed maximum deviation of ± 11 percent.

TABLE OF CONTENCTS

CHAPTER PAGE

CHAPTER PAGE

LIST OF TABLES

LIST OF FIGURES

LIST OF SYMBOLS

A	=	Area, unless otherwise specified
C_p	=	Heat Capacity
D	=	Diameter
h	=	Heat Transfer Coefficient
K	=	Thermal Conductivity
m	=	Mass Flow Rate (mass/time), unless otherwise specified
q''	=	Heat Flux
Q	=	Heat
n	=	constant
f	=	constant
ΔT	=	Temperature Drop, or Difference
$\frac{dt}{dx}$	=	Temperature Gradient
r	=	Thermal Contact Resistance, unless otherwise specified
T	=	Temperature
ρ	=	Density
Pr	=	Prandlt number
Re	=	Reynolds number
St	=	Stanton number
Sc	=	Schmidt number
V	=	Velocity
δx	=	Length of Element
μ	=	Dynamic Viscosity
U	=	Overall Heat Transfer Coefficient

U_c	=	Overall Heat Transfer with Contact Resistance Term
X	=	Width of Cooling Channel
Y	=	Depth of Cooling Channel
P	=	Pressure
NU	=	Nusselt number
Δx	=	Conduction Thickness

Subscripts

∞	=	free stream
w	=	wall
c	=	coolant
m	=	mass
H	=	hydraulic
1	=	surface one
2	=	surface two

CHAPTER I

INTRODUCTION

The fuel cell may be regarded as a continuously fed battery which converts the chemical energy of conventional fuel (such as natural gas and oxygen (from air) into electrical energy. Such a unit would not be reversible and cannot strictly be called a storage device; it is an energy conversion device or an electricity generator.

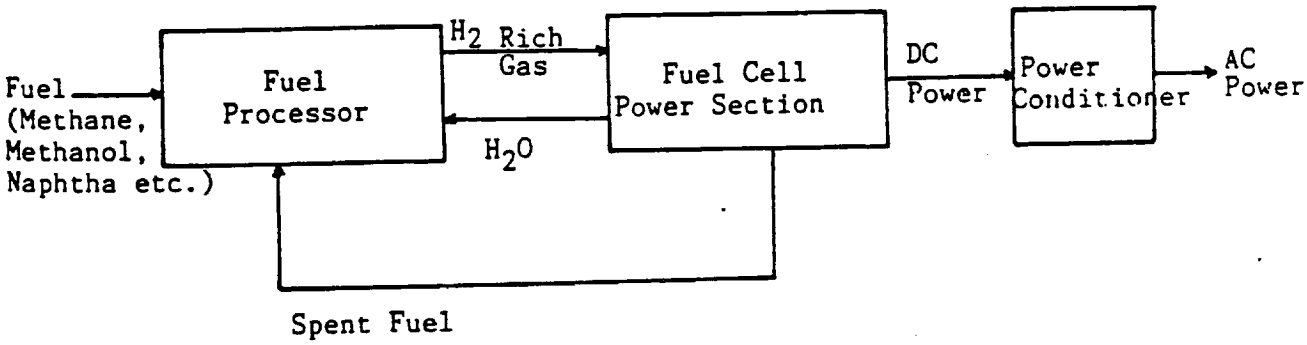

Figure 1 -Fuel Cell Power Plant Module

Figure 1 is a block diagram of a phosphoric acid fuel cell (PAFC) power plant with three principal modules: the fuel processor, the fuel cell power section, and the power processor.

Natural gas, methanol, and naphtha are principally considered for fuel cell use. Production of hydrogen, which is the major function of the fuel processor, occurs by reaction of the fuel with steam.

The major components in the fuel processor subsystem are the reformer, two shift converters, and several heat exchangers. The reformer is basically a nonadiabatic, nonisothermal catalytic reactor which can operate as high as 1200 °C and 10 atm.

Within the fuel cell power section, hydrogen and oxygen react with a continuous production of DC electricity, waste heat, and steam (as a reaction product). The oxygen is obtained from air and the waste heat can be removed by the cooling system of the fuel cell stack.

The heart of the power section is composed of a stack of several fuel-cell modules with four or five of such modules being sandwiched between two plates of the cooling system. The basic fuel-cell module can be made of two 30 cm x 40 cm bipolar plates, which function as gas diffusion electrodes, and a phosphoric acid matrix which is sandwiched between them.

The design and performance of the cooling system for the fuel-cell stack has significant effects on the operation and performance of the fuel-cell power modules.

In turn, these effects have direct influence on the capital and operating cost of the fuel-cell power plant and the cost of electric energy produced.

In addition to removal of heat generated by the electrochemical reaction, the stack cooling system must be so designed that surfaces of the electrodes are kept at a reasonably uniform temperature of 200 °c for optimum operation and to prevent the production of thermal stresses that can cause distortion and subsequent failure of the electrode plates.

The objective of this study is to analyse the heat transfer in the cooling system and to develop a correlation for the overall heat transfer coefficient in terms of the local heat transfer coefficient,coolant thermophysical properties,fluid flow characteristics,thermal contact resistance and cooling channel configuration.

1.1 Overall Heat Transfer Coefficient In a Fuel Cell Stack

In some phosphoric acid fuel cell power plants, the stack is arranged in such a way that each pair of cooling plates is sandwiched between five or more fuel cells modules.

Sigle cell assemblies are stacked in a series-connected bipolar mode. The directions of flow channels for air and hydrogen fuel are perpendicular to each other . In addition to the DC power generated, heat is produced as a result of the chemical reaction between hydrogen and oxygen. This heat is removed from the cell stack by coolant such as (air, water,etc...) passing through channels in cooling plates located approximately every fifth cell so as to maintain the

cells at the desired temperature. Figure 2 is a schematic illustration of a fuel cell stack.

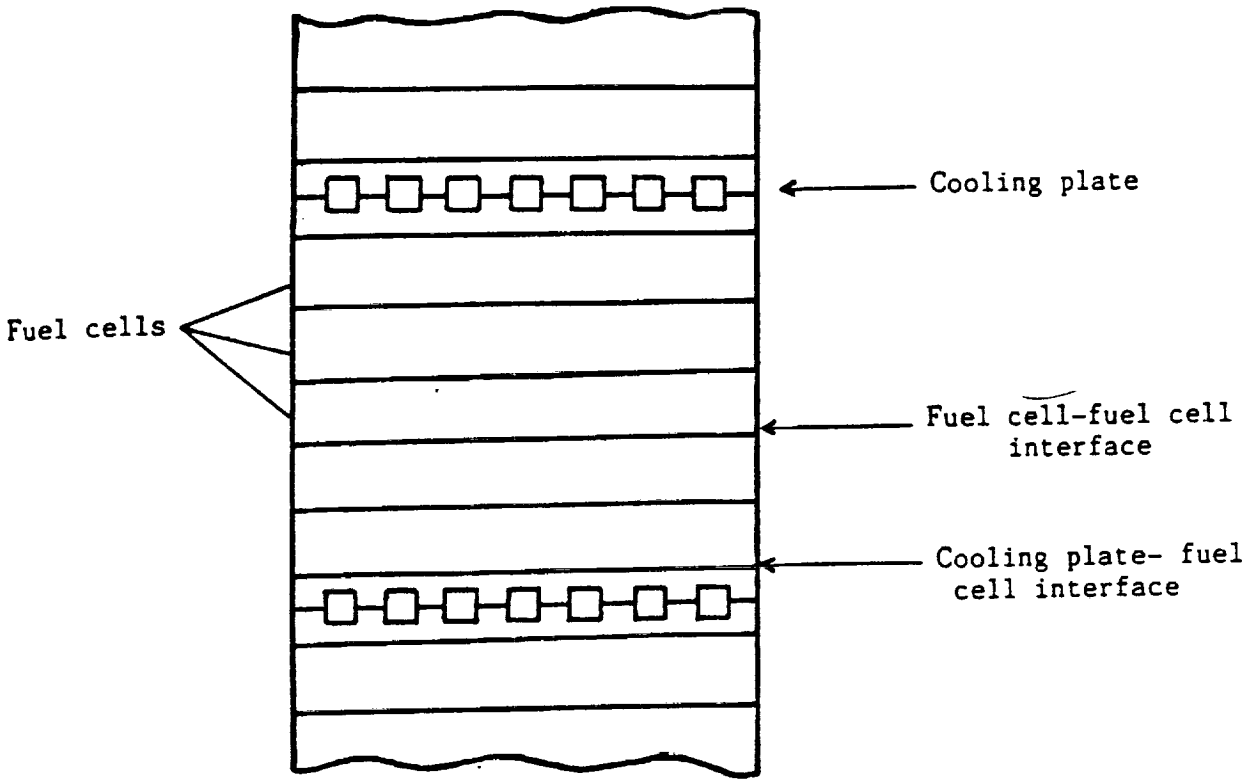

Figure 2 -Fuel Cell Stack

The overall heat transfer in the fuel cell stack may be represented by conduction through the cell plate, convection at the fuel cell - cooling plate interface which is due to thermal contact resistance, conduction through the cooling channel wall and the convection between the channel wall and the cooling fluid. More details about the overall heat transfer coefficient for the fuel cell stack and its representation in terms of a mathematical function will be

discussed at a later chapter.

1.2 Convective Heat Transfer Coefficient

Engineering applications of convective heat transfer and mass transfer are extremely varied. In a multifluid exchanger we are concerned solely with the heat transfer rate between the fluids and the solid surfaces of the heat exchanger separating the fluids. Calculation of the temperature of a cooled turbine blade or the throat of a rocket nozzle involves convective heat transfer. The aerodynamic heating of a high-speed aircraft is a convective heat transfer process, but it also becomes a mass-transfer process when temperatures are so high that gas dissociates, forming mass concentration gradients.

Obviously, the combination heat transfer, mass transfer, and chemical reaction problem is the most challenging of the convective problems. Nevertheless, the bulk of this project is devoted to convective heat transfer. It is convenient in most cases to define a convective heat transfer conductance, or coefficient, such that the heat flux at the surface is the product of the conductance and a temperature difference. Thus:

$$q'' = h (T_1 - T_2) \qquad (1)$$

The conductance h is essentially a fluid mechanic property of the system, whereas the temperature difference is, of course, a thermodynamic quantity. The usefulness of Eq. (1) lies largely in the fact that in a great many

technical applications it is close to being directly proportional to ($T_1 - T_2$), T_1 and T_2 are temperatures of surfaces one and two respectively, as the linearity of the applicable differential equation reveals. Nevertheless, numerous nonlinear problems are encountered where h itself is a function of the temperature difference. It is important to note that this does not distroy the validity of Eq. (1) as a definition of h, although it may well reduce the usefulness of the conductance concept.

1.3 Thermal Contact Resistance

As mentioned previously in section 1.1, that contacts between the fuel-cell plate and the cooling plate in a fuel cell stack resulted in the existence of thermal contact resistance. This parameter is needed in the evaluation of the overall heat transfer coefficient for the system. Therefore, some historical background and definition about thermal contact resistance may be briefly discussed in the following paragraphs.

In the past, thermal resistances of contacts between solids received little attention, the contacts being assumed to be either perfect or resulting in constant additional resistance. However, the quest for higher efficiencies required improved designs and materials pushed to the limits of their performance, and so the assumptions came to be increasingly questioned. This resulted in the investigation of the variation of the thermal contact conductance with material properties, applied load, temperature, and fluid environment. Hence, it is necessary to define thermal

contact resistance.

1.3.1 Contact Resistance

Whenever there is a flow of heat between two material, with thermal conductivities K_a and K_b , placed together under a load which is less than the load required for compressive yielding of the bulk material, actual contact between the surfaces occurs only at a discreet number of locations. This results in a temperature discontinuity across the interface.

The lines of flow of heat converge in passing through a contact area which is smaller in size than the boundaries of the solids in contact. Thus, thermal contact resistance occurs because not all of the volume of the solids in contact is equally available for the conduction of flow of heat. There is an undirectional flow of heat away from the contact surface, but near the interface the flow becomes three-dimensional. The interface is a region of disturbance which extends into the specimen by approximately the distance separating two consecutive perfect contacts (54).

From the basic Fourier equation, the linear temperature distribution some distance away from the interface is given by:

$$\frac{q}{A} = K_a \frac{dt}{dx} = K_b \frac{dt}{dx} \qquad (2)$$

This may be extrapolated to the interface to determine the effective temperature drop (ΔT) across the interface, Figure 30 . If the thermal contact conductance h may be

defined by :

$$h = \frac{q/A}{\Delta T} \tag{3}$$

then

$$h(\Delta T) = K \frac{dt}{dx} \qquad \text{or} \qquad h = K \frac{dt/dx}{\Delta T}$$

The thermal contact resistance r is defined by:

$$r_c = \frac{1}{h} \tag{4}$$

Thus, if the heat flux and the temperature drop across the interface are known, one can determine the thermal contact resistance. It is important to realize that there is no localized interface contact resistance but rather a region of influence in the neighborhood of the contact.

CHAPTER II

REVIEW OF LITERATURE

Estimation of the temperature profiles in an operating fuel cell is important for estimation of the power density distribution, thermal stability, and cooling requirements. Only a limited amount of information on this subject has been reported in the past. Baker and co-workers recognized this need and have performed a comprehensive steady state heat transfer in electrochemical systems (3,4,5). They studied various limiting and special cases to determine the maximum temperature of a stack; a two dimensional heat transfer analysis was carried out in the case of thick stacks where heat transfer in the direction of stacking was neglected. In the case of thin stacks, three dimensional heat transfer was considered with each wall at a different temperature. Infinite series solutions were developed for both thick and thin stacks. The authors estimated the maximum stack temperature for the constant wall temperature case. An approximate formula to predict the effect of finite resistance to heat transfer at the wall, the effect of cold or hot feeds, or non-uniformity of heat generation

was also carried out by using the method of Green's function.

A single fuel cell with no lateral heat transfer and no conduction of heat through the cell in the direction perpendicular to the gas flow was considered (4). Heat transfer by conduction in the direction of the gas flow was considered negligible in comparison to the heat transfer by convection, and analytical expressions for the electrolyte, fuel and air temperature profiles were derived.

Alkasab and Lu (6) have developed a heat transfer model for the phosphoric-acid fuel-cell stack combining mass, energy and electrochemical analysis. The derived three-dimensional mathematical model was utilized to develop a Fortran computer program in which this computer simulation included the determination of the effects on steady state temperature distribution in the cell plate and in the stacking directions: thermal conductivity, average current density, cell-plate dimensions, cell-plate size, coolant flow rate, cooling channels configurations, and inlet temperature of process air.

Industries such as Westinghouse and Energy Research Corporation (45) have used a unique technique for cooling fuel cell stacks. One of the reactant gases, rather than a liquid, is used as the stack coolant. In the cooling gas scheme, the air feed stream is either split inside the manifold into both a reactant stream and a coolant stream which flow independently through the fuel cell stack and are either merged in the exit manifold or maintain separate

reactant and cooling streams.

Engelhard (46) has also developed a low cost cooling plate that can be made of conventional materials using conventional furnace brazing techniques. The coolant is a dielectric liquid. This cooler offers a potential cost reduction over other liquid and ebullient liquid coolers. A complete 5 Kw power plant incorporating a methanol reformer and a utility grid compatible power processor has been built and tested.

United Technologies Corporation (47) has used an intercell cooling or two-phase water cooling method. Thin-walled, 2-pass copper tubes with stainless steel headers are the latest design. The acid environment requires the copper tubes to be coated with a thin teflon protective film; however, this somewhat reduces heat transfer. The chief disadvantage of these intercell coolers is their relatively high cost. The probability of cooler failure due to penetration of the film and subsequent corrosion of the copper has not yet been established.

Table I (48) displays comparison of separate gas cooling to the two other commonly accepted cooling methods: process gas cooling and liquid cooling.

The estimates are based on selected methods. No effort was made to optimize any of them; however, all systems are reasonable and are consistent for comparison purposes.

Westinghouse has recently made a more detailed study of gas cooling. Under Doe Contract (49, 50) they developed

TABLE 1

*Comparison of Cooling Schemes for Phosphoric Acid Fuel Cell System (48)

	Separate Gas Cooling	Process Gas Cooling	Liquid Cooling
1. Construction Simplicity	Simple	Simple	Complex
2. Electrolyte	Low	High	Low
3. Reliability	High	High	Low
4. External Heat Exchange	Fair	Fair	Good
5. Cost of Cooling Subsystem, % Stack Cost	5	5	25-50
6. Total Differential Temperature °F	45	60	20

a lumped parameter fuel cell stack simulation code that calculates reactant gas compositon, current-voltage characteristics, and heat transfer characteristics for a gas-cooled fuel cell stack. In the model, the cell area is broken down to a grid of finite elements so that power and heat generation can be calculated as functions of temperature and reactant composition, as each varies from from point to point in a cell.

Also, in the previous studies concern was primarily with the analytic evaluation of the conductance, or heat-transfer coefficient, under various conditions. The results of the evaluation were used, together with other heat transfer theory, for the analysis and design of fuel-cell systems. Some of these results have significant application outside the realm of fuel-cells, and there are cases where the conductance concept loses its useful significance. In these cases it will be more convenient to work directly with temperatures and heat transfer rates than to employ a conductance (41).

Many authors (34) considered tubes with various flow cross section shape: a circular tube, rectangular tubes and triangular tubes. They considered heating and cooling from two surfaces and the effects of a peripheral heat flux variation around a tube. Next, they also considered a class of problems where the velocity profile is fully developed and remains fixed while the temperature profile is fully developed and remains fixed while the temperature profile develops. After this they became concerned with

thermal-entry-length solutions for circular tubes and also, for rectangular tubes. A method was developed whereby the thermal-entry-length solutions for constant heat flux and constant surface temperature can be used to solve for the temperature distribution resulting from an arbitrary axial distribution of surface temperature or heat flux (34).

The cooling channel configuration is important in analyzing and studying the overall performance of the fuel cell cooling system. However, until now emphasis has been primarily on analytic solutions, and experimental results have been referred to only where they serve to validate the assumptions used in building a mathematical model of the heat-transfer process. Nevertheless, experiments can and do form a primary source of convection heat-transfer data for engineering applications; if the flow geometry is complex, it is often far easier to perform experiments than to attempt to deduce heat-transfer rates by analysis. Since the present work deals mainly with the convective heat transfer analysis, it becomes essential to investigate and acquire an experimental technique to measure the heat transfer coefficient where knowledge of it in engineering is required for a very wide range of activities. Numerous straight-forward and ingenious techniques have been used to determine the convective heat transfer coefficient experimentally. Moreover, in general, the scope of this review is confined to techniques for determining the steady state heat transfer coefficient and to summarize the available techniques along with a selection of their

applications.

2.1 Experimental Techniques for Measuring the Convective Heat Transfer Coefficient

Baughn (80 has recently summarized some methods of directly measuring heat transfer for forced convection in ducts, so the examples chosen for each technique are for flat surfaces. Davenport (9) used a straight forward technique for the mean heat transfer coefficient for the air-side of lowered surfaces in water cooled heat exchanger specimens. It was simply based on evaluation of the enthalpy change from the measured mass flow and temperature change of a liquid on the other side of the test surface.

Many authors considered electrical heating, which is the most common experimental technique of determining local and mean heat transfer coefficients. The electrical power energy input is easy to measure but the energy losses have to be carefully evaluated.

Three techniques have recently been used. Kim et al. (10) used 12 copper plates 460 mm wide, 50 mm long and 6 mm thick for a study of full coverage film cooling in a wind tunnel. The plates were heated by resistance wires installed in slots machined into the back side of each plate. To minimize the energy loss from the back of the plates, heated water tubes were used.

Eriksen and Goldstein (11) used 18 stainless steel foil heaters 203 mm wide, 50 mm long and 0.25 mm thick for film cooling studies in a wind tunnel. The foil was electrically heated and backed with 50 mm of styrofoam, and

had thermocouples on its surface. Blair (12), on the other hand, obtained a more detailed knowledge of the heat transfer coefficient distribution by using 144 separate 1 mm thick composite heaters on an area 508 mm x 1220 mm , again for film cooling studies in a wind tunnel. The heaters were backed with about 25 mm of rigid urethane foam, and the infrared technique was used to measure the wall temperature (13).

Another technique is to use electrically conducting wall coatings. Two types are commercially availble: a transparent type of vapor-deposited gold on polyester film 0.2 mm thich * and a carbon impregnated coating on a plastic sheet 0.31 mm thick. These have been successfully used with liquid crystal sheets ** for a variety of flat and curved geometries by Hippensteele (14). This combination gives local qualitative and quantitative data.

Heat flux sensors were used with the Fourier heat-conduction equation to obtain local heat transfer coefficients. It is important that they do not disrupt the gas flow at the wall or alter its temperature. Crawford et al. (23) have used foil-type sensors on flat, film-cooled

---

*From Sierracin/Index Products, Chatworth, CA, USA.

**Such as those from Liquid Crystal Technology LTD, LONDON, UK.

surfaces, while Hay and West (24) have constructed and applied slug-type sensors to swirling flow in a pipe. Miniature sensors which are about 25 times smaller, i.e. 0.7 mm x 0.2 mm x 0.8 micrometer thick, have been developed by Portrat, et al. (17) for turbomachinery.

Other methods of indirectly measuring heat transfer were conducted. For example, mass transfer experiments are easier to set-up, have cleaner boundary conditions, are easier to study, and are more accurate than the corresponding heat transfer process. The heat and mass transfer analogy approach where the gas concentration at the walls plays the same role in the mass transfer process as does the wall temperature in the heat transfer process, i.e. :

$$h\,(T_w - T_\infty) = h_m\,(C_w - C_\infty) \qquad (5)$$

The simplest and most useful form of the analogy was proposed by Chilton and Colburn (55).
This is :

$$St \cdot (Pr)^{2/3} = St_m \cdot (Sc)^{2/3} \qquad (6)$$

and where the flow fields are identical for the heat and mass transfer systems:

$$h = h_m\,C_p\,(Sc/Pr)^{2/3} \qquad (7)$$

So, by measuring h_m , h can be determined.

A comprehensive account of the analogies between mass, heat and momentum transfer is given by Sherwood et al. (56).

2.2 Thermal Contact Resistance

Jacob and Starr (21) investigated thermal contact resistance of interface joints between various metals in vacum as a function of pressure at room temperature and at the temperature of boiling nitrogen 93 °K.

Brunot and Buckland (22) investigated the dependence of thermal contact resistance on laminated and cold rolled steel joints of various surface roughness and contact pressures. As expected, contact resistance decreases with increased pressure. Their test on solid steel blocks with various degrees of smoothness indicate that the smoother the surface, the lower the resistance. They infer that it is probably " due to the thinner layer of air or the larger area of contact encountered ". Another conclusion is that tests on laminated steel blocks indicate that if a thick metal shim is used between the two surfaces, the hardness of the shim has little effect. If aluminum foil is substituted, the resistance is lowered as pressure is increased. They ascribe this to the fact that the laminations are embedded deeper in the foil, so that there is more effective conformity between surfaces. The effect of interstitial fluid on thermal contact resistance was not measured.

Weillis and Ryder (23) determined the dependence of thermal contact resistance of joints on pressure, surface

finish, temperature, interstitial fluid, heat flow, and temperature drop. Their results show a linear dependence of thermal contact conductance of dry steel joints and an exponential dependence for aluminum and bronze. Other significant results are the decrease in thermal resistance with a decrease in surface roughness of both dry and oil-filled joints, and a higher resistance of dry joints to oil-filled joints. The effect of the oil decreases at higher pressures. The thermal resistance is decreased by copper-plating on the surface of a joint.

Barzelay et al. (24) investigated the effect of heat flow, the temperature of the joint and later also investigated (25) the effect of pressure and dissimilar metal combinations on thermal contact resistance. They found that for the same metal combination the thermal contact resistance depended upon the direction of heat flow, whether heat flowed from steel to aluminum or from aluminum to steel. They found that, other factors remaining the same, the thermal contact conductance for aluminum to aluminum contact was greater than that for aluminum to steel contact, which in turn was greater than for steel to steel contact. The least value was observed for steel to aluminum contact. The reason for this was not satisfactorily explained by the authors, as pointed by Powell et al. (26).

They also found that interface conductance increased with pressure and with the mean temperature at the interface. Another conclusion was that surface roughness alone was not

a dominant parameter in determining thermal conductance of contacts; overall flatness had a more important role in determining the configuration of surface matching.

It appears that the majority of researchers have not included the effects of this parameter (contact resistance) in their analysis that involved fuel cells. Also, in the evaluation of the overall heat transfer coefficient, the terms " contact pressure " and " contact resistance " were not considered either. More details about the approach used in measuring the contact resistance and the significance of it will take place in a later chapter.

CHAPTER III

SYSTEM DESCRIPTION

In this chapter, a general description of the apparatus and the test procedure are presented. Also, shematic views for devices used are illustrated, and measuring instruments and other equipment are described.

3.1 Construction of the Fuel Cell

The objective of this task is to design and construct an experimental set-up that simulates the output and working conditions that prevail in the fuel-cell module and the cooling system of a phosphoric acid fuel-cell stack. The set-up is assumed to simulate a fuel-cell module operating at an average temperature of about 190 °C and one atmospheric pressure, having an ouput of 0.8 volt and an average current density of about 0.325 amp/cm^2.

The fuel-cell module shown in Figure 3 consists of two 0.30 m x 0.41 m mating graphite plates with an upper plate thickness of 6.35 mm and a lower one of 9.5 mm. Nichrome wire was used to hold the heating loops as shown in Figure 4 .

As was stated before, graphite is the principal

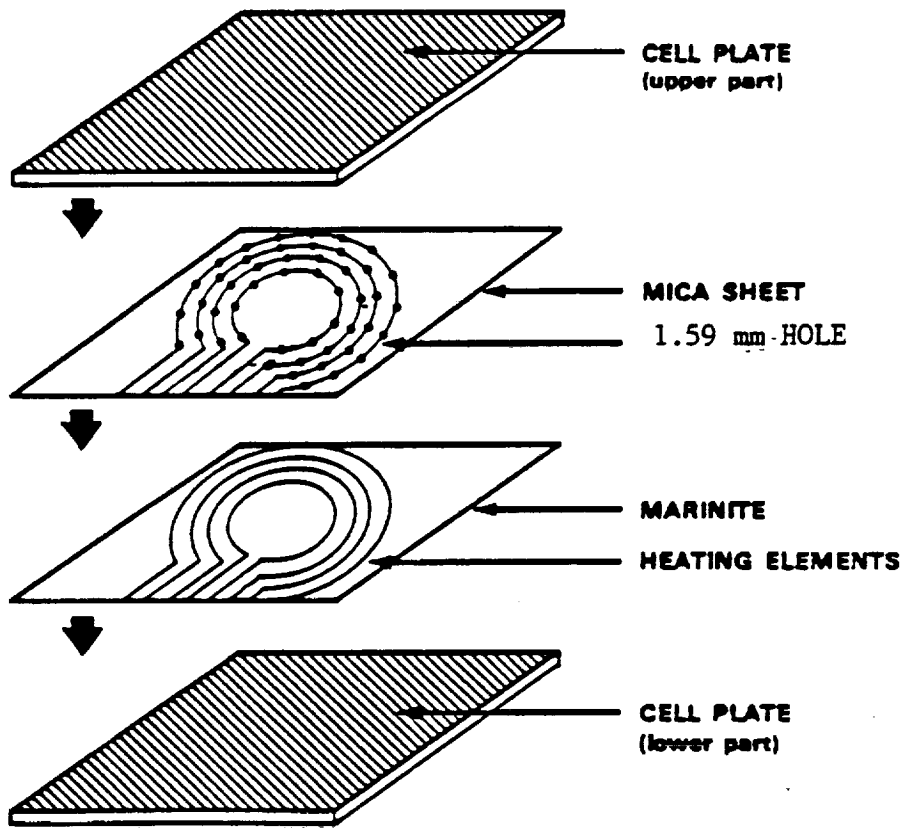

FIGURE 3 - ILLUSTRATIVE CELL CONFIGURATIONS

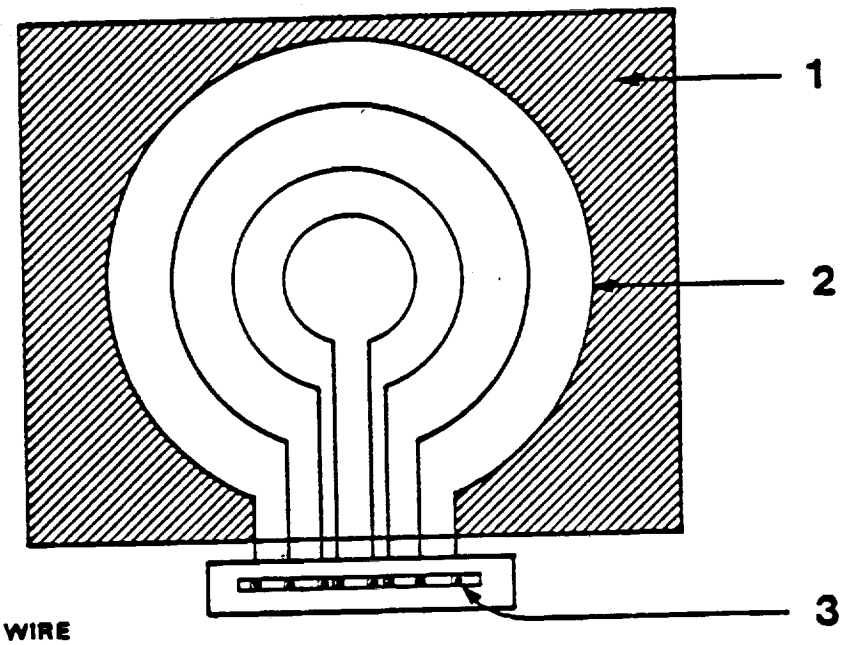

1. MARINITE
2. NICROME WIRE
3. ELECTRICAL CONNECTIONS

Figure 4 - Heating Elements Configuration

material used to construct fuel cells. Contact with nichrome heating elements caused circuit shortage because the graphite is an electrically conductive material; therefore, the use of marinite became necessary in order to electrically insulate the heating elements.

Marinite is structural insulation not affected by moisture or high humidity, and will not rust or corrode. In addition, it withstands a temperature of up to 650 °C . A sheet of marinite 0.25 x 0.38 m^2 with a 6.35 mm thickness was sandwiched between the two plates, after milling 4 circular loops of grooves 4.76 mm in diameter in each plate to fit the heating elements. This sheet of marinite was inserted into the lower plate of the cell module covering an area of 150 inches square. The face with circular grooves which contained the heating elements was in touch with the bottom part of the lower plate. In order to prevent electrical contact between the nichrome wire and the upper plate, a very thin sheet of mica was inserted in between. Thus, the heating elements, the marinite and the mica were sandwiched between the two graphite fuel-cell plates and bolted together, forming the simulated fuel cell module.

3.2 The Experimental Set-up

A general view of the test installation is shown in Figure 5 , a top view is shematically illustrated in Figures 6 , 7 , 8 , and a close-up of the pressure loading system showing the location of the test assembly is shown in the shematic of Figure 9 .

The set-up consists of the following:

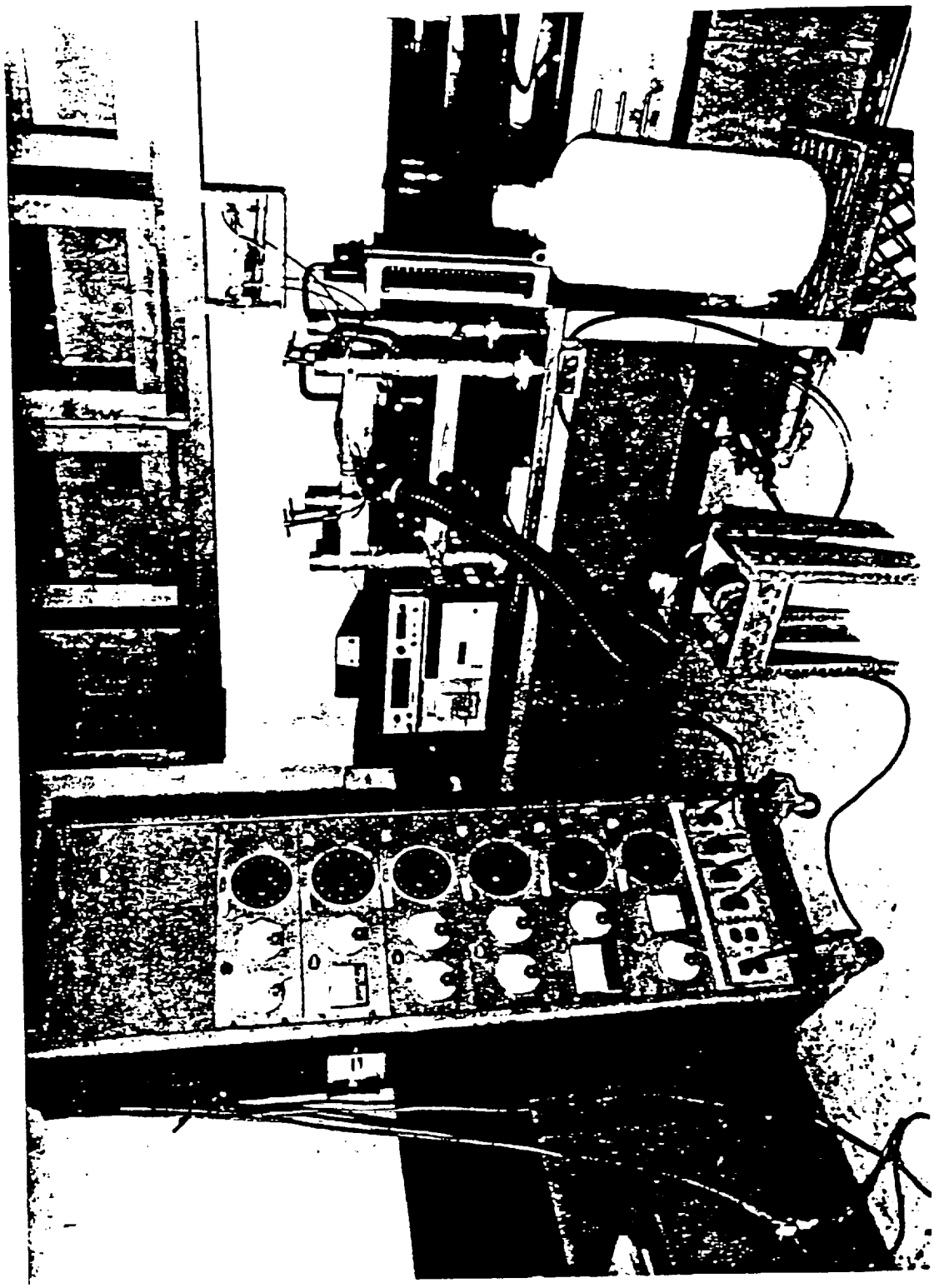

Figure 5 - The Experimental Set-up (Air Case Shown)

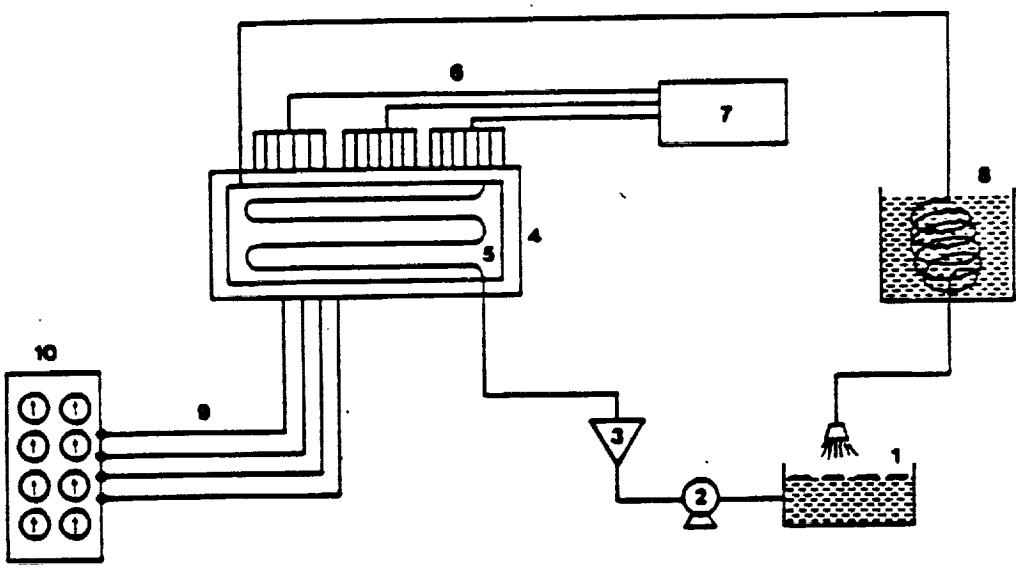

1 TANK FOR COOLANT (OIL)
2 PUMP
3 FLOW METER
4 FUEL CELL PLATE
5 COOLING PLATE (SERPENTINE TYPE SHOWN)
6 THERMOCOUPLES CONNECTED TO DATA LOGGER
7 FLUKE DATA LOGGER
8 OIL COIL ICE BATH
9 WIRE CONNECTIONS TO HEATING ELEMENTS
10 POWER SUPPLY

Figure 6 - Flow Diagram of the Apparatus when Oil is Used as a Coolant

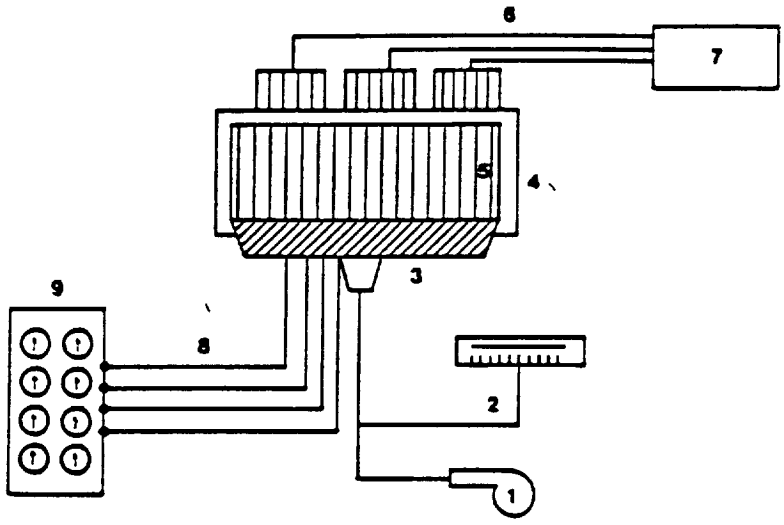

1 BLOWER
2 PITOT TUBE
3 MANUFOLD
4 FUEL CELL PLATE
5 COOLING PLATE (STRAIGHT CONFIGURATION SHOWN)
6 THERMOCOUPLES CONNECTED TO DATA LOGGER
7 FLUKE DATA LOGGER
8 WIRE CONNECTIONS TO HEATING ELEMENTS
9 POWER SUPPLY

Figure 7 - Flow Diagram of the Apparatus when Air is Used as a Coolant

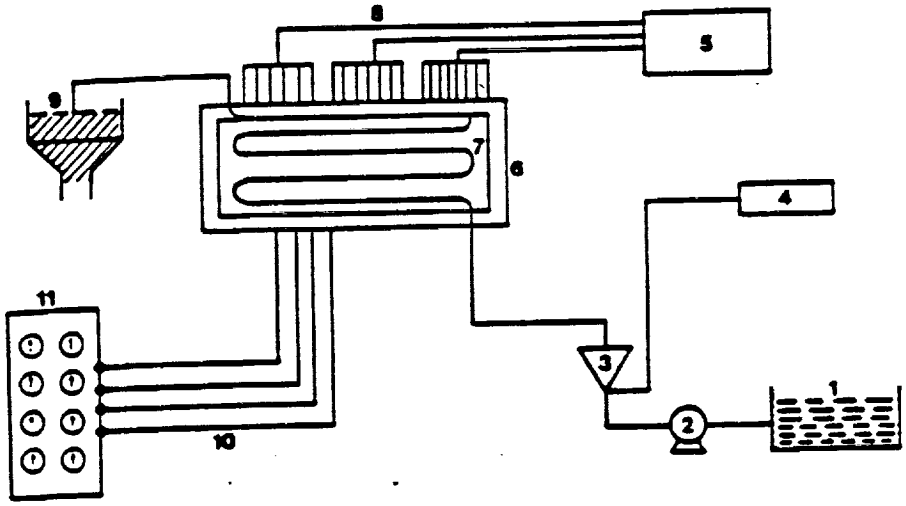

1. TANK FOR COOLANT (WATER)
2. PUMP
3. FLOW METER
4. CMC UNIVERSAL PRESET COUNTER
5. FLUKE DATA LOGGER
6. FUEL CELL
7. COOLING PLATE (SERPENTINE TYPE IS SHOWN)
8. THERMOCOUPLES CONNECTED TO DATA LOGGER
9. DRAINER
10. WIRE CONNECTIONS TO HEATING ELEMENTS
11. POWER SUPPLY

Figure 8 - Flow Diagram of the Apparatus when Water is Used as a Coolant

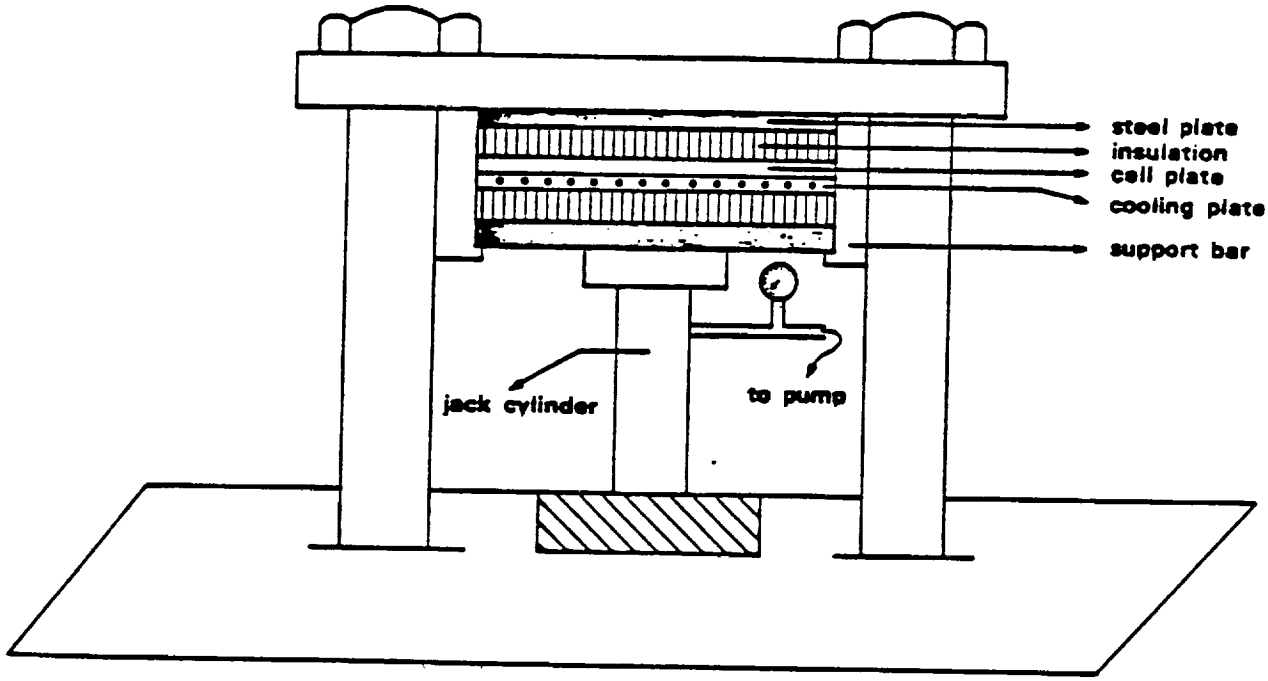

Figure 9 - Schematic View of the Stack Pressure Loading System

1- Fuel-cell module

2- Fuel-cell cooling plates

3- Power supply unit

4- Temperature measurement and recording equipment and instruments.

5- Coolant circulations and fluid flow measuring devices.

6- Stack pressure loading system

3.2.1 Fuel-Cell Module

Heat generation in the fuel-cell module was implemented by supplying the required amount of wattage to simulate an actual operating fuel cell from the power supply. The heat source consisted of 4 loops of coils of 80-20 nickel-chromium alloy resistance wire. These coils were centrally positioned inside machined circular grooves in the marinite sheet with the ends of each coil loop connected to the power supply. The terminals of the coil were electrically insulated by compacted magnesium oxide which has the unique quality of being a good insulator at high temperature, and at the same time a good heat conductor Figure 4 . Each heating loop was connected to an autovariac which supplies it with 120 volt A.C. By varying the voltage across each loop, the shape of isotherms across any section in the heat assembly also could be varied. This gave an additional control in order to get a uniform heat flux across the cross sectional area of the fuel cell plate.

3.2.2 Cooling Plates

The cooling system consisted of two types of cooling

plate configurations and three different types of coolants. The serpentine configuration was used for oil and water and the straight channel configuration for air.

A. Serpentine Configuration

As shown in Figure 14 , this configuration consisted of two mating plates of graphite, size 0.30 x 0.41 m^2 , and a copper tube 9.5 mm in diameter, 3.66 m long. The copper tubing was inserted as loops inside the cooling plate. Grooves were machined in each half of the cooling plate to fit four and a half loops of the copper tubing. The coolant was circulated through the system by the use of a pump with a variable speed motor and a maximum capacity of 5 gpm. The variable speed motor provided control of the coolant flow and the ability for it to operate at different flow rates.

B. Straight Channel Configuration

The straight channel configuration is shown in Figures 15 , 16 . This cooling plate was built from graphite of the same dimensions as that of the serpentine type. Two mating halves were constructed with each half having a total of 30 half channels; the combination of the two halves formed the straight channel configuration.

In this configuration, air was forced through the manifold system by a blower, a 51 mm diameter plastic tube was used to connect the blower outlet to the manifold system inlet. To minimize corrosion, the manifold was fabricated from steel and the tube was constructed from heavy duty plastic.

3.2.3 Power Control Unit

This unit consisted of the metal panel where a set of 6 variacs, ammeters and voltmeters are dispersed in series of 3. Each independent set of one (variac, voltmeter, ammeter) was connected to the heating loop by a heavy duty electric wire. Monitoring the amount of electric heat in each loop was easily managed and the amount of power was measured with considerable accuracy. This instrument obtained its electric power from the main switch that is provided by the university in the lab.

3.2.4 Temperature Recording Devices and Instrumentations

In this experiment, measurement of temperature was the most important factor and the most sensitive aspect as far as accuracy is concerned. Thermocouples type T copper-constantan were used for measuring the temperature. Over 100 temperature measurements were needed during the operation. Therefore, a data acquisition system was installed, type Fluke (Model 2200 B), along with an extender chassis (Model 2201 A) giving the system a capacity of accomodating 100 channels. Basically, this unit is designed to scan and measure analog input data, and then output the measurement data in digital form. Output data is displayed and can be recorded. The control section operates under program control to select input channels, and scale the resultant measurement readings for display of recording purposes.

A total of 72 thermocouples Figure 13 , were installed to measure the surface temperature of the cell plate.

Four thermocouples, which measured the wall temperature, were attached on the plate centerline along the length and at four locations 0.15m apart axially from each other. The temperature for inlet and outlet of coolant were also measured and monitored by the Data Logger. Thermal contact resistance temperatures were recorded. Other temperature measurements such as room and surroundings were obtained by a Fluke Digital thermometer. The thermocouples were a 24 Gauge or 0.25 mm in diameter, which were glued to the lower cell plate through holes 1.59 mm in diameter made on the upper plate, and then were connected to the Data Logger. Also, the rest of thermocouples were glued to their locations using Viton cement which not only holds the thermocouples in place but withstands high temperature and provides good heat conduction.

3.2.5 Coolant Circulation and Flow Rate Equipment and Instruments

Flow rate for the cooling air was determined by using a pitot tube. The flow is manually controlled by varying the speed of the blower motor; this arrangement was done by using a variac to draw different voltages across the blower motor in order to obtain the desired flow rate.

Water flow rate was measured by using a turbine flow transducer, an inline metering device utilizing a bladed rotor to generate flow information. It has the ability to measure liquid and gas under high temperature and pressure conditions with accuracy and reliability. It was connected to a flow counter CMC (Model 614 A) where a digital readout

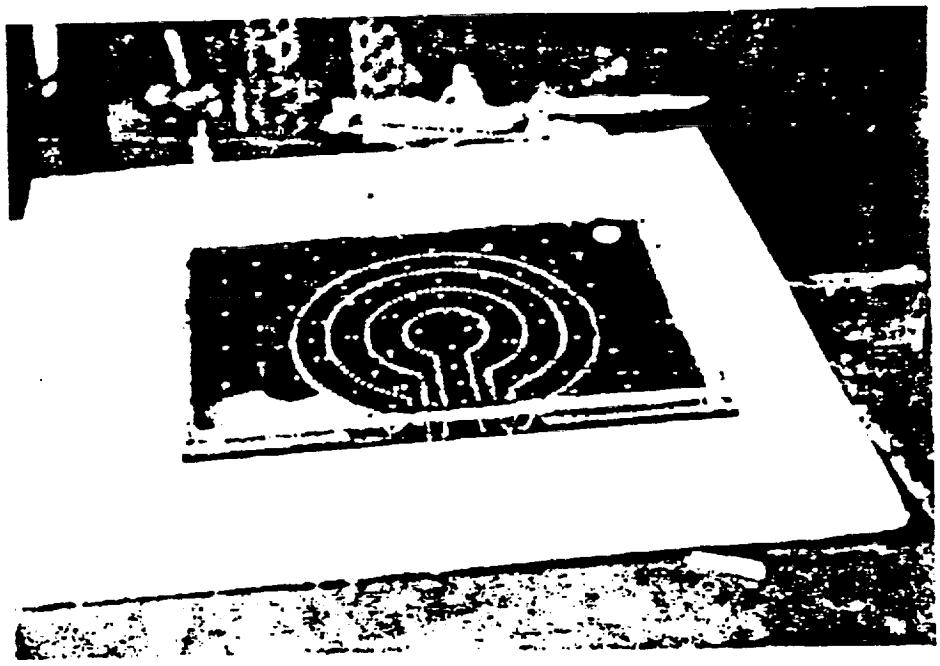

Figure 10 - View of the Mica Sheet over the Heating Elements

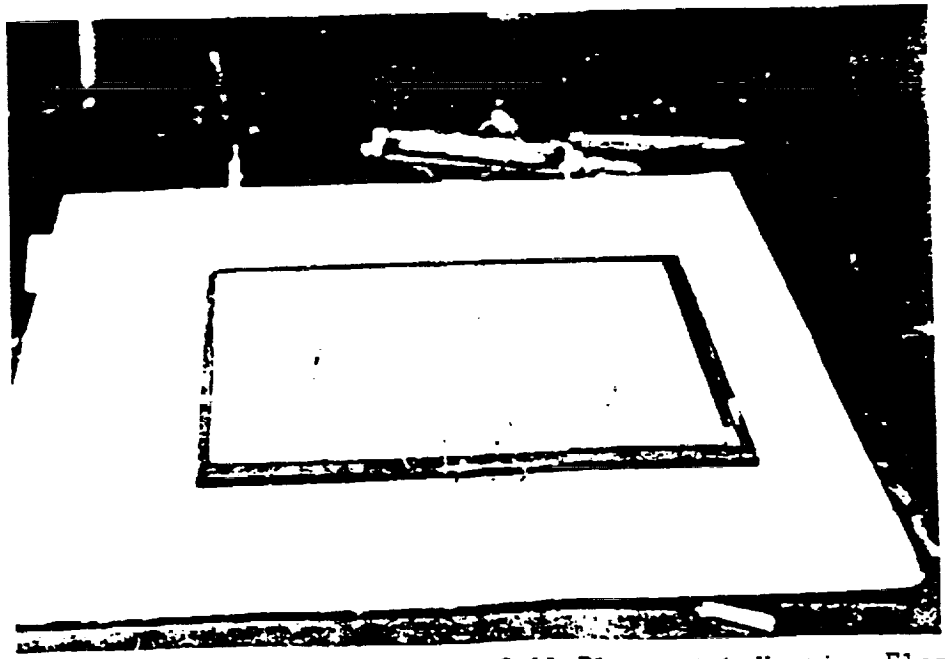

Figure 11 - Lower Part of the Cell Plate with Heating Elements inside Grooves of Marinite

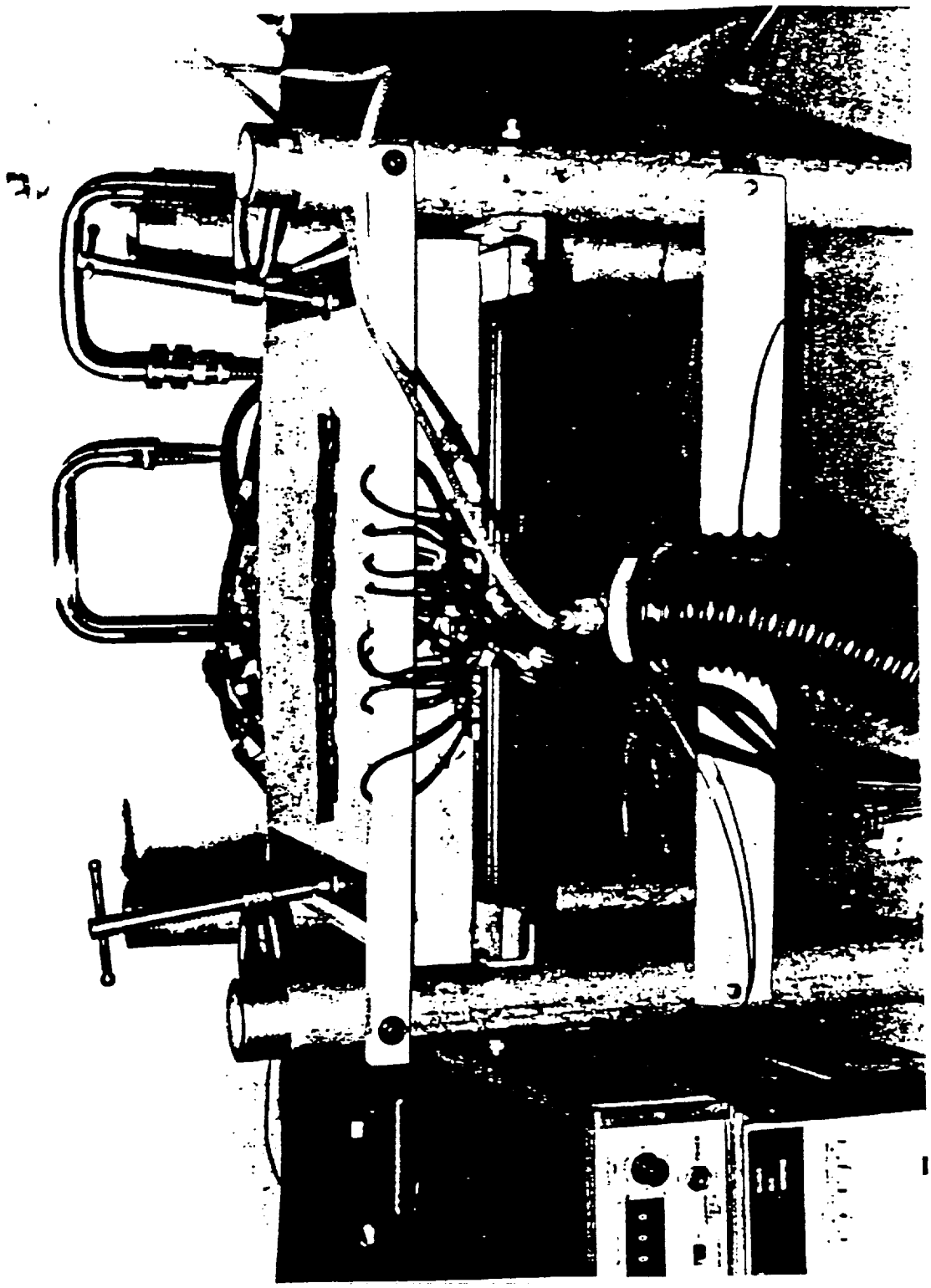

Figure 12 - View for the Fuel Cell Module

of the frequency is obtained, and a calibration curve of frequency versus gallon/minute was established. A mechanical flow meter (Model 1110 B) Brooks with a maximum capacity of 0.40 gpm was used to determine the flow rate of oil. A certificate of calibration was provided by the manufacturer and a manual calibration was imposed to check over the data. Water and oil flow rates were manually controlled by a special valve attached to the pump used in this experiment.

3.2.6 Stack Loading System

This system simulated the pressure applied to the fuel-cell stack to hold the fuel-cell module and the cooling plate together. As shown in Figure 12 , the stack of the fuel-cell module and the cooling plate were sandwiched between two steel plates having a thickness of 12.71 mm each. Pressure was applied to the stack by a 4 ton capacity hydraulic jack and measured by gauge as shown in Figure 9 .

3.3 Test Procedure

A shematic of the flow system is shown in Figure 6 . The test began by applying electrical power to the heating elements in the fuel cell module. Temperatures at different locations in the cell plate were monitored until a uniform heat generation and an average cell temperature of 190 °C were obtained. At this point, the cooling system was put into operation with coolant using oil, water and air as coolants. The oil and water were circulated through the serpentine passages or the air was forced through the cooling channels.

When oil was used as a coolant, a cooling coil, which is shown in Figure 6 , has been designed and built so that the oil is cooled to 21 °C which is the oil inlet temperature used in this experiment. Temperatures were monitored again until steady state conditions were achieved. Tests were conducted for various interface pressure (0 to 3448 Kpa).

Temperatures were digitally recorded and were continuously available on a 5 minute update cycle. The control of temperature of the coolant was achieved by an isothermal bath (oil case); the copper coil was contained in a 50 liter capacity reservoir tank. The bath temperature was controlled with simultanuous hot and cold water. The temperature was monitored by the Data Logger during the test period providing continuous reading for the inlet temperature. Bath temperature was sensed by a thermocouple installed in conjunction with the experimental thermocouple network. Water temperature was pumped from the reservoir tank while the temperature monitored by the Data Logger and controlled by a similar method as oil achieved the desired temperature. Air temperature was maintained between 20 °C and 23 °C during all the test period, an average of 21 °C was used in carrying out the mathematical calculations. The wall temperatures were measured at 4 stations 15.25 cm axially apart from each other. An arithmetical average for all four was used in the calculation. Twelve thermocouples were installed to measure the temperature drop across the interface: three were stationed at 3 locations 6.33 cm axially

apart from each other, 2 sets in the cell plate and the other 2 in the cooling plate. The effective temperature drop was found by linear extrapolation to the interface as shown in Figure 30 .

The pressure was measured by a zero to 6895 Kpa gauge; the gauge had been calibrated by the general instrument corporation with a piston gauge which has been compared with master piston gauges. Furthermore, the calibration certificate suggests an accuracy of 0.1 percent for the gauge employed in the program.

The heat was supplied by the loops of nichrome wire, gauge 30 of about 8.8 ohms at room temperature. The electrical input power was determined from the current and voltage measurements. All measuring instruments in this part were calibrated and carried certifications of the test showing a maximum deviation from nominal of 0.01 percent.

The coolant flow rates were measured by flow meters except for air where a pitot tube was employed, power input was constant during the test period. Conditions were then changed by varying one of a number of parameters which included the coolant flow rate, the interface pressure, as well as the cooling plate configurations. Each test was repeated three or four times and measurements were recorded accordingly.

For completness, the experimental work included careful insulation of the (cell/cooling) plate to minimize heat losses. Non-asbestos millboard type Binder-Cement that withstands temperatures of up to 538 °C was used for this

purpose. In order to assess the magnitude of the heat loss, the apparatus was operated at low power with no coolant flow and the wall temperature was measured. These data were then used to correct the power input in normal operation. The total heat loss was found to be approximately 1 % of the heat input. The corrected power input was employed in the evaluation of the average fluid temperature gradient. Data reduction followed the normal pattern of the evaluation of Reynolds numbers, thermal contact resistance, and finally average heat transfer coefficient (i.e. heat transfer coefficient based on average surface heat flux and average wall temperature to the average fluid temperature difference).

FUEL CELL PLATE
THERMOCOUPLE LOCATIONS

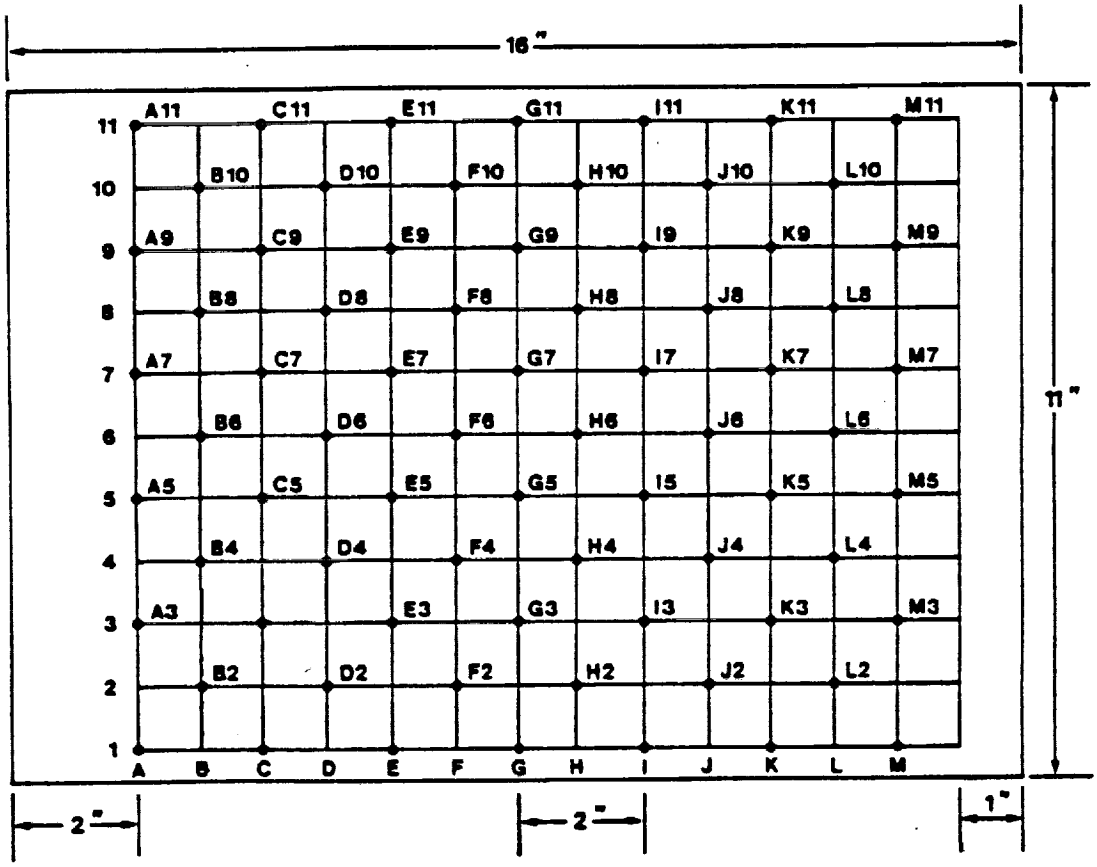

Figure 13 - Locations of Thermocouples

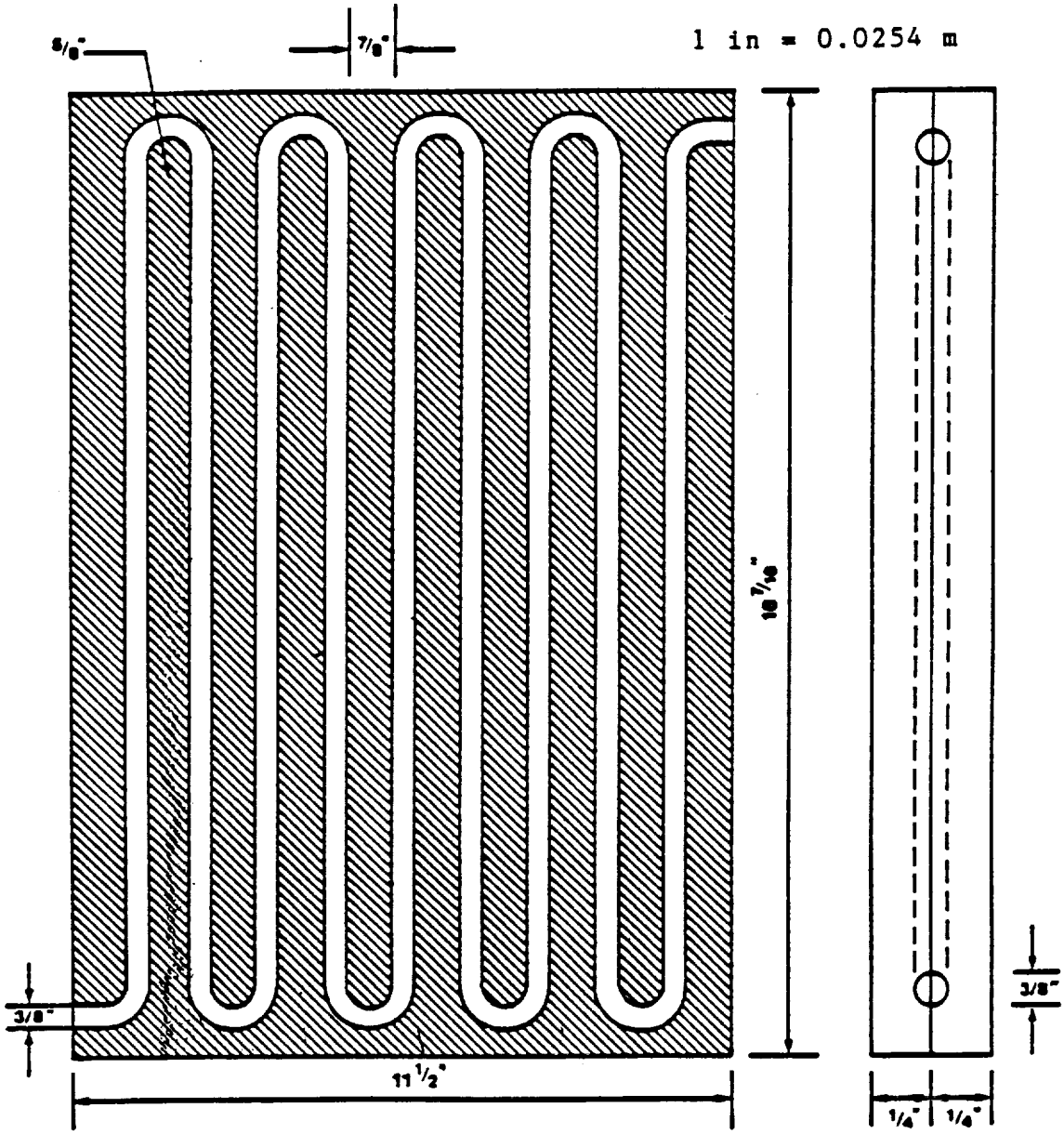

FIGURE 14 – SERPENTINE COOLING PLATE GEOMETRY

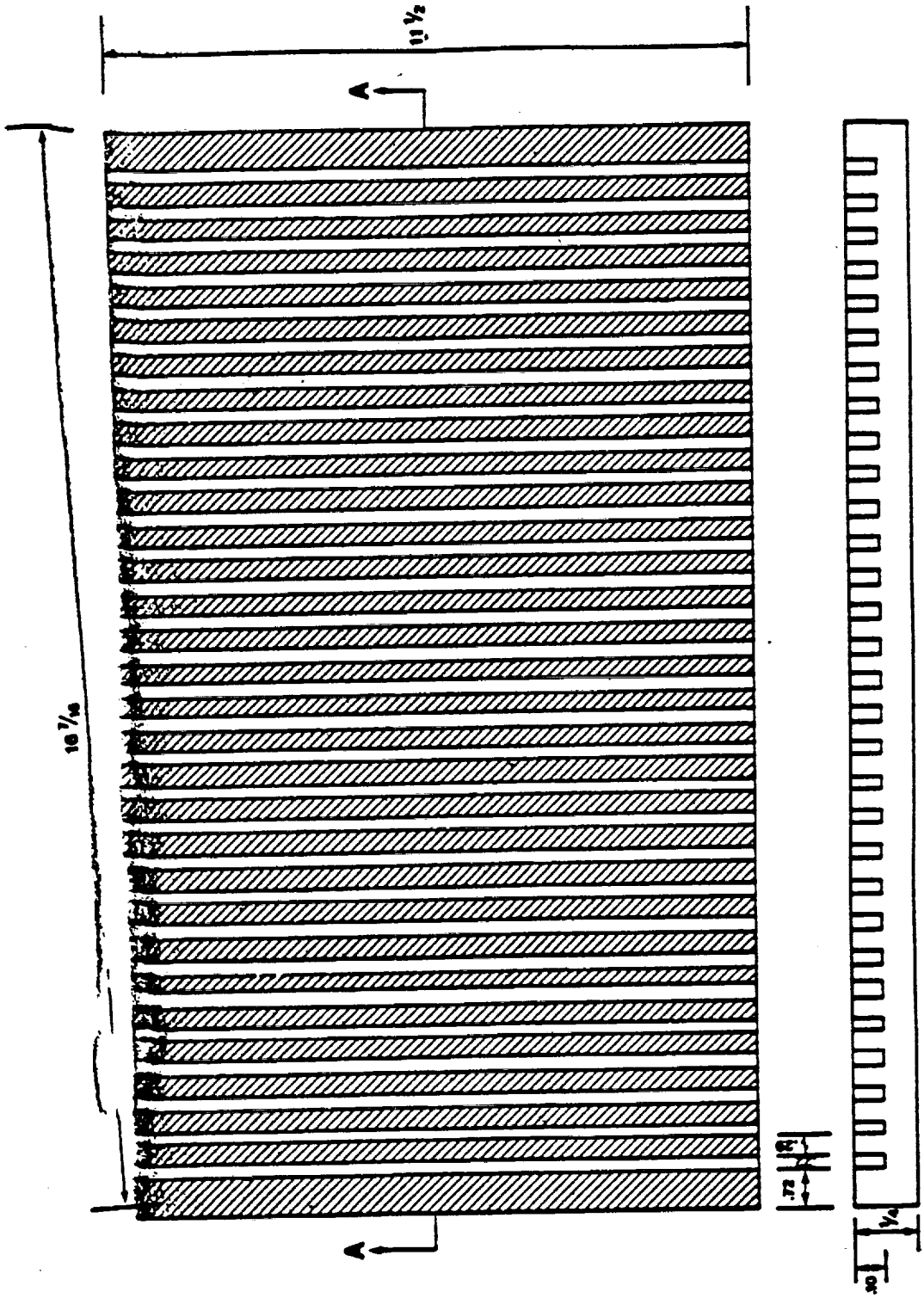

1 in = 0.0254 m

Figure 15 - Detailed Drawing of the Straight Channels Configuration

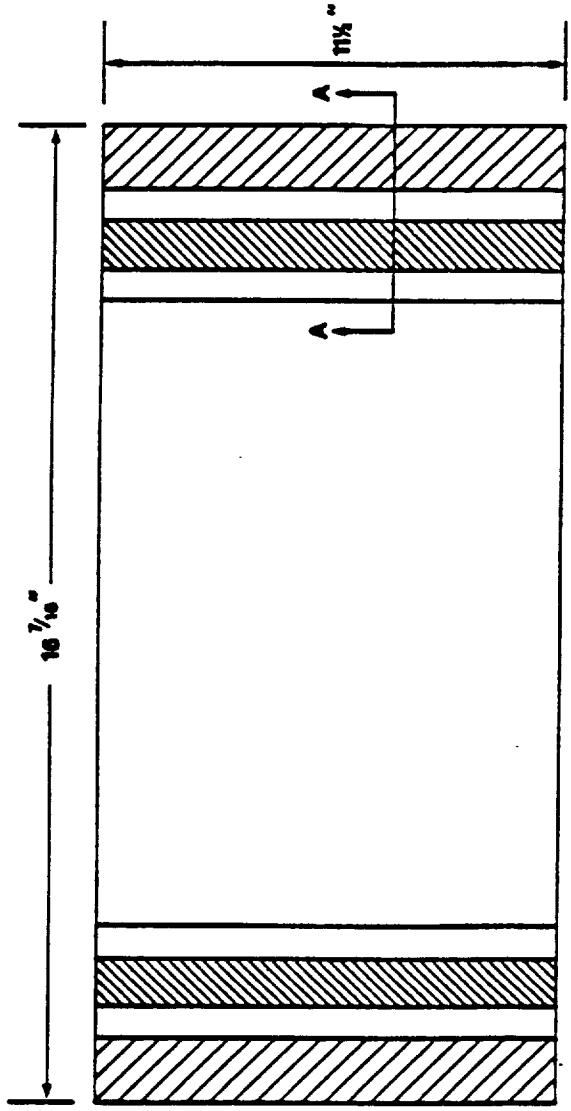

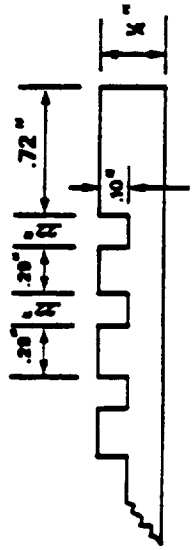

1 in = 0.0254 m

FIGURE 16 – SECTION A-A AS SHOWN FOR STRAIGHT CHANNELS CONFIGURATION

CHAPTER IV

ACCURACY OF DATA

Since there could be many sources of error with varying degrees of influence for different sets of readings, it is therefore appropriate to discuss individually these sources of error and their influence on the final result.

4.1 Errors Due to Thermocouple Readings

Any error in the thermocouple readings is of great significance as it is from this, directly or indirectly, that all the numerical results were obtained. Each of the thermocouples used in these tests were made of wire from the same lot and read on the same Data Logger.

Obviously, the significance of this error would depend, on the temperature drop across the interface which is used in the evaluation of the thermal contact resistance. However, the accuracy of measuring the overall heat transfer coefficient depends on the accuracy of the thermal contact resistance values. At high pressure the minimum of temperature drop across the interface is found to be 2 °C as seen in Figure 30 . When scales were used, the temperature drop across the interface varied from 2 °C to

6 °C . Inlet temperature of the coolant was between 20 °C and 22 °C for all types of coolants. Obviously, the maximum error, due to thermocouple readings, in presence of the Data Logger was not more than 1 percent.

4.2 Errors Due to Heat Leaks

There are possible paths through which the surroundings can exchange heat energy with the test module where the essential measurements are taking place.

The first is by convection through the body of the test module. To eliminate the convective component of heat transfer to the surroundings, the fuel cell module has been insulated. The quality and the thickness of the insulation used were such that heat loss to the surroundings was expected to be insignificant. It was calculated to be about 15 watts which is less than 2 percent of the total heat generation. This could result in some percentage of error in the calculation of the heat transfer coefficient and conductance values.

The second source of error was in the uncertainty of the uniformity of the heat flow which could be caused by:

a. Heat loss

b. Non-uniformity in the heat path

The non-uniformity of heat flow has two origins: the first is the non-uniformity inherent in the very nature of contact resistance; the second is the disturbance created by the thermocouple insertion. Nothing can be done with the first one. The second one was minimized by spot-welding the tip of the thermocouple to a small brass

sphere 1.27 mm in diameter. This is done so that an average temperature over a small region at the center could be measured. In this way any inaccuracies due to thermocouple bead not being exactly at the center were diminished. Moreover, in order to have uniform horizontal isotherms in the cell plate itself, the latter must have boundary conditions. This was achieved by the use of graphite in the construction of both the cell plate and the cooling plate. Besides, this material was chosen because its electrical resistivity did not vary with temperature, resulting in a uniform heat flux.

Precise measurements of the axial location of thermocouple was necessary for the accurate calculation of the temperature gradient. This is especially important in the determination of the temperature drop across the interface.

Although thermocouples were placed as close as possible to the interface, a linear extrapolation of the axial temperature gradient could have been inaccurate when the temperature drop was unusually small or when a radial gradient of sufficient magnitude was present. However, any error due to this extrapolation was assumed negligible.

4.3 Errors Associated with Observation of the Properties to be measured

This section is a brief discussion of errors made due to errors in calibration and readability of pressure gauge, flow meters, voltmeter and ammeters.

As indicated earlier, the pressure gauge has an

accuracy of 0.1 percent. This means that for a range of maximum pressure of 6895 Kpa used in the present research, the pressure gauge had an error ±6.9 Kpa. To account for errors in readability and calibration we shall adopt a maximum of ±35 Kpa.

The test flow meters have an accuracy of 0.05 percent for the turbine flow transducer and 0.1 percent for the Brooks instrument type. The error due to measurements of flow from the pitot tube is accounted to be about 1 percent. Thus, the maximum combined error due to flow rates measurements would amount to 0.4 percent. Other measurements such as readings of voltage, current and heat losses along thermocouple wires, were assumed to be about one percent.

Nevertheless, the error in calculating the heat transfer coefficient for 3 different tests under the same conditions for oil, water and air was found to be less than one percent. However, all the above factors might have influenced the values presented for heat transfer coefficient and thermal contact resistance to an estimated ± 10 percent in the extreme.

The energy balance for the coolant includes convective heat transfer between coolant and channel walls and convection by the coolant. The energy balance for the coolant, for a unit length along the channel, can be written as

$$hS\,(T_w - T_c) - \frac{mC_p\,dT_c}{dx} = 0 \qquad (8)$$

where

h	= Heat Transfer Coefficient	$w/m^2.°C$
S	= Perimeter of Cooling Channel	m
T_c	= Average Coolant Temperature	°C
T_w	= Average Wall Temperature	°C
m	= Cooling Mass Flow Rate	Kg/hr
C_p	= Specific Heat of the Coolant	KJ/Kg.°C
x	= Distance from the Edge	m

The boundary condition is:

$T_c = T_i$, at inlet at $x = 0$

In carrying out this mathematical analysis the following assumptions were made:

(a) Thermal conductivities, specific heats, and densities of all fluids involved are assumed to be constant.

(b) The heat flux at the wall is constant.

(c) The edges of fuel cell plate and cooling plate are assumed to be adiabatic.

(d) The coolant flow is assumed to be steady.

Thus, if the flow enters at temperature T_i , the solution from Eq. (8) yields a value of the exit temperature, T_o , in the following form.

$$T_o = T_i + (T_w - T_i)(1 - e^{-\phi}) \qquad (9)$$

where,

$$\phi(x) = \frac{hSx}{m.C} \qquad (10)$$

Eq. (9) was solved numerically on the IBM 370 computer for five different flow rates and for air, oil and water properties. Comparison of both the calculated and the measured values for the exit coolant temperature are presented in Appendix (B).

5.2 Heat Transfer Analysis for the Serpentine Configuration

In tube flow, the heat flux q" is usually defined by the relation,

$$q" = mC_p (T_{b_2} - T_{b_1}) \qquad (11)$$

or,

$$q" = h (T_w - T_b) \qquad (12)$$

and,

$$h = \frac{q"}{A (T_w - T_b)} \qquad (13)$$

where,

A = Total Surface Area for Heat Transfer m^2

T_w = Average Wall Temperature °C

T_b = Average Fluid or Bulk Temperature °C

Subscripsts 1 and 2 refer to inlet and outlet conditions.

In deriving the mathematical relation for the convective

heat transfer coefficient in the serpentine cooling plate configuration, the followings were led to be :

1- Wall temperature is the logarithmic average of the measured temperatures at various locations at the wall.

2- T_b , is the logarithmic average of the inlet and oulet temperatures of the coolant.

The heat transfer rate through the surface of the cooling plate was determined from the measurements of the electrical power dissipated by the nichcrome heating elements in the cell plate, the outer wall temperature, and the mean of the cooling fluid temperature as expressed in Eq. (13).

The electrical power was determined from the heating elements current and voltage measurements. The inaccuracy in the current and voltage measurements was estimated to be less than 5 percent. This is believed to be the major uncertainty in the heat transfer measurements. Check measurements were made of the voltage drop across the heating loops. This gave an upper limit of the power generated in the cell plate, since it included losses due to contact resistance. Measurements showed a little variation in the electrical resistance per heating loop over the surface of the cell plate.

The outer wall temperature was measured with thermocouples at various locations as shown in Figure 19 . Inlet temperature of coolant was measured with a thermocouple located in a well mixed location at the entrance to the test section. The outlet temperature was

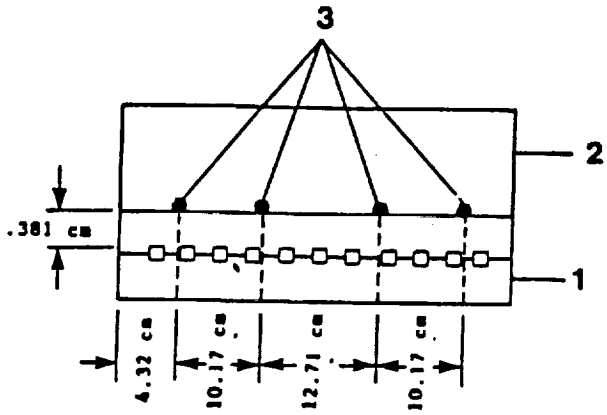

1 - Cooling Plate

2 - Fuel-Cell Plate

3 - Thermocouple Location At The Wall

Figure 18 -Measurements of Wall Temperature

measured in the settling chamber at the manifold in the air case and at a probed thermocouple inside the copper tube in the oil and water cases.

Reynolds and Nusselt numbers were determined from the following relations,

$$Re = \frac{V.D}{\nu} \qquad (14)$$

where,

V = Velocity m/sec

D = Cooling Channel Diameter m

ν = Dynamic Viscosity of the Fluid m^2/sec

$$NU = \frac{h\ D}{K} \qquad (15)$$

where

K = Thermal Conductivity of Coolant w/m.°C

For oil and water Eq. (13) was used in the calculations of the heat transfer coefficient.

5.3 Heat Transfer Analysis for the Straight Channel Configuration

The heat transfer coefficient for the cooling air was determined from the energy balance between the heat removed by the coolant and the convective heat transfer between the channel walls and the coolant.

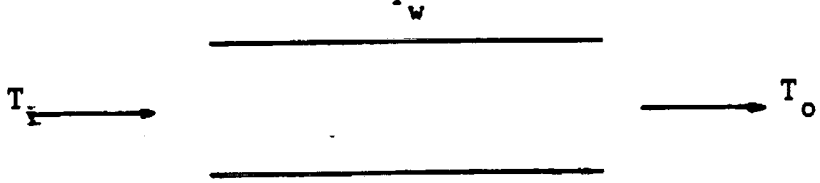

Figure 13 - Geometry of Cooling Channel (Straight)

At steady state the energy balance can be written as follows:

$$hA\ (T_w - T_c) = m.C_p\ (T_o - T_i) \qquad (16)$$

and

$$h = \frac{m.C_p(T_o - T_i)}{A\ (T_w - T_c)} \qquad (17)$$

where

m = Cooling Air Flow Rate — Kg/hr

A = Heat Transfer Area for the Cooling Channel — m^2

T_o = Outlet Temperature of Air — °C

T_i = Inlet Temperature of Air — °C

T_c = Average of Inlet and Outlet Temperature of Air — °C

T_w = Wall Temperature — °C

In this analysis the hydraulic diameter is used for evaluating Reynolds number. This is so because most of the velocity change in a turbulent flow takes place very close to the wall surface and is relatively independent of the proximity of other wall surfaces. For this reason the shape of the flow tube cross section has little effect on the shear stress at the wall, except where sharp corners are involved. The hydraulic diameter is defined by:

$$D_H = \frac{2xy}{x + y} \qquad (18)$$

x = Width of Cooling Channel — m

y = Depth of Cooling Channel — m

5.4 The Overall Heat Transfer Coefficient

The heat-transfer process may be represented by the network shown in Figure 20 , and the overall heat transfer is calculated as the ratio of the overall temperature difference to the sum of the thermal resistances.

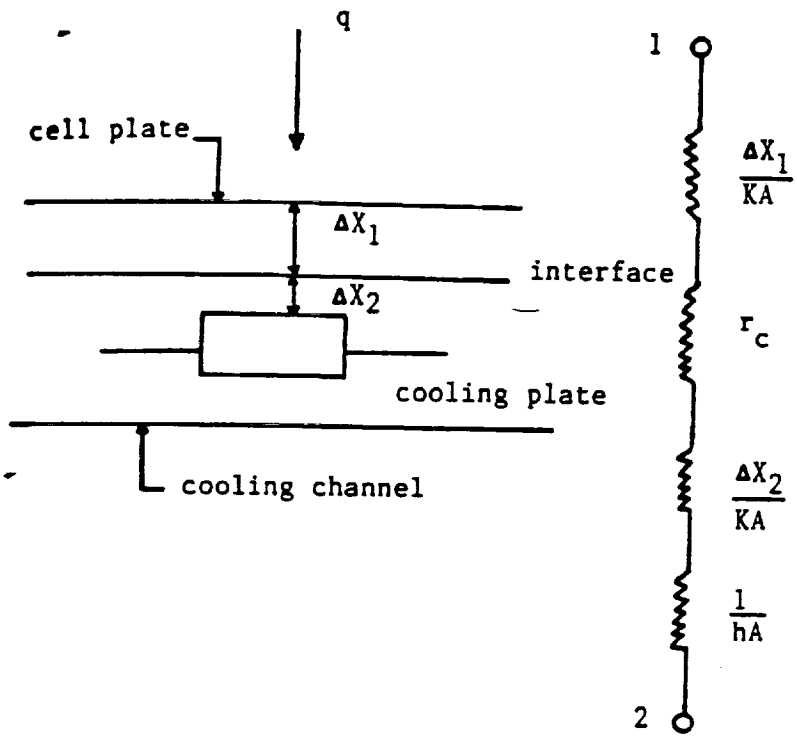

Figure 20 -Overall Heat Transfer through the (Cell/Cooling) Plate Unit.

This is represented by the following relation,

$$q = \frac{T_s - T_c}{\frac{1}{hA} + \frac{\Delta x_1}{KA} + \frac{\Delta x_2}{KA} + r_c} \qquad (19)$$

where,

T_s = Source or Cell Temperature °C

T_c = Mean Fluid Temperature °C

Δx_1 = Distance, Fuel Cell - Interface m

Δx_2 = Distance, Interface - Cooling Channel Wall m

Observe that the value 1/hA is used to represent the convection resistance. The overall heat transfer by combined conduction and convection is expressed in terms of an overall heat-transfer coefficient U , defined by the relation,

$$q = UA\,\Delta T_{overall} \qquad (20)$$

where A is the total heat transfer area. In accordance with Eq. (19) the overall heat transfer coefficient would be:

$$U = \frac{1}{\left[\frac{1}{h} + r_c + \frac{\Delta x}{K}\right]} \qquad (21)$$

where,

r_c = Thermal Contact Resistance °C.m/w

Δx = Sum of Δx_1 and Δx_2 m

K = Graphite Thermal Conductivity w/m.°C

Thermal contact resistance between the cooling plate and the fuel-cell plate was measured for various interface pressures and a correlation was developed relating the contact resistance with interface pressure. More details pertaining to this correlation will be presented in an upcoming section.

5.5 Experimental Correlations

Mathematical correlations for the local heat transfer

coefficient in terms of Nusselt number and Reynolds number for all coolants oil, water and air are presented. Also, the thermal contact resistance and the temperature drop across the interface as a function of interface pressure are also shown.

This arrangements permitted the presentation of the experimental results in their most general form in order to establish the basic relationships between the essential parameters, and to specify the significant parameters themselves.

In an attempt to correlate the results (Appendix B), a computer program was developed to handle various types of curve fitting procedures including linear, polynomial, exponential, power and reciprocal functions. The least squares techniques and Gauss-Siedel approach, as well as other algorithms, were utilized in the development of this computer code. It also included graphics subroutine which enabled comparison of the various types of functions simultaneously on the screen of the graphic terminal.

Thus, the experimental data shown in Tables 1.1 through 1.5 were correlated by using the following functional variation,

$$h = C \ Re^{m} \ Pr^{n} \qquad (22)$$

where C, m and n are constants to be determined from experimental data. Figure 21 shows the dependence of the heat transfer coefficient on Reynolds number. By using all

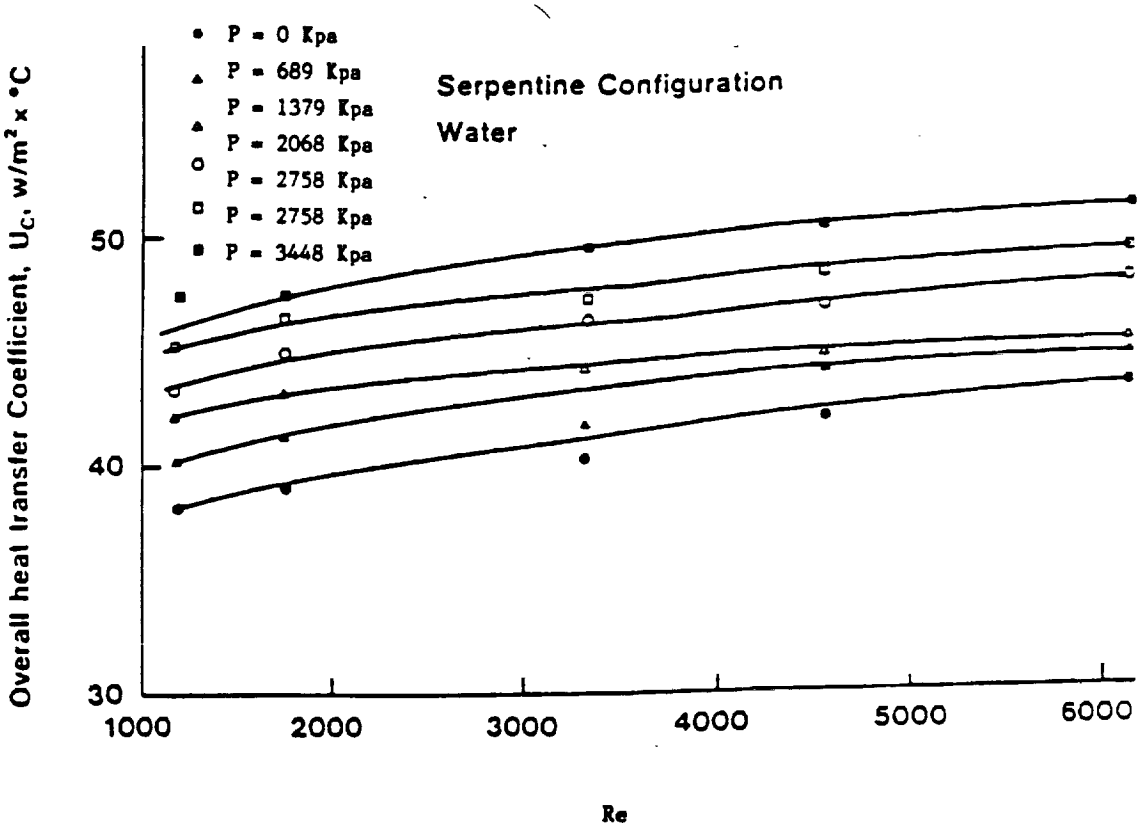

Figure 21 - Variation of the Overall Heat Transfer Coefficient with Re and P for serpentine configuration with water as coolant

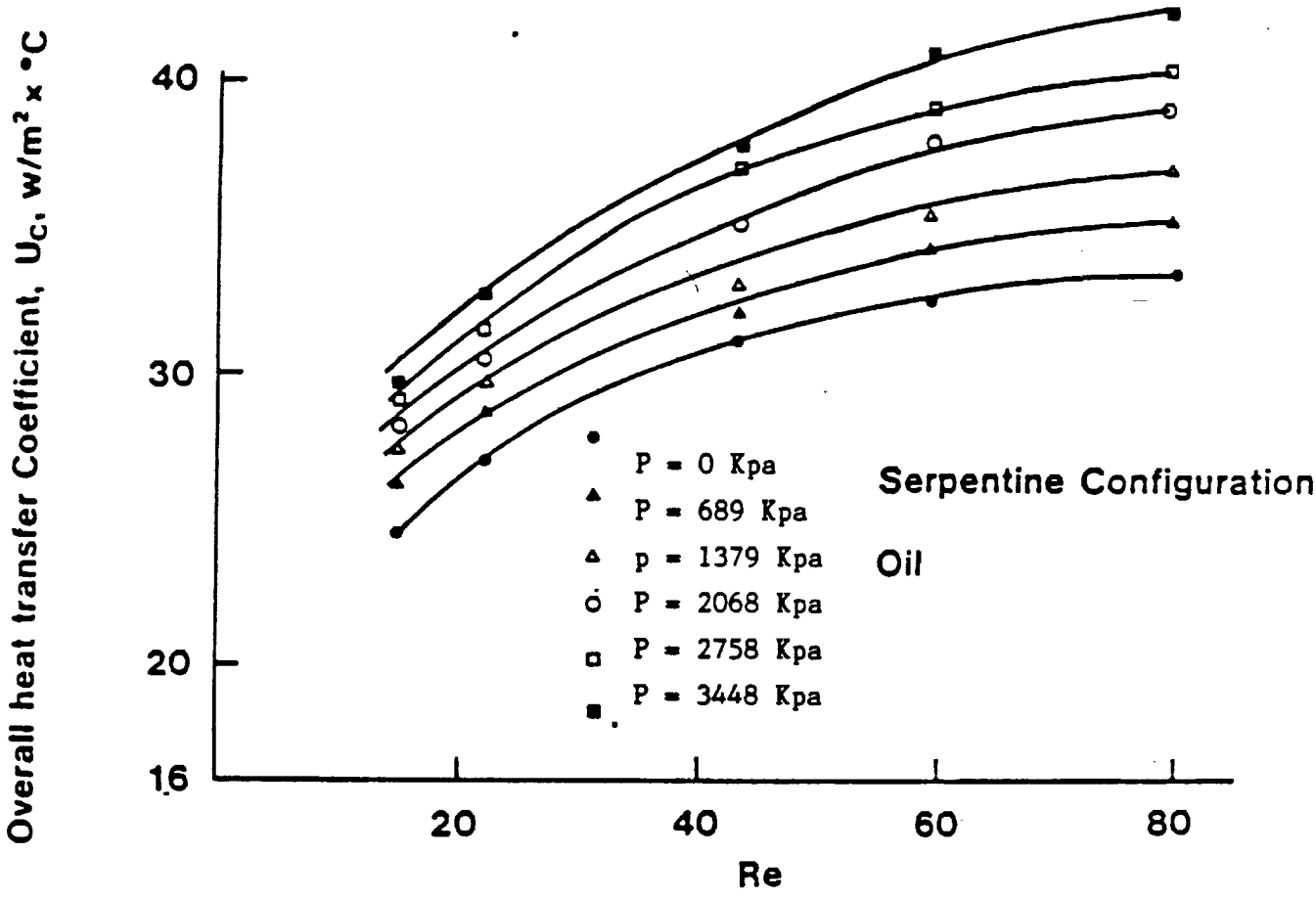

Figure 22 - Variation of the Overall Heat Transfer Coefficient with Re and P for serpentine configuration with oil as coolant

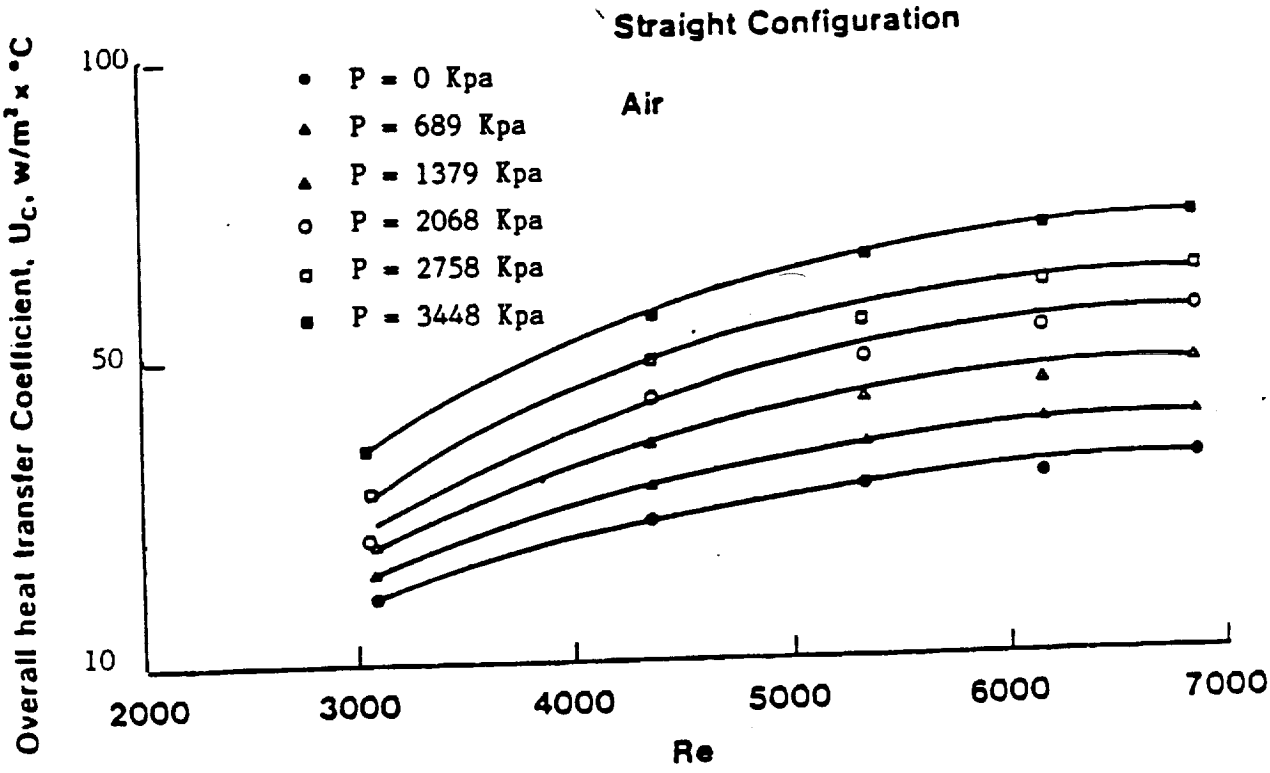

Figure 23 - Variation of the Overall Heat Transfer Coefficient with Re and P

the experimental data (Appendix B) as input to the computer program, a final value for m was determined as well as value for the constants n and C .

Final correlations for all three coolants used are represented as follows:

(a) Serpentine Configuration (Oil)

The correlation equation which represents the heat transfer coefficient when oil is used as a coolant in terms of Nusselt number and Reynolds number is represented by,

$$h = 16.444\ Re^{0.2144}\ Pr^{0.00769} \tag{23}$$

and,

$$NU = 0.7501\ Re^{0.2142}\ Pr^{0.00394} \tag{24}$$

(b) Serpentine Configuration (Water)

Also, similar equation was developed for the heat transfer coefficient when water is used as a coolant in terms of the same parameters as (a) , this equation is given by,

$$h = 31.088\ Re^{0.05779}\ Pr^{0.01433} \tag{25}$$

and,

$$NU = 0.3259\ Re^{0.05632}\ Pr^{0.0385} \tag{26}$$

(c) Straight Channel Configuration (Air)

For the straight channel configuration and the cooling air, the heat transfer coefficient in terms of Nusselt number and Reynolds number can be written as follow:

$$h = 0.004338\ Re^{1.0730}\ Pr^{0.04085} \tag{27}$$

and,

$$NU = 0.0005138\ Re^{1.0966}\ Pr^{0.237} \tag{28}$$

(d) Correlation of the Thermal Contact Resistance

Similarly, correlations of the experimental data for thermal contact resistance, effective temperature drop across the interface as a function of interface pressure were developed. Measured values of thermal contact resistance versus interface pressure were plotted for the serpentine and the straight channel configurations as shown in Figures 24 and 25 . These plots were then utilized to obtain the following correlations:

1- Straight Channel Configuration

The following equation was developed for the contact resistance in terms of the interface pressure from the experimental results.

$$r_c = 0.001581\ e^{(-0.001413\ P)} \tag{29}$$

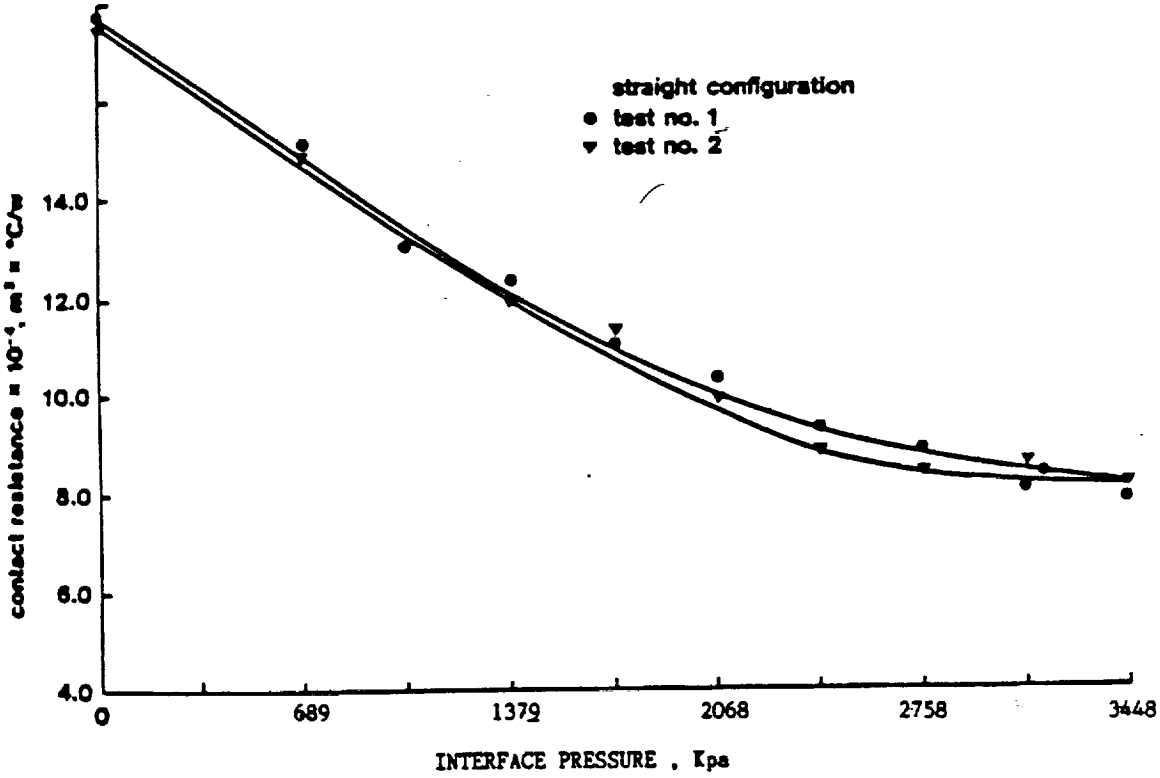

Figure 24 - Variation of Contact Resistance with Interface Pressure for straight configuration

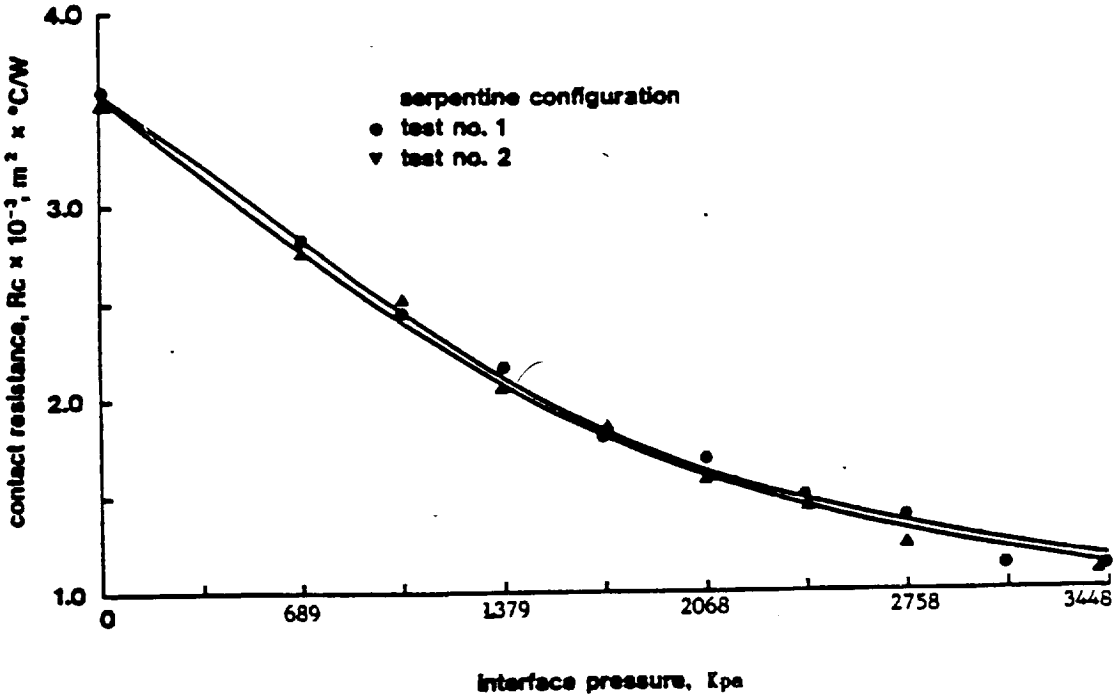

Figure 25 - Variation of Contact Resistance with Interface Pressure for serpentine configuration

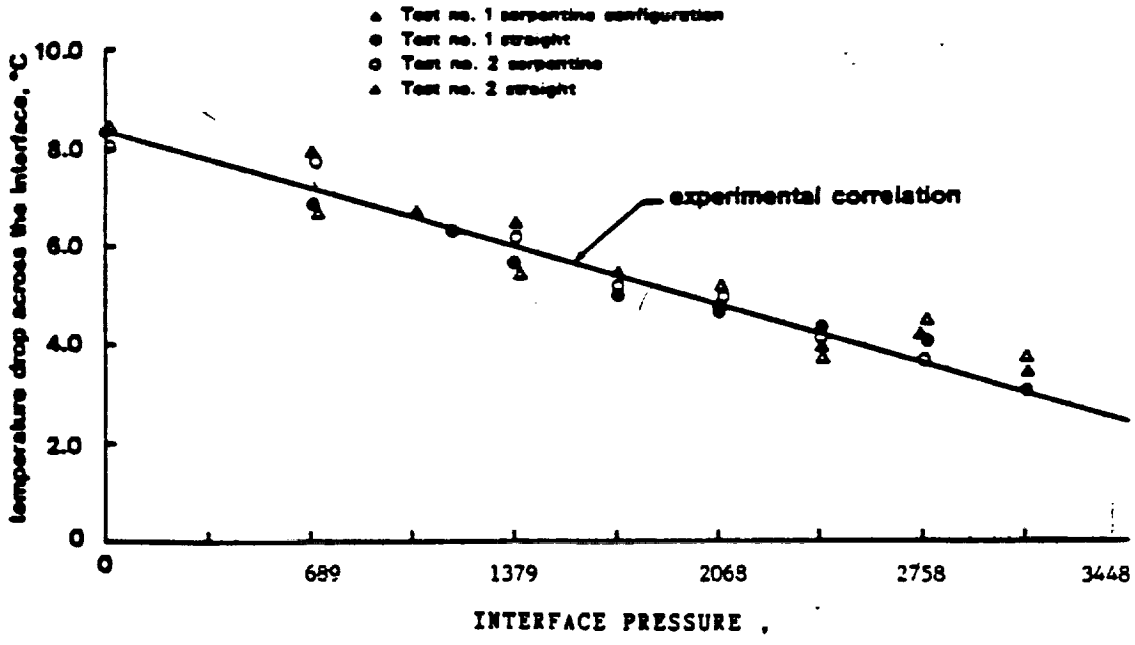

Figure 26- Effective Temperature Drop across the Interface versus Contact Pressure for serpentine and straight configurations

2- Serpentine Configuration

Thermal contact resistance in terms of the interface pressure was formulated for this configuration and it can be written as follows:

$$r_c = 0.00357\ e^{(-0.002356\ P)} \qquad (30)$$

During this course of analysis and testings all the measurements for the temperatures used for the evaluation of the thermal contact resistance were taken without any coolant flowing through the cooling system.

Also, experimental data for effective temperature drop for both serpentine and straight configurations were combined and plotted against interface pressure as shown in Figure 26 . The plot was then used to obtain the following correlation:

$$\Delta T = 7.986 - 0.9597 \times 10^{-2} p \qquad (31)$$

Results obtained from using the interval estimation technique (38) showed that these correlation equations have a confidence level of 95 percent.

5.6 Thermal Contact Resistance Measurements

Figure 27 shows the locations of thermocouples that have been used for collecting temperature measurements for the thermal contact resistance on the cell plate and the cooling plate.

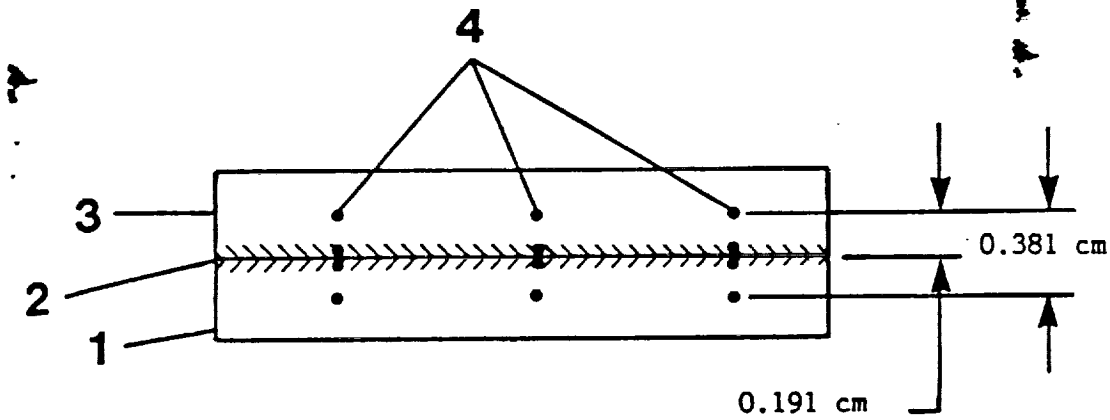

1 - Cooling Plate

2 - Interface

3 - Fuel-Cell Plate

4 - Thermocouples

Figure 27 -Locations of Thermocouples at the Interface.

Thermocouples located at positions shown in Figure 28 were used to measure the temperature in the fuel-cell plate during the test period and Figure 29 indicates the locations of thermocouples used in the cooling plate.

The determination of the temperature drop across the cell and the cooling plates interface was carried out by means of recording temperature measurements of thermocouples.

Three thermocouples were inserted through 5.1 cm deep holes positioned axially at 6.35cm from each other and 1.91 mm from the interface. This arrangement was done in both the cooling plate and the fuel cell plate.

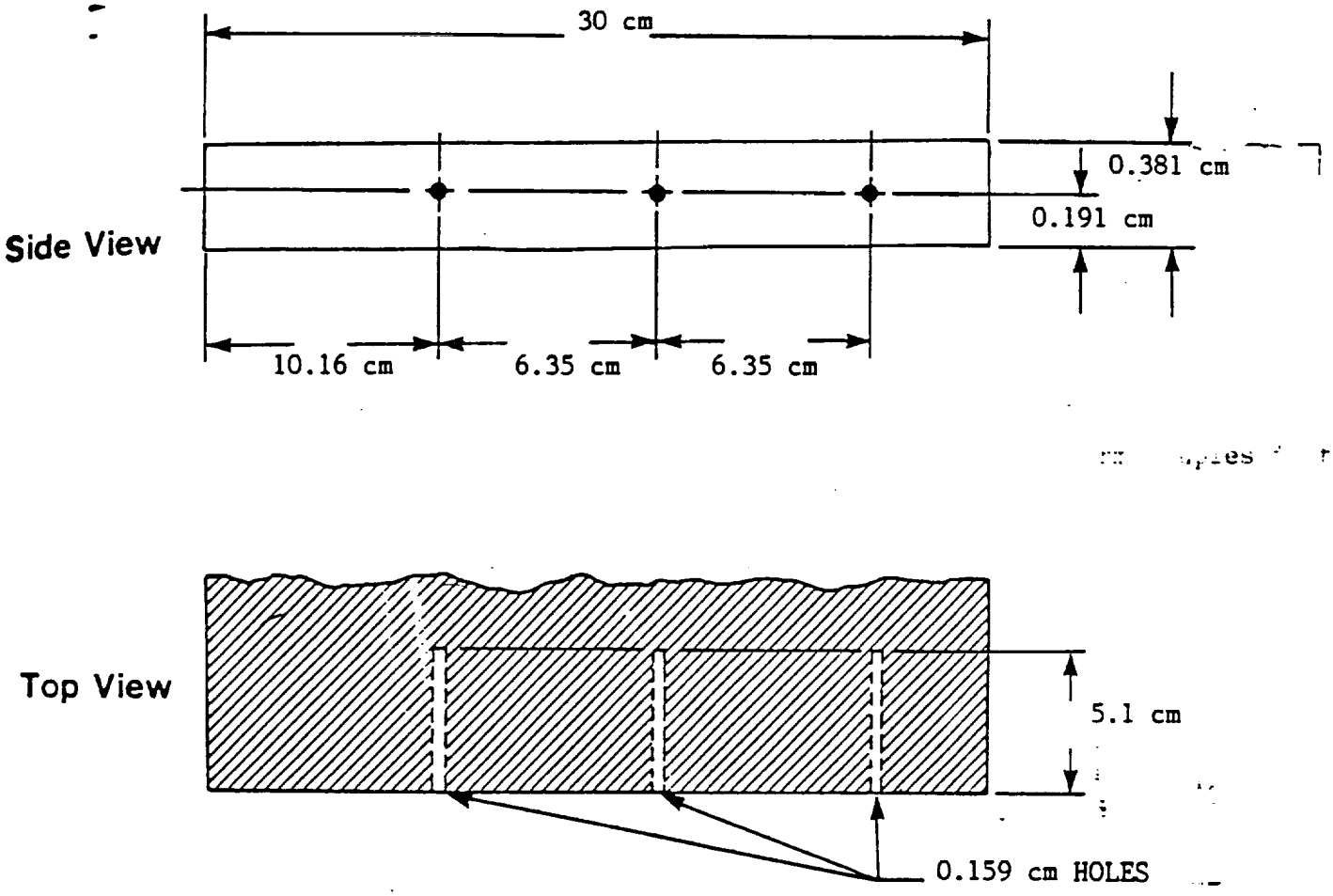

Figure 28 -Locations of Thermocouples in the Cell Plate

Also, six thermocouples were positioned along the interface in each plate as shown in Figure 27 . These thermocouples were accommodated in a shallow grooves so that good surface

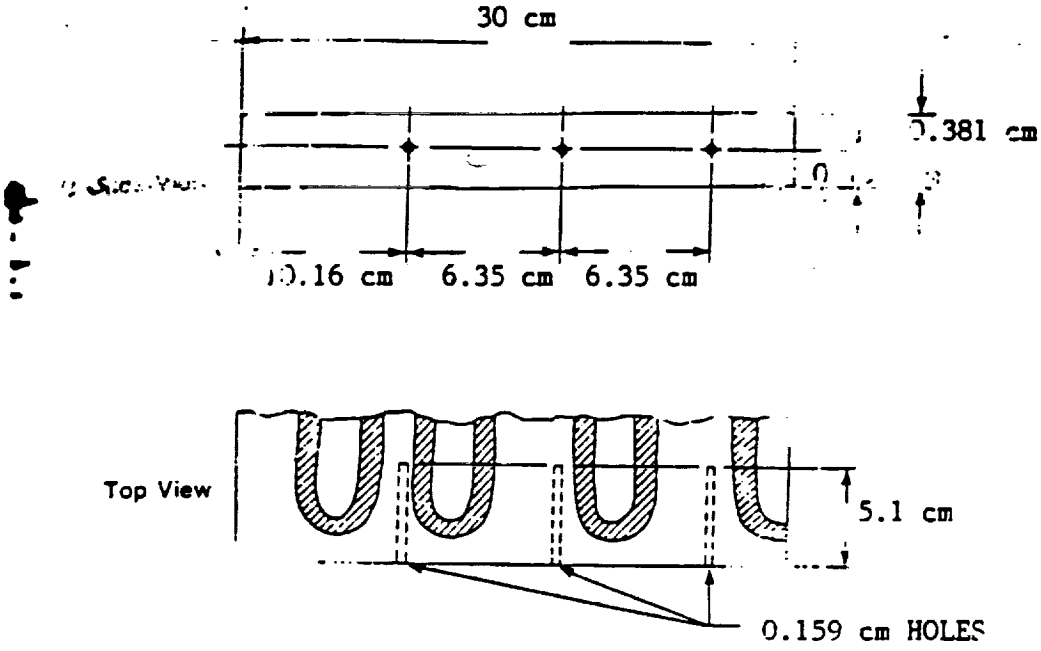

Figure [illegible] Locations of Thermocouples in the Cooling Plate

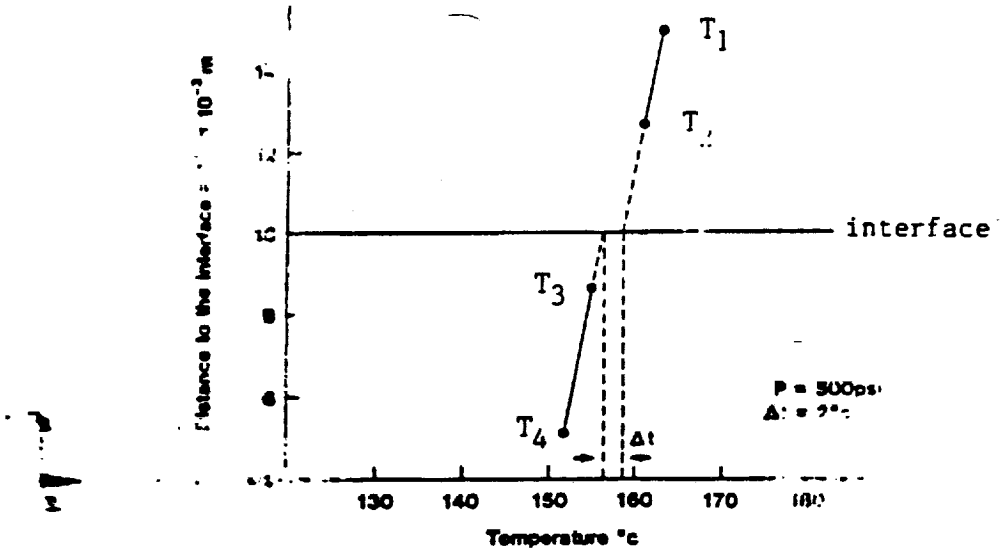

Figure 30 -Linear Extrapolation of Temperature Drop across the Fuel-Cell/Cooling Plate Interface.

contact between the two surfaces could be maintained. In order to ensure good contact between the cooling plate and the fuel-cell plate , graphite powder was injected to the contact area so as to minimize the existence of air initially contained in the unit. Application of pressure was implemented by the use of a hydraulic jack as shown in Figure 9 . The heat was determined from current and voltage measurements and the temperature drop across the interface was found by linear extrapolation as shown in Figure 30 . Thermal contact resistance was then evaluated by using Eq. (4)

5.7 Analysis of Experimental Results

In this section, an evaluation of the performance of the two types of cooling plates is presented. The variation of the overall heat transfer coefficient with the clamping pressure and Reynolds number for all three coolants is shown in Figures 34 through 37 . Also, Tables 1.1 to 3.5 (Appendix B) were used to plot Figures 31 through 33 for Nusselt number versus Reynolds number for oil, water and air and for straight and serpentine configurations.

1- The Nu-Re Relationship

The Nu-Re relationship for all coolants and the two types of cooling plates is shown in Figure 31 . The values of Nu varied from 4 to 8 for air, 1 to 3 for oil, and 0.4 to 0.6 for water (Appendix B). It can be noted that air has produced the highest Nusselt number in comparison to oil and water. This has been so because the straight configuration has a large heat transfer area and the

2- The U-Re Relationship

Tables 1.1 through 3.5 (Appendix B) were used to plot Figures 35 and 37 where the variation of the overall heat transfer coefficient with the clamping pressure and the Reynolds number (Re) is shown. It can be seen from Figure 35 that the overall heat transfer coefficient has increased as Reynolds number and the clamping pressure increased. This can be clearly seen in Figures 35 and 37 where P = 0 Kpa and P = 3448 Kpa . The values of the overall heat transfer coefficient for oil, water and air increased about 20 % when the clamping pressure varied from 0 to 3448 Kpa . Water produced higher overall heat transfer coefficient than oil and air. This was expected due to the nature of water for being a good coolant. Air at clamping pressure of 3448 Kpa gave higher value for the overall heat transfer coefficient than water at Reynolds numbers over 6000 .

5.8 Concluding Remarks

In this section an overall evaluation for all the experimental observations in relation to the cooling system and the two cooling plates used in this experiment is implemented.

In an attempt to evaluate each cooling plate configuration, it may be concluded that many factors should be considered in order to reach an optimum design for best cooling system. Such factors would be construction simplicity, reliability, type of coolant and cost. The straight channel configuration which includes the air

cooling is by far the simplest in construction. Besides, in real fuel cell application, it keeps the cathodic reactant air separate from the cooling system gas (air). This improves electrical performance due to higher oxygen concentration of the cathode as well as reducing the need for acid resistant heat exchangers in the cooling stream (48) .

The disadvantage of using the serpentine cooling system lies in its construction complexity and cost. It involves passing the liquid coolant through cooling plates inserted at regular intervals in the stack. The coolant may remain in the liquid phase at all times using only its sensible heat to cool the stack, or the coolant may partially vaporize using latent heat for part of the cooling load. The coolant must be either separately manifolded or supply lines must be connected to each individual cooling plate. Standard heat transfer materials, such as copper, are corroded by phosphoric acid and must be protected if it is to be used. Finally, the liquid itself and coolant lines, if electrically conductive, provide a possible shorting path in the cell (Shunt currents which result in parasitic losses) which must be minimized.

However, in air cooling most air leaks could be ignored, but a leak in the stack liquid cooling system could cause a shutdown while the leak was repaired or the defective cooling plate replaced.

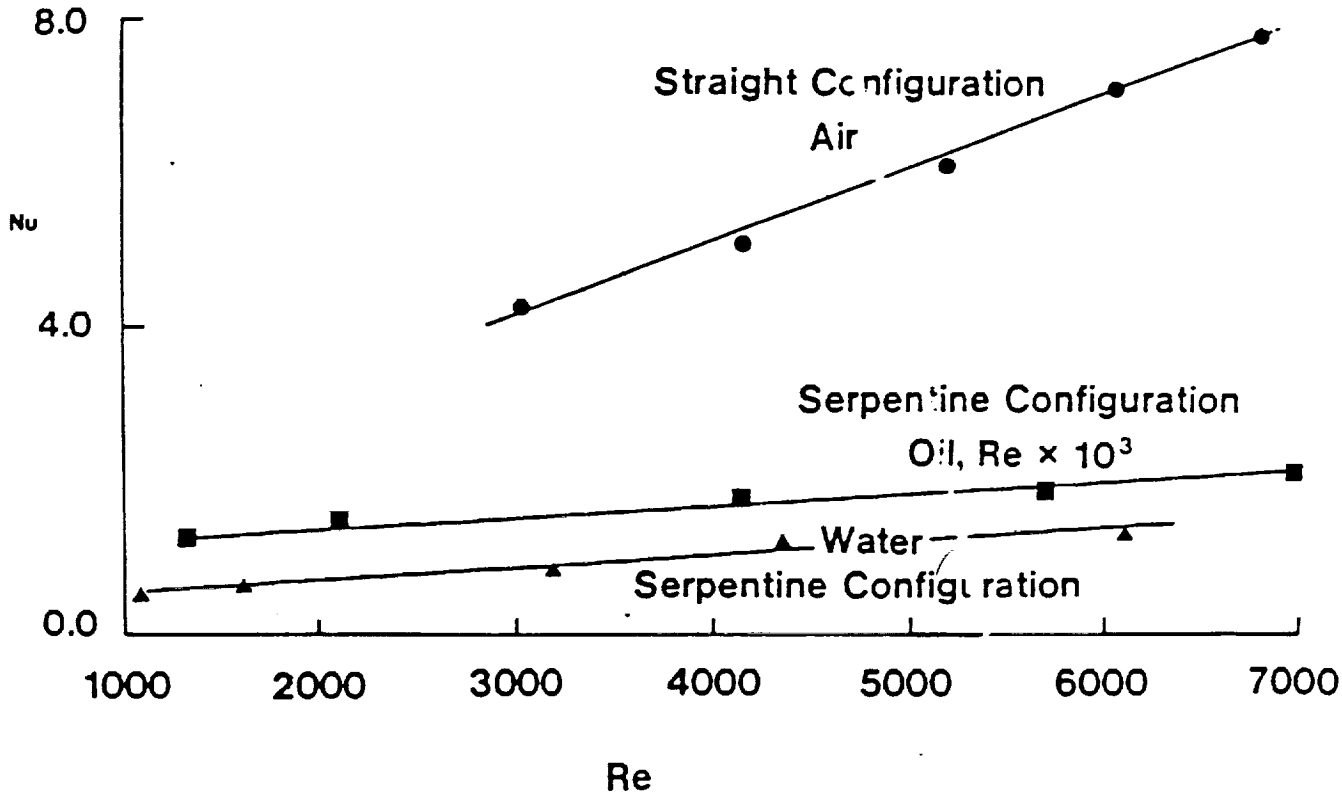

Figure 31 -Nusselt Number versus Reynolds Number for Straight and Serpentine Configurations with Air, Oil and Water as Coolants.

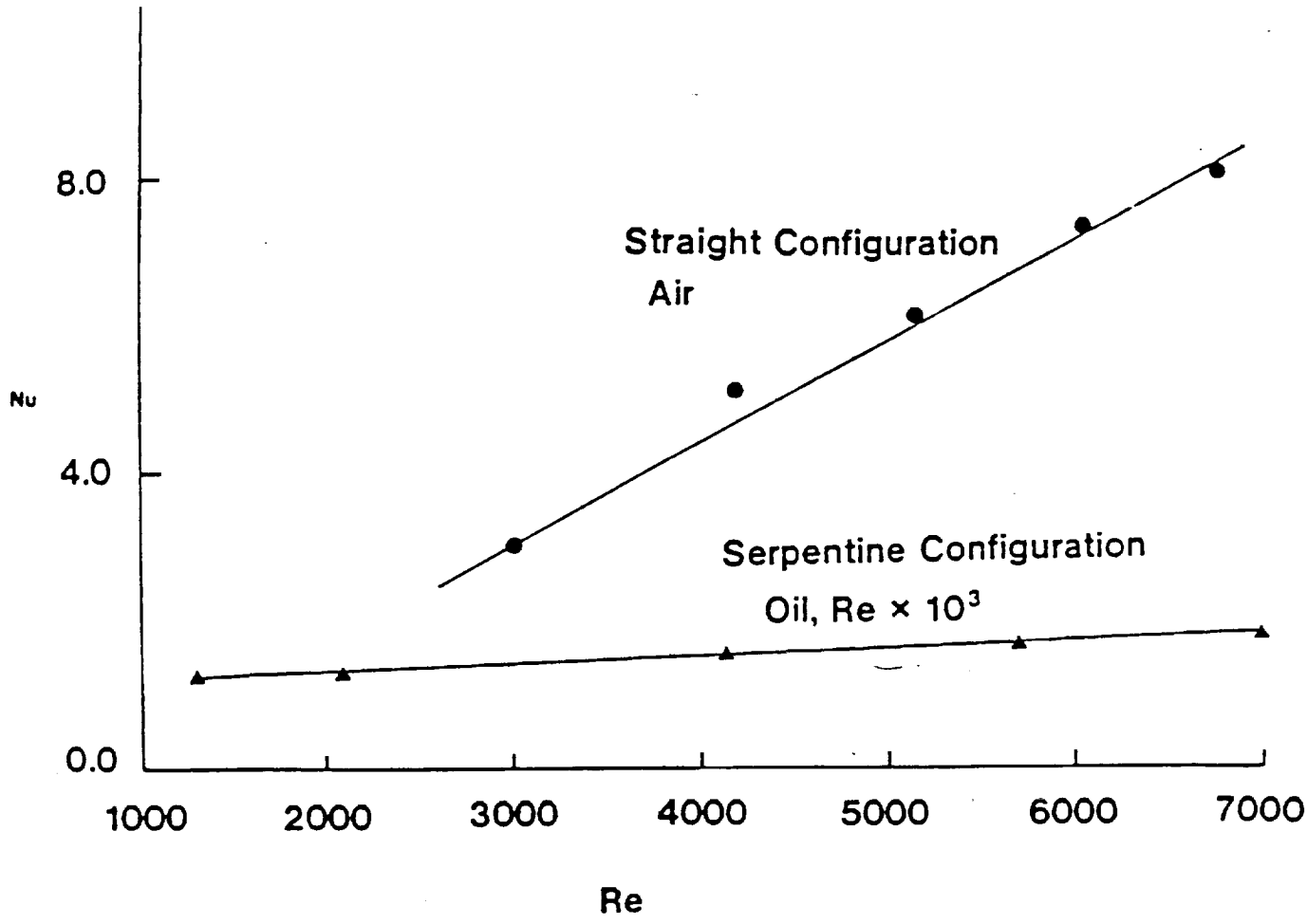

Figure 32 -Nusselt Number versus Reynolds Number for Straight and Serpentine Configurations with Air and Oil as Coolants.

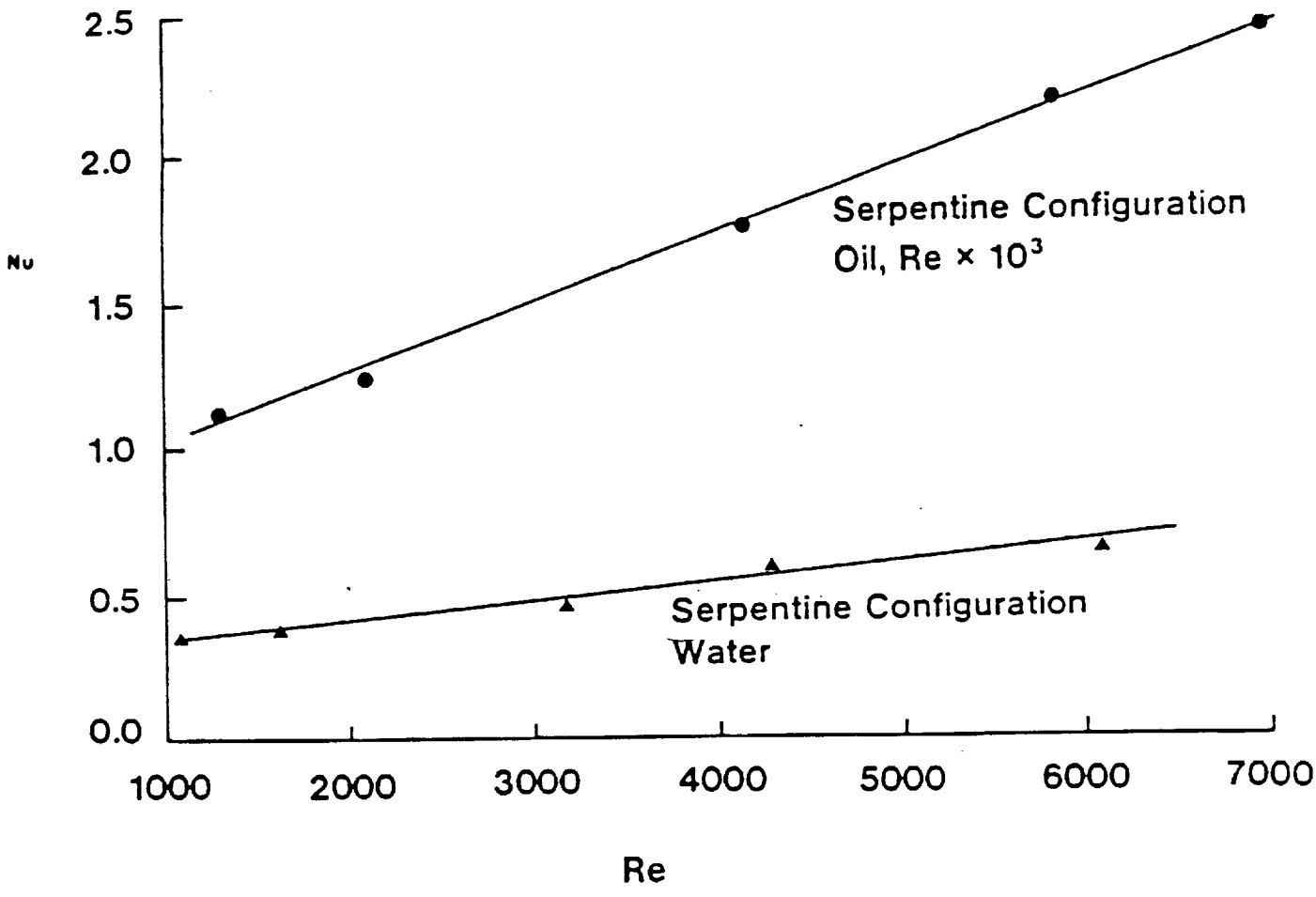

Figure 33 -Nusselt Number versus Reynolds Number for Serpentine Configuration with Oil and Water as Coolants.

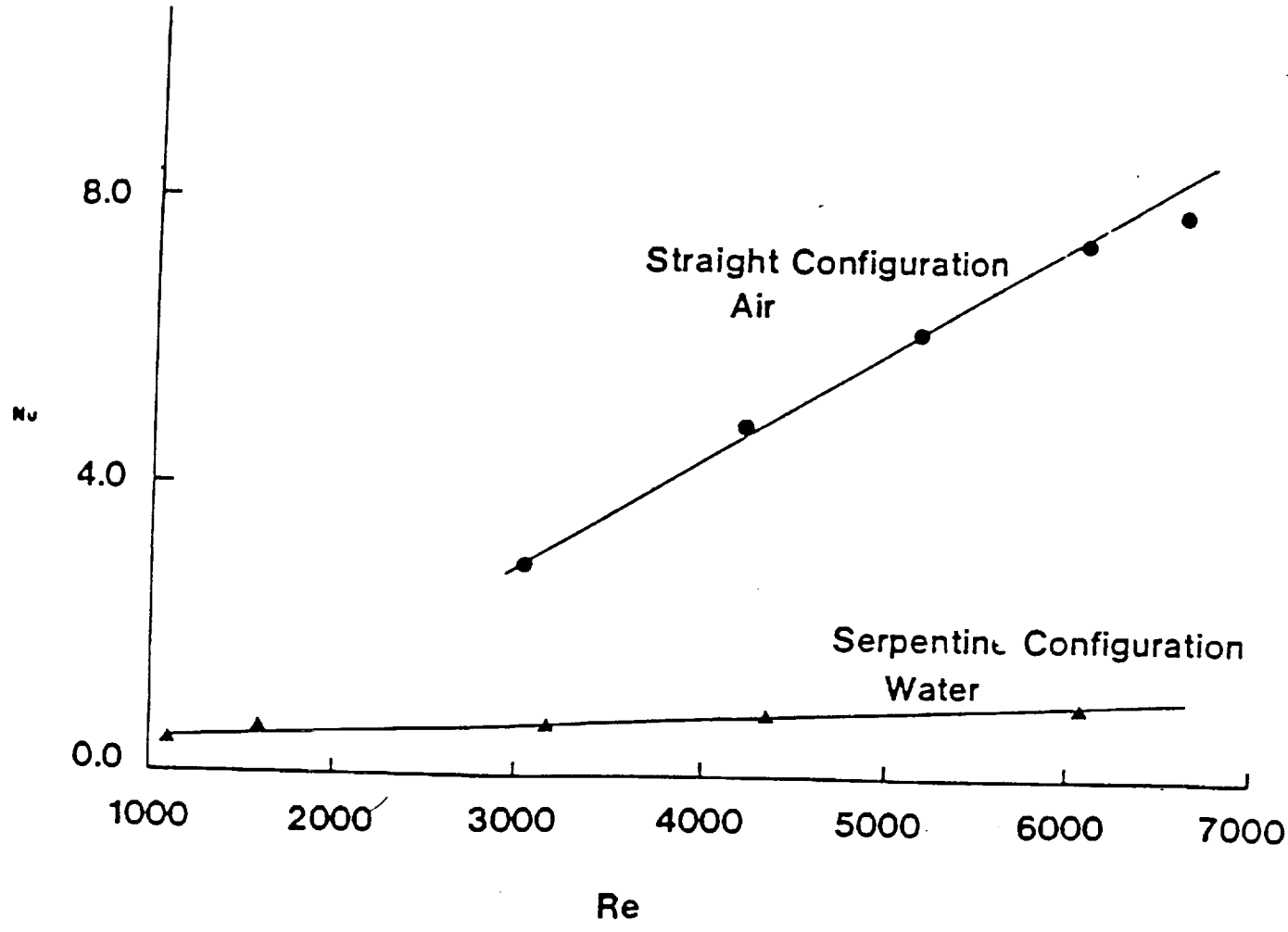

Figure 34 -Nusselt Number versus Reynolds Number for Straight and Serpentine Configurations with Air and Water as Coolants.

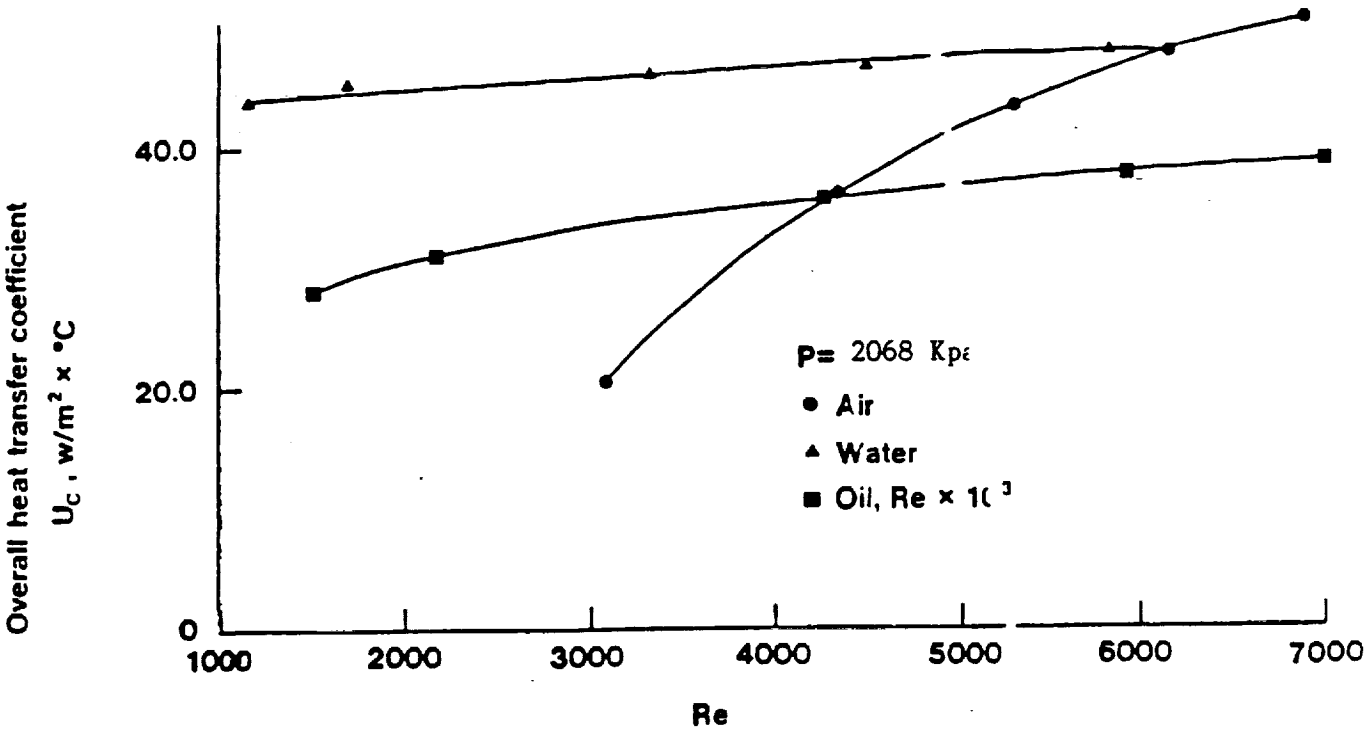

Figure 36 -Overall Heat Transfer Coefficient versus Reynolds Number for Serpentine and Straight Configurations with P = 2068 Kpa

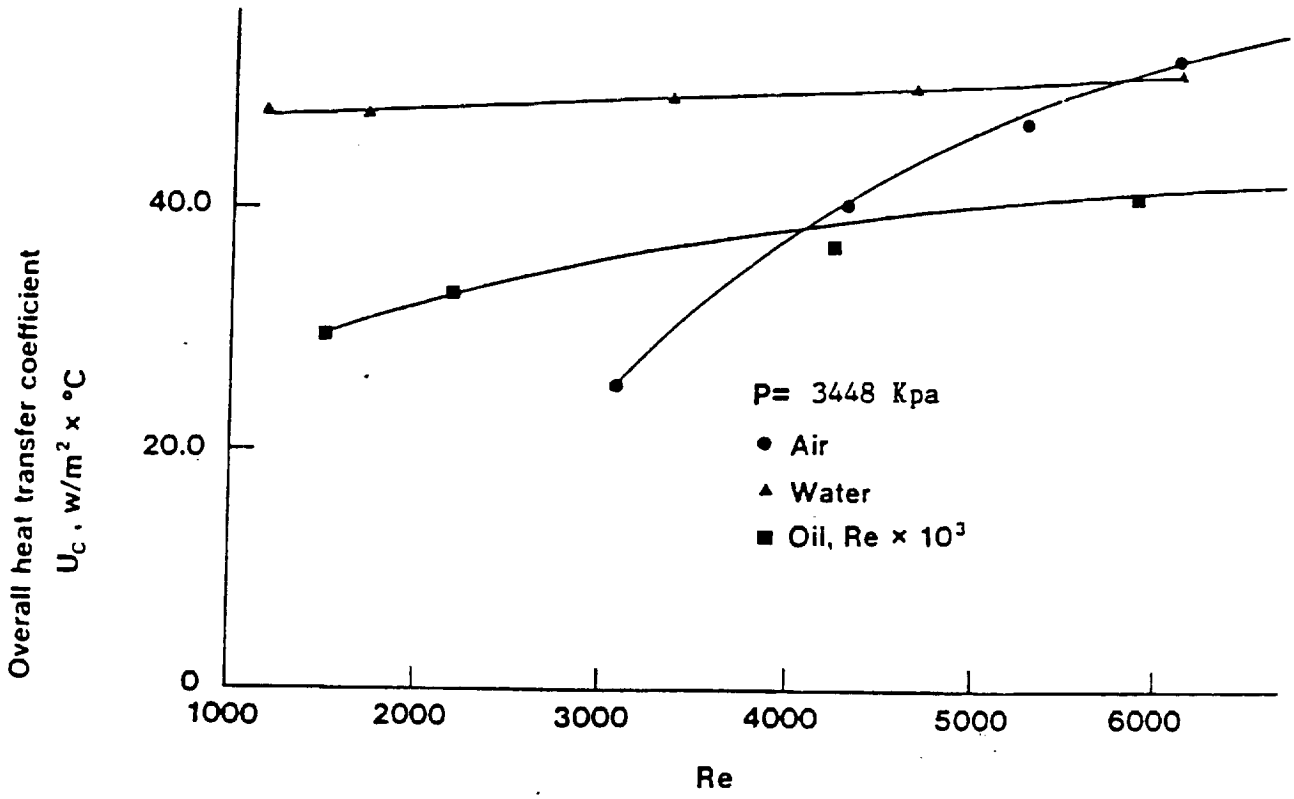

Figure 37 -Overall Heat Transfer Coefficient versus Reynolds Number for Serpentine and Straight Configurations with P = 3448 Kpa.

CHAPTER VI

EFFECTS OF HEAT TRANSFER COEFFICIENT ON ELECTRODE TEMPERATURE DISTRIBUTION AND OTHER STACK PARAMETERS

The quantity of electrical energy produced in phosphoric acid fuel cells is accompanied by approximately equal amounts of generated heat energy. Removal of this excess heat energy is accomplished by the flow of reactant gases and the system of cooling plates.

The fuel cell heat generation is not evenly distributed across the cell plate because of depletion of reactant gases. This results in non-uniform temperature distributions. The experimental heating elements do not provide exact simulation of fuel cell heat generation, but they do load the forward edge of the plate at the coolant entrance.

The work reported in this chapter is directed towards comparing the steady state temperature profiles for the experimental simulation of the fuel cell with the results obtained by Alkasab and Lu (6) in their computer simulation model. Also, effects of other parameters such as stack

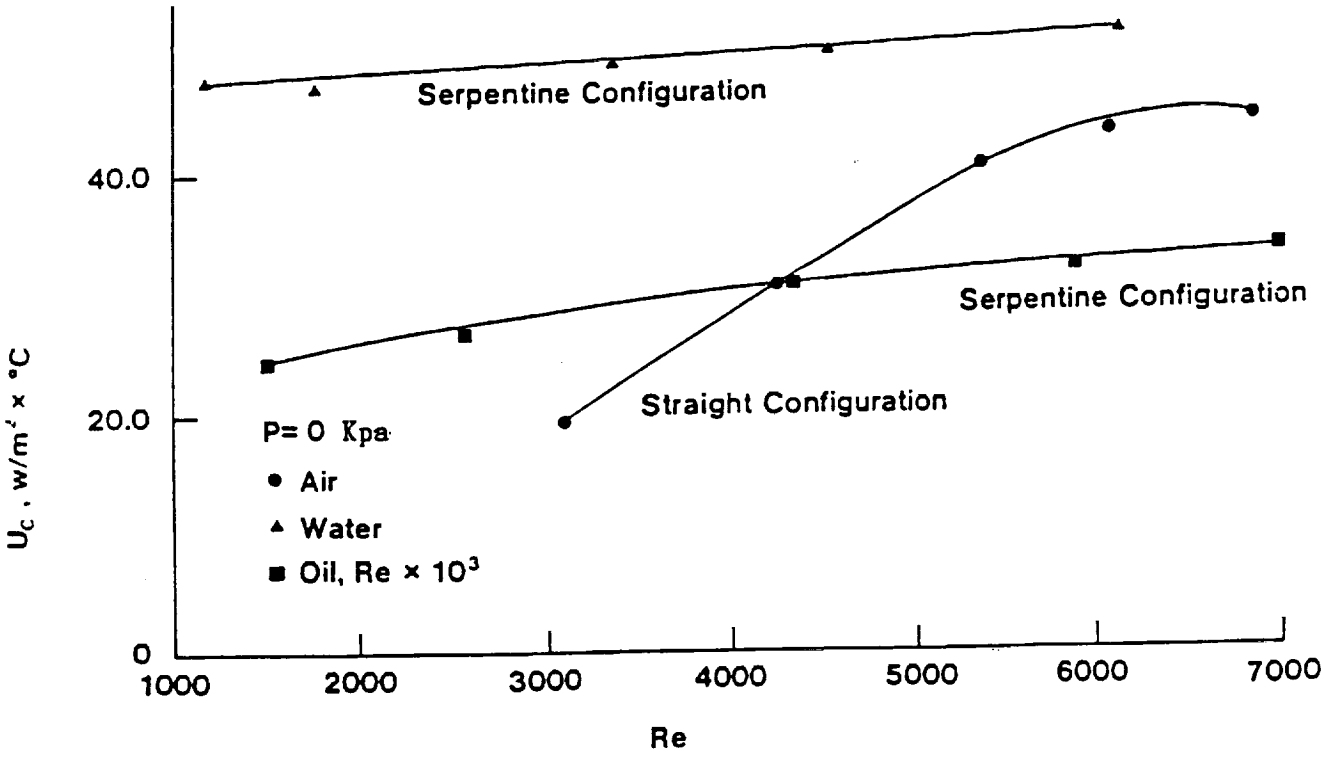

Figure 35 -Overall Heat Transfer Coefficient versus Reynolds Number for Serpentine and Straight Configurations with P = 0 Kpa.

pressures and coolant flow rates with air, water and oil. A mathematical correlation was developed to relate the average fuel-cell plate temperature with the air cooling flow rate and the stack clamping pressure. This correlation is represented by the following equation.

$$\frac{T_{av}}{T_{max}} = 0.8916 - 0.0926 \frac{P \cdot m}{P_{max} \cdot m_{max}} \qquad (32)$$

where,

T_{av} = Average cell Temperature °C

T_{max} = 190 °C

P_{max} = 500 psi

P_{min} = 0 psi

m_{max} = 46.62 Kg/hr

m_{min} = 0 Kg/hr

Figure 38 shows the variation of the fuel cell plate average temperature as function of the above parameters.

6.2 Effects of Cooling System Parameters on the Temperature Distribution

The temperature contour lines are very sensitive to many parameters such as the heating rate, coolant flow rate, stack clamping pressure and geometry of the cooling plate.

Figures 39 and 40 show the effect of flow rate on temperature distribution when a serpentine cooling plate is used. Temperature measurements for the surface of the

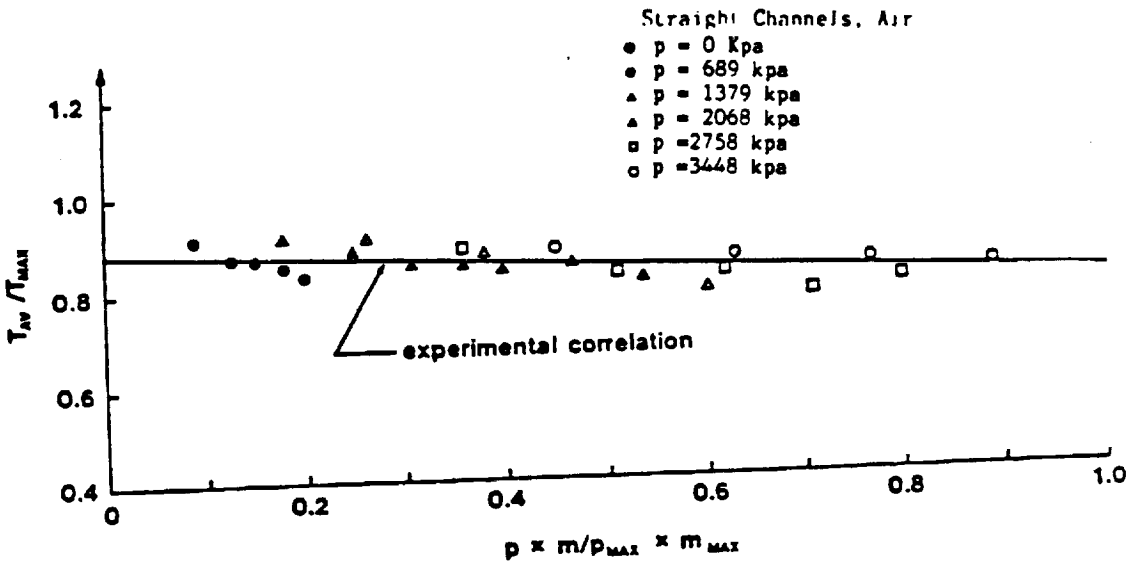

Figure 38 -Variation of Average Fuel Cell Temperature with Coolant Flow Rate and Interface Pressure for Straight Configuration with Air as Coolant.

C-2

clamping pressure and coolant flow rate on the temperature distributions as well as the variations of the operating fuel cell temperature and system efficiency with the stack clamping pressure are discussed.

6.1 Temperature Distributions

In actual operation, the heat dissipation across the fuel cell plate is of asymmetrical type. Since only one curved boundary (the fuel cell plate) transfers energy to the flow. The experimental module was built in a manner where a real simulation of the actual operation was implemented.

The temperature variations are an indication of the local heat generation rate where these are changed by the coolant flow rate. The temperature distribution for the fuel cell module was obtained by measuring the temperatures at seventy-two locations on the surface of the fuel-cell plate. Isotherms defining the temperature distribution across the surface of the fuel cell plate were drawn for various test cases including all three of the coolants used in this investigation. The average fuel cell temperature was calculated by obtaining the mathematical average of the temperature for all of the isotherms.

These temperature profiles were a function of stack clamping pressure as well as the coolant flow rate. The clamping pressure showed to have a significant effects on the temperature distributions.

Figures 69 through 74 (Appendix A) show the variations in the shapes of the isotherms for various stack clamping

See page 79 to find Page (83)

cell plate were taken as mentioned in the previous section at seventy-two locations and from these measurements a set of isotherms was generated for all coolants used in this experiment under various conditions and stack clamping pressures.

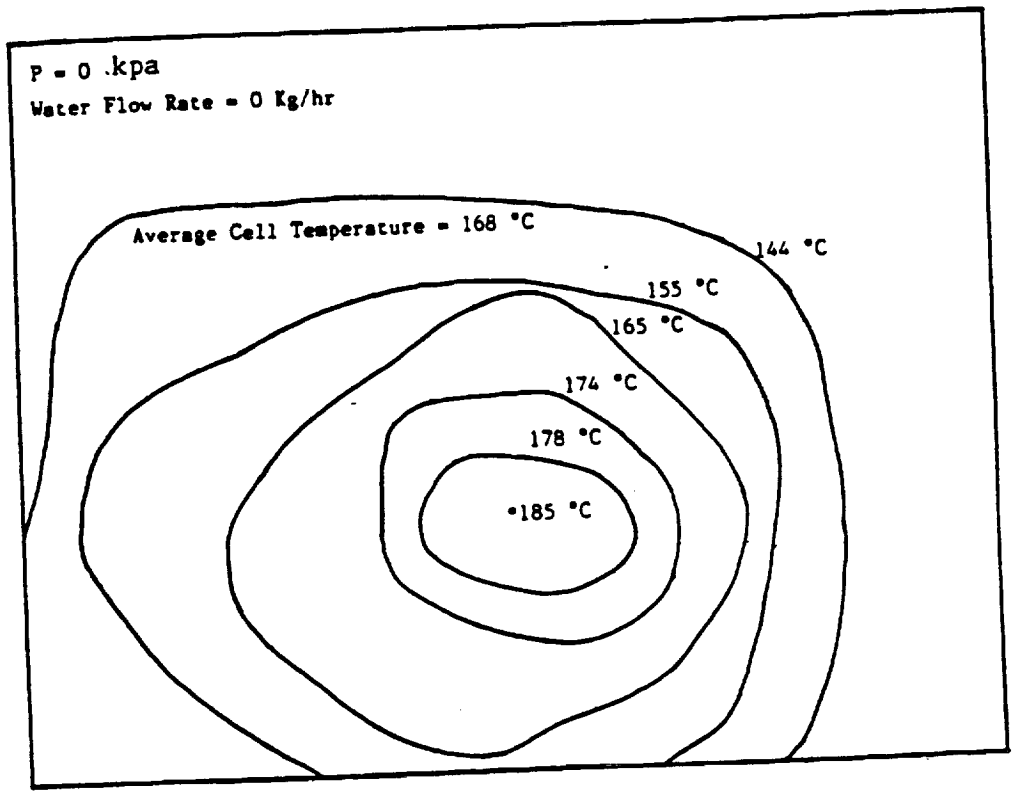

Figure 39 -Effects of Coolant Flow Rate and Stack Clamping Pressure on the Temperature Distributions (Serpentine, Water Cooling)

It can be noted from Figures 39 and 40 that the highest temperature on the cell plate was always close to the center because of the heating elements distributions in the cell plate and it was decreasing in the direction of the cooling flow. Also, the effects of the clamping pressure on the temperature distribution is clearly noticed. For example, in considering Figure 39 , where serpentine cooling plate is used and there is zero clamping pressure and zero coolant flow rate, the temperature at the center is 185 °C . While at the maximum clamping pressure of 500 psi and zero flow rate the temperature rose to 190 °C resulting in a 5 °C increase as shown in Figure 40 .

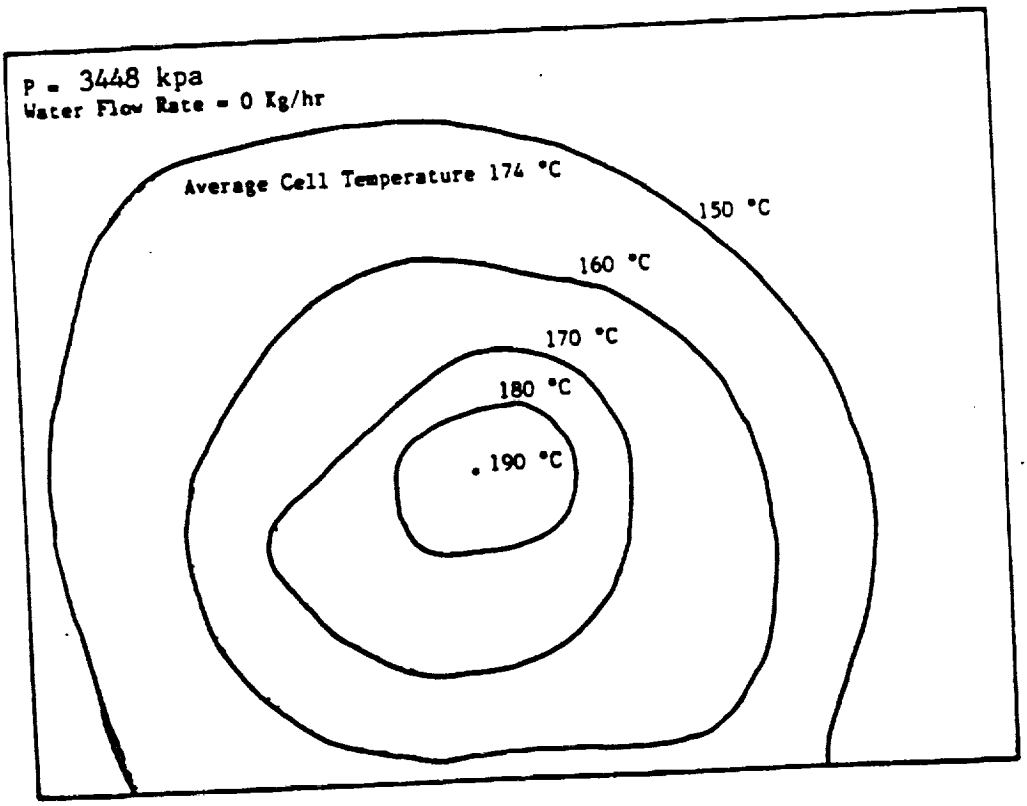

Figure 40 - Effects of Coolant Flow Rate and Stack Clamping Pressure on the Temperature Distributions (Serpentine, Water Cooling)

Obviously, the increase of temperature is due to the influence of the clamping pressure on the system which resulted in producing a better contact between the cell plate and the cooling plate. Consequently, this resulted in a better temperature uniformity and a smaller temperature differential in the water cooling flow direction. Also, the average cell temperature increased from 168 °C to 174 °C which is within 2 percent of the average cell temperature obtained by Westinghouse measured data .

Similar variations of the temperature distributions under the influence of stack clamping pressure and coolant mass flow rate have been also observed for oil and air. It can be noticed from Figures 41 and 42 that, when the stack clamping pressure increased from zero psi to 500 psi under the same coolant flow rate, the average cell plate temperature increased by 2 °C. Also, as the coolant flow rate increased, the temperature decreased by 15 °C at a flow rate of 88.20 Kg/hr.

Another important result is that the contour lines of temperature corresponded to break closer to each other under the effect of higher stack clamping pressure.

It may be concluded that most of the heat generated is removed through the cooling plate. But from a cost view point, the greater the flow rate of coolant the greater the auxiliary power needed to recycle the coolant and the more coolant that is used, the lower the mean temperature will be, but the greater the temperature difference between plates will be in stack cooling situations. Lower peak

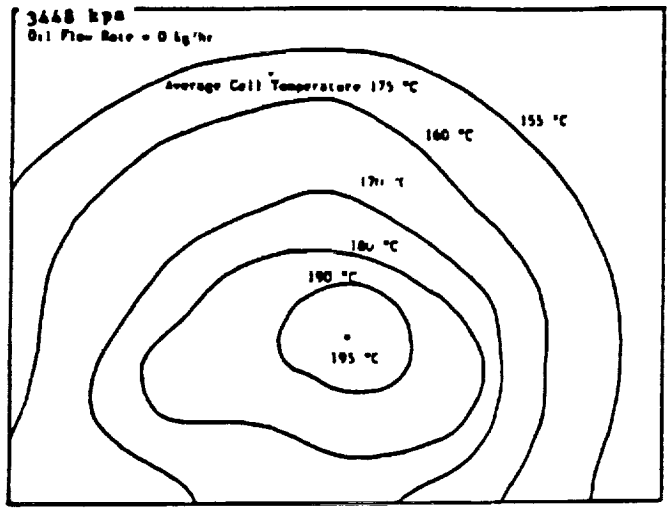

Figure 41 -Effects of Coolant Flow Rate and Stack Clamping Pressure on the Temperature Distributions. (Serpentine, Oil Cooling)

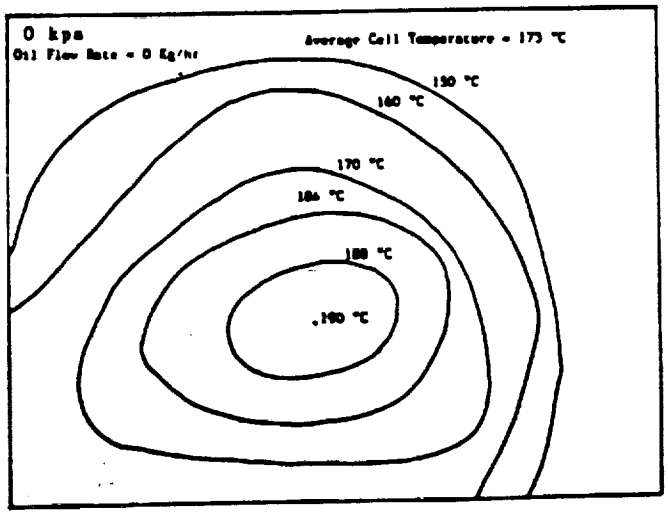

Figure 42-Effects of Coolant Flow Rate and Stack Clamping Pressure on the Temperature Distributions. (Serpentine, Oil Cooling)

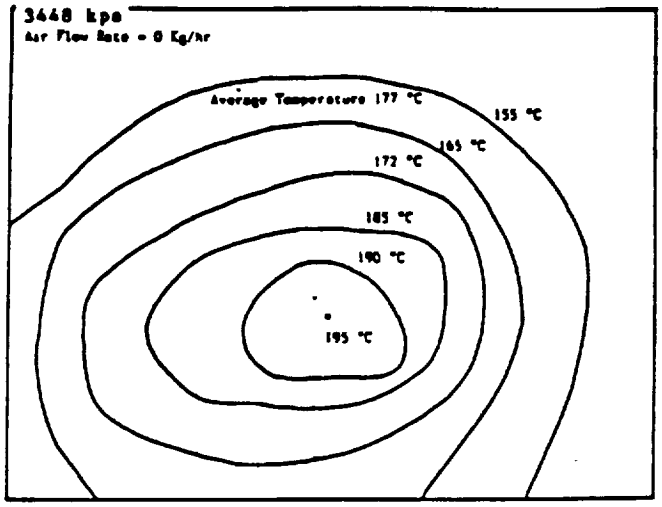

Figure 43 Effects of Coolant Flow Rate and Stack Clamping Pressure on the Temperature Distributions. (Straight, Air Cooling)

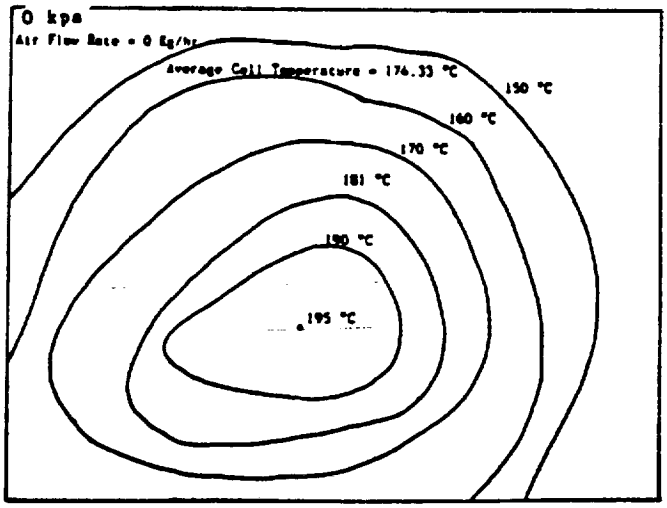

Figure 44 -Effects of Coolant Flow Rate and Stack Clamping Pressure on the Temperature Distributions. (Straight, Air Cooling)

temperature means a more uniform temperature distribution and lower average temperature means that less auxiliary power will be required to pump the coolant.

6.3 Thermal Analysis

The energy balance equations for the fuel cell plate, cooling plate, process air and coolant were developed by Alkasab and Lu (6). In their analysis, they considered a phosphoric-acid fuel cell stack similar to that shown in Figure 45 . In such a stack, it was assumed that the number of fuel cell modules contained between each pair of cooling plates to be five, and the repeating stack components to consist of a half cooling plate and two and a half fuel cell modules.

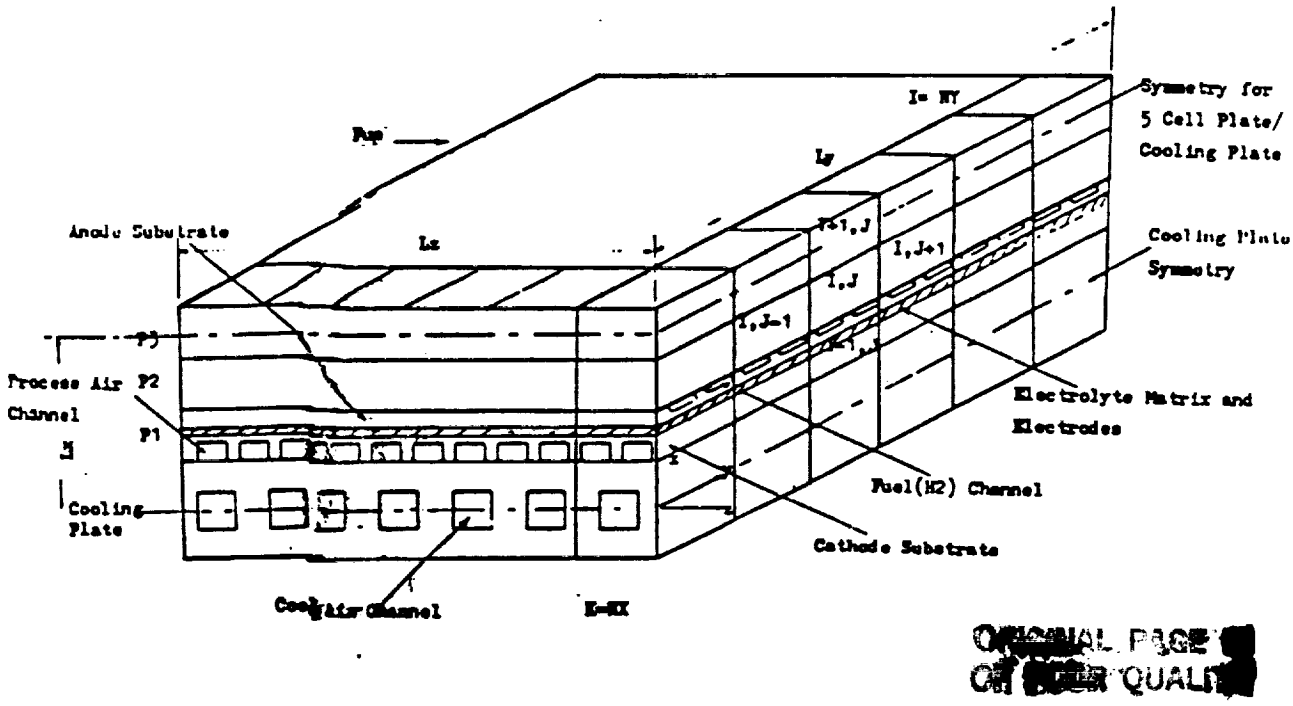

Figure 45 Geometry of a Strip of Element for the Thermal Analysis Model

The mathematical model developed by reference (6) includes four energy balance equations for the fuel cell plate, cooling plate, process air, and coolant are as follow.

Fuel cell on process air side in air flow direction

$$t\ Ky\ \frac{\delta^2 T}{\delta y^2} + Kx\ \frac{\delta T}{\delta x}\bigg|_{x+t} - Kx\ \frac{\delta T}{\delta x}\bigg|_{x} - \frac{Cp\,mp}{\rho_p}\ \frac{\delta T_p}{\delta y} + (V^* - V)I = 0 \qquad (33)$$

Cooling plate in coolant direction

$$t'Ky\ \frac{\delta^2 T}{\delta y^2} + 2\ Kx\ \frac{\delta T}{\delta x}\bigg|_{\frac{x+t'}{2}} - \frac{C_c m_c}{\rho_c}\ \frac{\delta T_c}{\delta y} = 0 \qquad (34)$$

Process air side

$$\frac{dT_p}{dy} = \frac{hp\ S}{mp\ C_p}\ (T - T_p) \qquad (35)$$

Coolant side

$$\frac{dT_c}{dy} = \frac{hc\ Sc}{mc\ C_c}\ (T - T_c) \qquad (36)$$

Boundary conditions

$x = 0$	$\delta T/\delta x = 0$	symmetric condition
$y = 0$	$\delta T/\delta y = 0$	adiabatic assumption
$x = Lx$	$\delta T/\delta x = 0$	symmetric condition

$y = Ly$ $\quad \delta T/\delta y = 0$ adiabatic assumption

$y = 0$ $\quad T_p = T_p$, inlet

$y = 0$ $\quad T_c = T_c$, inlet

where m = mass flow rate, Kg/hr-channel

C = heat capacity, J/Kg-K

K_y = effective thermal conductivity of cell in flow direction, J/hr-m-K

K_x = effective thermal conductivity of cell in stacking direction, J/hr-m-K

t = thickness of cell including fuel and air channel, m

x1 = effective conduction distance from plate to upper cell plate, m

x2 = effective conduction distance from plate to lower cell plate, m

p = pitch of channel, m

x1' = effective conduction distance from cooling plate to upper cell plate, m

Lx, Ly = height and length of one slice, respectively, m

V* = H/ZF , V

t' = thickness of cooling plate, m

h = heat transfer coefficient, J/hr-m^2-K

S = perimeter of the channel, m

Subscription

p = process air

c = coolant

These simultaneous ordinary differential equations and the corresponding boundary conditions were solved by the finite-difference method.

6.4 Relation of Experimental Results-Computer Model

The mathematical model of fuel cells that was described in the previous subsection, was developed into a computer program by reference (6) to facilitate performing the necessary calculations.

This computer program was used in predicting the distribution of the temperature profiles in the fuel-cell stack. Experimental correlations developed,by the present investigation, and the overall heat transfer coefficient were incorporated into the computer program of reference (6). The modified program was then utilized to predict the temperature distribution in the fuel cell stack, and the results were compared with those obtained by reference (6).

In considering the overall analysis for the cooling system, reference (6) considered the cooling factor to be a function of the heat transfer characteristics, plate size, and stack construction. The latter is primarily to specify the number of power plates between a pair of cooling plates. The heat transfer characteristics is a function of the type of coolant (gas or liquid), cooling plate design, and the thermal conductivities of the plate material. In comparing the current experimental results with those available in the literature and reference (6), only the straight channel and the serpentine configurations were considered.

The developed computer model was modified to meet the

cooling configurations used in this experiment. Also, factors such as thermal conductivities of plate material, plate size, and current densities were kept constant throughout the analysis. However, coolant mass flow rate, inlet and outlet temperature of the coolant, thermophysical properties and dimensions of the cooling channel were supplied to the program as input data.

The program was run on the IBM 370 in NASA Lewis Research Center. The temperature of each grid on the cell plate, from outer-most plate to central plate was obtained. Also the average operating temperature, the operating pressure, and the DC output voltage for the specified stack were calculated. A difference between the results generated using the reference (6) data and the current experimental data is apparent. The difference is in the range of 5 to 11 percent.

6.5 Comparison of Experimental Results

In this section, examination of the results obtained by the computer analysis describing major effects on the steady state temperature distribution and other aspects in relation to the effects of coolant and stack clamping pressure on the variations of temperature are presented.

The computer outputs representing the temperature distribution on the fuel cell plate under the influence of the above parameters may be discussed as follows, these are representative outputs from:

a) Water Cooling

Figure 46 and 47 show the numeric distribution of the

```
TEMPERATURE(C)

 210. 210. 209. 209. 208. 208. 207. 206. 205. 204. 202. 200.
 209. 209. 208. 208. 207. 207. 206. 205. 204. 203. 201. 199.
 207. 207. 207. 206. 206. 205. 204. 203. 202. 201. 200. 198.
 205. 204. 204. 203. 203. 202. 202. 201. 200. 199. 197. 195.
 202. 201. 201. 200. 200. 199. 199. 198. 197. 196. 195. 193.
 198. 198. 197. 197. 197. 196. 195. 195. 194. 193. 192. 190.
 195. 194. 194. 193. 193. 193. 192. 191. 191. 190. 188. 187.
 191. 191. 190. 190. 190. 189. 189. 188. 187. 186. 185. 184.
 188. 187. 187. 187. 186. 186. 185. 185. 184. 183. 183. 181.
 184. 184. 184. 184. 183. 183. 183. 182. 182. 181. 180. 179.
 182. 182. 182. 181. 181. 181. 180. 180. 179. 179. 178. 177.
 180. 180. 180. 180. 179. 179. 179. 178. 178. 177. 177. 176.

 THE AVERAGE OPERATING TEMPERATURE IS  0.46404E 03 K
THE OPERATING PRESSURE IS 1.0  ATM
THE FULL DC POWER OUTLET IS  0.57120E 01 KW-DC
 TERMINATED: STOP
```

Figure 46 –Computer Output for Temperature Distributions Generated by Experimental Data (Water Flow Rate = 47.50 Kg/hr , Current Density 0.325 am/cm^2 , Stack Clamping Pressure = 0 Kpa)

```
TEMPERATURE(C)

 196. 195. 195. 195. 195. 194. 194. 193. 192. 192. 190. 189.
 194. 194. 193. 193. 193. 192. 192. 191. 191. 190. 189. 187.
 191. 190. 190. 190. 190. 189. 189. 188. 188. 187. 186. 185.
 187. 187. 186. 186. 186. 186. 185. 185. 184. 184. 183. 182.
 182. 182. 182. 182. 182. 181. 181. 181. 180. 180. 179. 178.
 178. 178. 177. 177. 177. 177. 177. 176. 176. 175. 175. 174.
 173. 173. 173. 173. 173. 172. 172. 172. 172. 171. 171. 170.
 169. 169. 169. 169. 168. 168. 168. 168. 168. 167. 167. 167.
 165. 165. 165. 165. 165. 164. 164. 164. 164. 164. 163. 163.
 162. 162. 162. 161. 161. 161. 161. 161. 161. 161. 160. 160.
 159. 159. 159. 159. 159. 159. 159. 159. 159. 159. 158. 158.
 159. 159. 159. 158. 158. 158. 158. 158. 158. 158. 158. 158.
1 THE AVERAGE OPERATING TEMPERATURE IS  0.44563E 03 K
 THE OPERATING PRESSURE IS 1.0  ATM
 THE FULL DC POWER OUTLET IS  0.52976E 01 KW-DC
```

Figure 47 –Computer Output for Temperature Distributions Generated by Experimental Data (Water Flow Rate = 47.50 Kg/hr , Current Density 0.325 am/cm^2 , Stack Clamping Pressure = 3448 Kpa

temperature in each finite difference on the cell plate at the final steady state under the influence of the stack clamping pressure.

Figures 46 and 47 were generated by the experimentally

developed heat transfer coefficients with water cooling and at zero and 3448 Kpa stack clamping pressures. The effects of the stack clamping pressure is clearly noticed since the average fuel cell plate temperature decreased from 193 °C to 176 °C when the stack clamping pressure increased from zero to 3448 Kpa.

```
TEMPERATURE(C)

 212. 212. 211. 211. 210. 209. 209. 208. 207. 205. 204. 202.
 211. 211. 210. 210. 209. 208. 208. 207. 206. 204. 203. 201.
 209. 209. 208. 208. 207. 207. 206. 205. 204. 203. 201. 199.
 207. 206. 206. 205. 205. 204. 204. 203. 202. 200. 199. 197.
 204. 203. 203. 202. 202. 201. 201. 200. 199. 198. 196. 194.
 200. 200. 200. 199. 199. 198. 197. 197. 196. 195. 193. 192.
 197. 197. 196. 196. 195. 195. 194. 193. 193. 192. 190. 189.
 193. 193. 193. 192. 192. 191. 191. 190. 189. 188. 187. 186.
 190. 190. 189. 189. 189. 188. 188. 187. 186. 186. 185. 183.
 187. 187. 187. 186. 186. 185. 185. 184. 184. 183. 182. 181.
 185. 184. 184. 184. 183. 183. 183. 182. 182. 181. 180. 179.
 183. 182. 182. 182. 182. 181. 181. 181. 180. 179. 179. 178.
 THE AVERAGE OPERATING TEMPERATURE IS  0.46608E 03 K
 THE OPERATING PRESSURE IS  1.0  ATM
 THE FULL DC POWER OUTLET IS  0.57493E 01 KW-DC
```

Figure 48 -Computer Output for Temperature Distributions Generated by Experimental Data (Water Flow Rate = 47.50 Kg/hr , Current Density 0.325 am/cm^2 , Stack Clamping Pressure = 3448 Kpa)

```
TEMPERATURE(C)

 222. 221. 221. 220. 219. 218. 217. 216. 215. 213. 211. 209.
 221. 220. 220. 219. 218. 218. 217. 216. 214. 213. 211. 208.
 219. 219. 218. 218. 217. 216. 215. 214. 213. 211. 209. 207.
 217. 217. 216. 215. 215. 214. 213. 212. 211. 209. 207. 205.
 214. 214. 213. 213. 212. 211. 210. 209. 208. 206. 205. 202.
 211. 211. 210. 209. 209. 208. 207. 206. 205. 203. 202. 200.
 207. 207. 206. 206. 205. 205. 204. 203. 202. 200. 199. 197.
 204. 203. 203. 202. 202. 201. 200. 199. 198. 197. 195. 194.
 200. 199. 199. 199. 198. 197. 197. 196. 195. 194. 192. 191.
 196. 196. 195. 195. 195. 194. 193. 193. 192. 191. 189. 188.
 193. 193. 192. 192. 191. 191. 190. 190. 189. 188. 187. 185.
 190. 190. 190. 189. 189. 188. 188. 188. 187. 186. 186. 185. 183.
 THE AVERAGE OPERATING TEMPERATURE IS  0.47496E 03 K
 THE OPERATING PRESSURE IS  1.0  ATM
 THE FULL DC POWER OUTLET IS  0.58938E 01 KW-DC
```

Figure 49 -Computer Output for Temperature Distributions Generated by Reference (6) Data (Water Flow Rate = 47.50 Kg/hr , Current Density 0.325 am/cm^2 , Stack Clamping Pressure = 0 Kpa)

Comparison between reference (6) data and the current experimental data is shown in Figures 48 and 49 , these temperatures were produced using water as coolant and with equal flow rates. The outputs of these temperatures showed an average cell temperature of 186.10 °C for the experimental data, while the reference (6) data for the same flow rate yielded an average fuel cell temperature of 204 °C. A difference of 11 percent is apparent between experimental and predicted results by (6).

b) Oil Cooling

Similarly for oil cooling, Figures 50 and 51 represent the numeric outputs of temperatures at the final steady state.

```
TEMPERATURE(C)

 222. 221. 221. 220. 219. 219. 218. 217. 215. 214. 212. 209.
 221. 221. 220. 220. 219. 218. 217. 216. 215. 213. 211. 209.
 220. 220. 219. 218. 218. 217. 216. 215. 213. 212. 210. 207.
 218. 218. 217. 216. 216. 215. 214. 213. 211. 210. 208. 206.
 216. 215. 215. 214. 213. 213. 212. 211. 209. 208. 206. 203.
 213. 213. 212. 212. 211. 210. 209. 208. 207. 205. 203. 201.
 210. 210. 209. 209. 208. 207. 206. 205. 204. 203. 201. 199.
 207. 207. 206. 206. 205. 204. 203. 202. 201. 200. 198. 196.
 204. 204. 203. 203. 202. 201. 201. 200. 199. 197. 196. 194.
 201. 201. 200. 200. 199. 199. 198. 197. 196. 195. 193. 191.
 198. 198. 198. 197. 197. 196. 195. 194. 193. 192. 191. 189.
 196. 195. 195. 194. 194. 193. 193. 192. 191. 190. 189. 187.
1 THE AVERAGE OPERATING TEMPERATURE IS  0.47743E 03 K
 THE OPERATING PRESSURE IS  1.0  ATM
 THE FULL DC POWER OUTLET IS  0.59286E 01 KW-DC
```

Figure 50 –Computer Output for Temperature Distributions Generated by Experimental Data (Oil Flow Rate = 16.66 Kg/hr , Current Density 0.325 am/cm^2 , Stack Clamping Pressure = 0 Kpa)

The temperature of the fuel cell plate decreased from 200 °C to 193 °C when the stack clamping pressure increased from zero to 3448 Kpa. Also, the average fuel cell plate

temperature varied between 190 °C and 200 °C at various coolant flow rate for the experimental data and between 175 °C and 204 °C for reference (6) data. The difference is about 10 percent.

```
 TEMPERATURE(C)

  196. 196. 196. 195. 195. 195. 194. 194. 193. 192. 191. 190.
  194. 194. 194. 194. 193. 193. 193. 192. 191. 191. 189. 188.
  191. 191. 191. 191. 190. 190. 190. 189. 189. 188. 187. 186.
  188. 187. 187. 187. 187. 186. 186. 185. 185. 184. 183. 182.
  183. 183. 183. 183. 182. 182. 182. 181. 181. 180. 180. 179.
  179. 178. 178. 178. 178. 178. 177. 177. 177. 176. 176. 175.
  174. 174. 174. 174. 174. 173. 173. 173. 173. 172. 172. 171.
  170. 170. 170. 170. 169. 169. 169. 169. 169. 168. 168. 167.
  166. 166. 166. 166. 166. 165. 165. 165. 165. 165. 164. 164.
  163. 163. 163. 162. 162. 162. 162. 162. 162. 162. 161. 161.
  160. 160. 160. 160. 160. 160. 160. 160. 160. 159. 159. 159.
  160. 160. 160. 159. 159. 159. 159. 159. 159. 159. 159. 158.
1 THE AVERAGE OPERATING TEMPERATURE IS  0.44644E 03 K
 THE OPERATING PRESSURE IS  1  ATM
 THE FULL DC POWER OUTLET IS  0.53205E 01 KW-DC
```

Figure 51 -Computer Output for Temperature Distributions Generated by Experimental Data (Oil Flow Rate = 16.66 Kg/hr , Current Density 0.325 am/cm^2 , Stack Clamping Pressure = 3448 Kpa)

```
 TEMPERATURE(C)

  215. 214. 214. 213. 213. 212. 211. 210. 209. 208. 206. 204.
  214. 213. 213. 212. 212. 211. 210. 209. 208. 207. 205. 203.
  212. 212. 211. 211. 210. 209. 209. 208. 206. 205. 203. 201.
  210. 209. 209. 208. 208. 207. 206. 205. 204. 203. 201. 199.
  207. 207. 206. 206. 205. 204. 204. 203. 202. 200. 199. 197.
  204. 204. 203. 203. 202. 201. 201. 200. 199. 198. 196. 194.
  201. 200. 200. 199. 199. 198. 198. 197. 196. 195. 193. 192.
  197. 197. 197. 196. 196. 195. 194. 194. 193. 192. 190. 189.
  194. 194. 193. 193. 192. 192. 191. 191. 190. 189. 188. 186.
  191. 191. 190. 190. 190. 189. 189. 188. 187. 186. 185. 184.
  188. 188. 188. 188. 187. 187. 186. 186. 185. 184. 183. 182.
  186. 186. 186. 185. 185. 185. 184. 184. 183. 182. 182. 181.
1 THE AVERAGE OPERATING TEMPERATURE IS  0.46924E 03 K
 THE OPERATING PRESSURE IS  1  ATM
 THE FULL DC POWER OUTLET IS  0.58043E 01 KW-DC
```

Figure 52 -Computer Output for Temperature Distributions Generated by Experimental Data (Oil Flow Rate = 24.87 Kg/hr , Current Density 0.325 am/cm^2 , Stack Clamping Pressure = 0 Kpa)

```
TEMPERATURE(C)

 196. 196. 195. 195. 195. 194. 194. 193. 193. 192. 191. 189.
 194. 194. 193. 193. 193. 193. 192. 192. 191. 190. 189. 188.
 191. 191. 190. 190. 190. 189. 189. 189. 188. 187. 186. 185.
 187. 187. 186. 186. 186. 186. 185. 185. 184. 184. 183. 182.
 182. 182. 182. 182. 182. 181. 181. 181. 180. 180. 179. 178.
 178. 178. 178. 177. 177. 177. 177. 176. 176. 176. 175. 174.
 173. 173. 173. 173. 173. 173. 172. 172. 172. 171. 171. 170.
 169. 169. 169. 169. 169. 168. 168. 168. 168. 168. 167. 167.
 165. 165. 165. 165. 165. 165. 164. 164. 164. 164. 164. 163.
 162. 162. 162. 162. 162. 161. 161. 161. 161. 161. 161. 160.
 160. 160. 159. 159. 159. 159. 159. 159. 159. 159. 159. 158.
 159. 159. 159. 159. 159. 159. 158. 158. 158. 158. 158. 158.
1 THE AVERAGE OPERATING TEMPERATURE IS  0.44579E 03 K
  THE OPERATING PRESSURE IS   1   ATM
  THE FULL DC POWER OUTLET IS  0.53028E 01 KW-DC
```

Figure 53 -Computer Output for Temperature Distributions Generated by Reference (6) Data (Oil Flow Rate = 24.87 Kg/hr , Current Density 0.325 am/cm^2 , Stack Clamping Pressure = 0 Kpa)

c) Air Cooling

For air cooling steady state temperature distributions are represented by Figures 54 and 55 under zero and 500 psi stack clamping pressures.

The average fuel cell plate temperature dropped from 192 °C to 176 °C as the stack clamping pressure increased from zero to 3448 Kpa. Also, the temperature distributions showed some difference under the influence of the heat transfer coefficients between experiment and predicted by (6). Nevertheless, the agreement was within 2 percent which is an indication of validity for the computer simulation. The average fuel cell temperature was about 190 °C for both experimental and reference (6) data.

```
TEMPERATURE(C)

 211. 210. 210. 209. 209. 208. 207. 207. 206. 204. 203. 201.
 210. 209. 209. 208. 208. 207. 207. 206. 205. 203. 202. 200.
 208. 208. 207. 207. 206. 205. 205. 204. 203. 202. 200. 198.
 205. 205. 205. 204. 204. 203. 202. 201. 200. 199. 198. 196.
 202. 202. 201. 201. 201. 200. 199. 199. 198. 196. 195. 193.
 199. 198. 198. 198. 197. 197. 196. 195. 194. 193. 192. 191.
 195. 195. 195. 194. 194. 193. 193. 192. 191. 190. 189. 188.
 192. 191. 191. 191. 190. 190. 189. 189. 188. 187. 186. 185.
 188. 188. 188. 187. 187. 187. 186. 186. 185. 184. 183. 182.
 185. 185. 185. 184. 184. 184. 183. 183. 182. 181. 181. 180.
 183. 183. 182. 182. 182. 181. 181. 181. 180. 179. 179. 178.
 181. 181. 181. 180. 180. 180. 179. 179. 179. 178. 177. 176.

 THE AVERAGE OPERATING TEMPERATURE IS  0.46466E 03 K
THE OPERATING PRESSURE IS    1  ATM
THE FULL DC POWER OUTLET IS  0.57235E 01 KW-DC
 TERMINATED: STOP
-
```

Figure 54 -Computer Output for Temperature Distributions Generated by Experimental Data (Air Flow Rate = 29.84 Kg/hr , Current Density 0.325 am/cm^2 , Stack Clamping Pressure = 0 Kpa)

```
TEMPERATURE(C)

 196. 195. 195. 195. 195. 194. 194. 193. 193. 192. 190. 189.
 194. 193. 193. 193. 193. 192. 192. 191. 191. 190. 189. 187.
 191. 190. 190. 190. 190. 189. 189. 189. 188. 187. 186. 185.
 187. 187. 186. 186. 186. 186. 185. 185. 184. 184. 183. 182.
 182. 182. 182. 182. 182. 181. 181. 181. 180. 180. 179. 178.
 178. 178. 177. 177. 177. 177. 177. 176. 176. 175. 175. 174.
 173. 173. 173. 173. 173. 173. 172. 172. 172. 171. 171. 170.
 169. 169. 169. 169. 169. 168. 168. 168. 168. 167. 167. 167.
 165. 165. 165. 165. 165. 165. 164. 164. 164. 164. 163. 163.
 162. 162. 162. 162. 161. 161. 161. 161. 161. 161. 160. 160.
 159. 159. 159. 159. 159. 159. 159. 159. 159. 159. 158. 158.
 159. 159. 159. 158. 158. 158. 158. 158. 158. 158. 158. 158.
1 THE AVERAGE OPERATING TEMPERATURE IS  0.44565E 03 K
 THE OPERATING PRESSURE IS    1  ATM
 THE FULL DC POWER OUTLET IS  0.52991E 01 KW-DC
```

Figure 55 -Computer Output for Temperature Distributions Generated by Experimental Data (Air Flow Rate = 29.84 Kg/hr , Current Density 0.325 am/cm^2 , Stack Clamping Pressure = 3448 Kpa)

```
 TEMPERATURE(C)

  212. 211. 211. 210. 210. 209. 208. 207. 206. 205. 203. 202.
  211. 210. 210. 209. 209. 208. 207. 207. 205. 204. 203. 201.
  209. 209. 208. 208. 207. 206. 206. 205. 204. 203. 201. 199.
  207. 206. 206. 205. 205. 204. 203. 202. 201. 200. 199. 197.
  204. 203. 203. 202. 202. 201. 200. 200. 199. 197. 196. 194.
  200. 200. 199. 199. 198. 198. 197. 196. 196. 194. 193. 192.
  197. 196. 196. 196. 195. 195. 194. 193. 192. 191. 190. 189.
  193. 193. 192. 192. 192. 191. 191. 190. 189. 188. 187. 186.
  190. 189. 189. 189. 188. 188. 187. 187. 186. 185. 184. 183.
  187. 186. 186. 186. 186. 185. 185. 184. 183. 183. 182. 181.
  184. 184. 184. 183. 183. 183. 182. 182. 181. 181. 180. 179.
  182. 182. 182. 182. 181. 181. 181. 180. 180. 179. 178. 178.
1 THE AVERAGE OPERATING TEMPERATURE IS  0.46584E 03 K
 THE OPERATING PRESSURE IS    1 ATM
 THE FULL DC POWER OUTLET IS  0.57450E 01 KW-DC
```

Figure 56 –Computer Output for Temperature Distributions Generated by Experimental Data (Air Flow Rate = 29.84 Kg/hr , Current Density 0.325 am/cm^2 , Stack Clamping Pressure = 0 Kpa)

```
 TEMPERATURE(C)

  210. 210. 209. 209. 208. 208. 207. 206. 205. 204. 202. 200.
  209. 209. 208. 208. 207. 207. 206. 205. 204. 203. 201. 199.
  207. 207. 206. 206. 205. 205. 204. 203. 202. 201. 200. 198.
  205. 204. 204. 203. 203. 202. 202. 201. 200. 199. 197. 195.
  201. 201. 201. 200. 200. 199. 199. 198. 197. 196. 194. 193.
  198. 198. 197. 197. 196. 196. 195. 195. 194. 193. 191. 190.
  194. 194. 194. 193. 193. 192. 192. 191. 190. 189. 188. 187.
  191. 190. 190. 190. 189. 189. 188. 188. 187. 186. 185. 184.
  187. 187. 187. 186. 186. 186. 185. 185. 184. 183. 182. 181.
  184. 184. 184. 183. 183. 183. 182. 182. 181. 181. 180. 179.
  182. 182. 181. 181. 181. 180. 180. 180. 179. 179. 178. 177.
  180. 180. 180. 179. 179. 179. 179. 178. 178. 177. 176. 176.
1 THE AVERAGE OPERATING TEMPERATURE IS  0.46387E 03 K
 THE OPERATING PRESSURE IS    1 ATM
 THE FULL DC POWER OUTLET IS  0.57089E 01 KW-DC
```

Figure 57 –Computer Output for Temperature Distributions Generated by Reference (6) Data (Air Flow Rate = 29.84 Kg/hr , Current Density 0.325 am/cm^2 , Stack Clamping Pressure = 0 Kpa)

6.6 Effects of Overall Heat Transfer Coefficient on the Efficiency of the Fuel-Cell Stack

The efficiency η, of the fuel-cell stack can be defined as,

$$\eta = \frac{E_s - E_p}{E_s + Q_s} \tag{37}$$

where,

E_s = Electric energy generated by the fuel-cell stack

E_p = Electric energy consumed by the pump to circulate the coolant.

Q_s = Heat generated by the fuel-cell stack

where E_p is directly proportional to the coolant mass flow rate. On the other hand, it can be shown that the mass flow rate is inversely proportional to the value of the overall heat transfer coefficient U_c . From equations (11) and (20) the following relation can be obtained,

$$\frac{T_s - T_i}{q} = \frac{1}{A_p}\cdot\frac{1}{U_c} + \frac{1}{2C_p}\cdot\frac{1}{m} \tag{38}$$

where T_s , T_i , q, A_p and C_p are assumed to be constant. Eq. (38) can also be written as,

$$\xi = \frac{1}{A_p}\cdot\frac{1}{U_c} + \frac{1}{2C_p}\cdot\frac{1}{m} \tag{39}$$

where,

$$\xi = \frac{T_s - T_i}{q}$$

Values of m were calculated for a range of values of U_c for air, oil and water, and the results were plotted against the experimental values of U_c and their corresponding m's . These plots are shown in Figures 58 , 59 and 60 respectively. It can be noted from these figures that the maximum deviation between the calculated and the measured values of U_c and m is about 14 percent for water, 16 percent for oil and 9 percent for air cooling.

Also, these figures clearly indicates that the higher the value of U_c , the lower is the value of the flow rate m. Since the work consumed by the pump to circulate the coolant is directly related to the flow rate, Eq. (37) shows that the higher is the value of U_c , the greater will be the efficiency of the fuel cell stack. Also, since U_c is directly proportional to the clamping pressure, one can conclude that the higher is the clamping pressure, the higher is the efficiency of the fuel-cell stack.

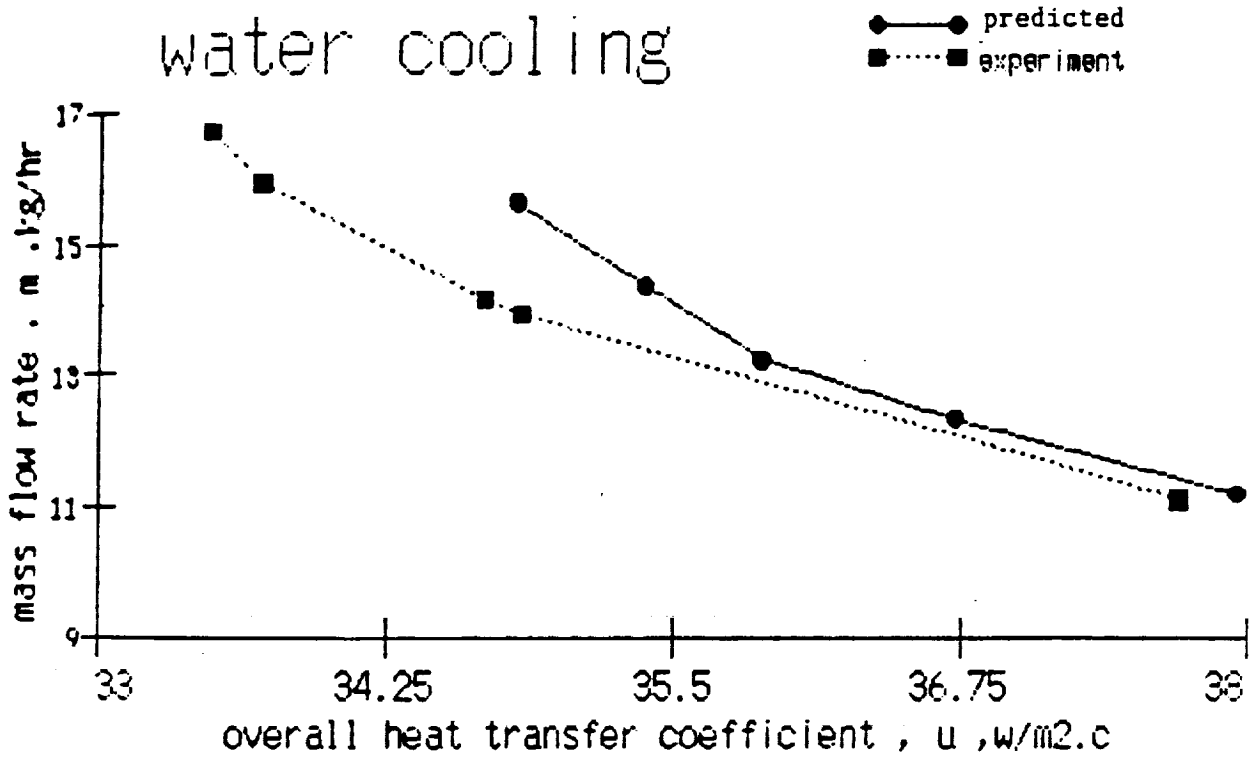

Figure 58 -Coolant Flow Rate Requirements, To maintain The Electrodes Temperature at 190 °c, As a Function Of The Overall Heat Transfer Coefficient.(Serpentine Configuration, Water Cooling)

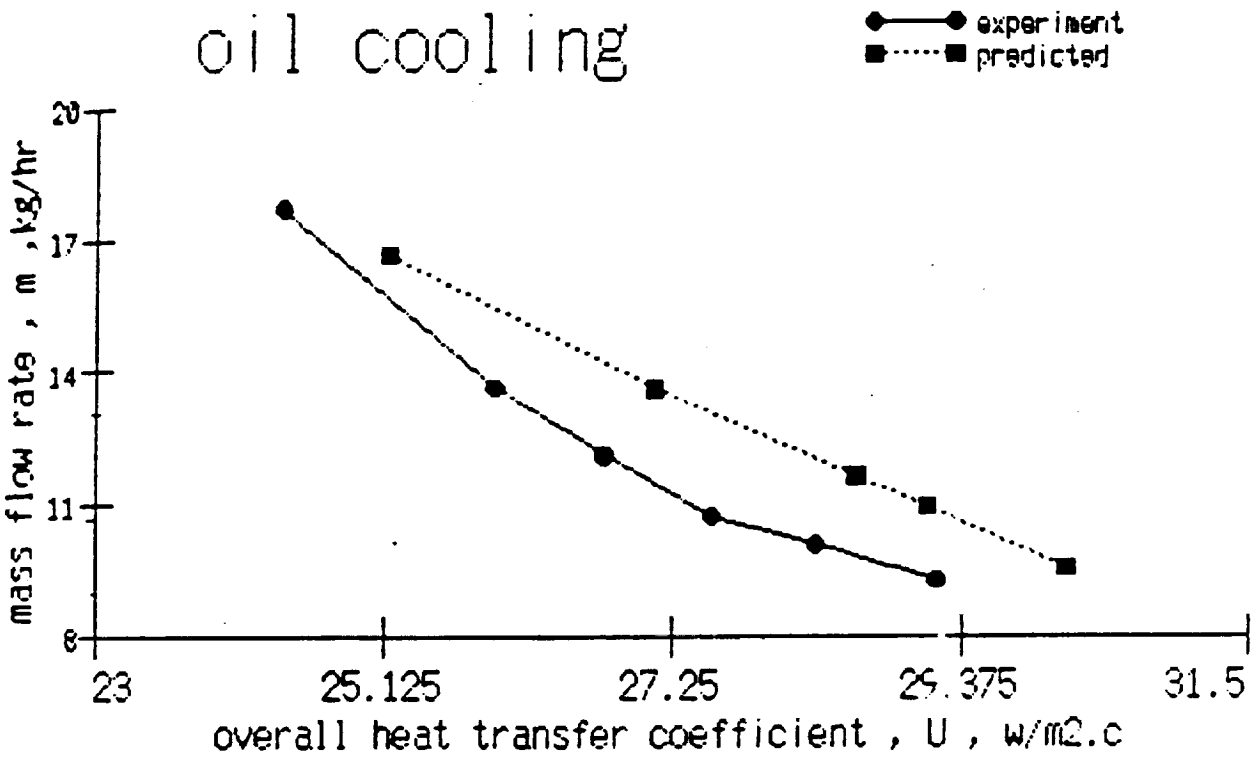

Figure 59 –Coolant Flow Rate Requirements, To Maintain The Electrodes Temperature at 190 °c, As Function Of The Overall Heat Transfer Coefficient. (Serpentine Configuration, Oil Cooling)

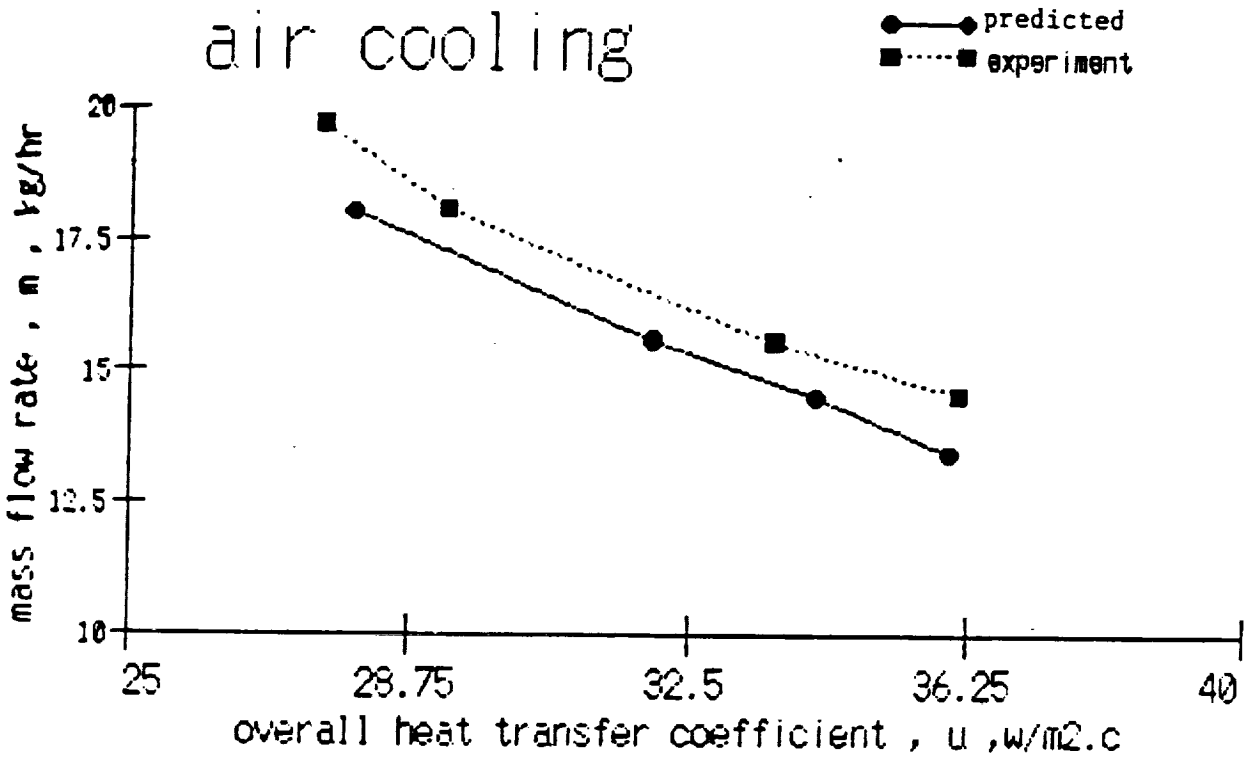

Figure 60-Coolant Flow Rate Requirements, To maintain The Electrodes Temperature at 190 °c,As a function Of The Overall Heat Transfer Coeficient.(Straight Configuration, Air Cooling)

CHAPTER VII

RESULTS AND DISCUSSIONS

Some of the important features pertaining to the results obtained during this course of investigation are discussed below.

While the investigation was primarily concerned with heat transfer, preliminary measurements of the thermal contact resistance were also made to evaluate its influence on the overall heat transfer coefficient. The values of the overall heat transfer coefficients for the three different coolants and the two different cooling plate configurations are plotted in Figures 61 , 62 and 63 . In all cases, the overall heat transfer coefficient increased with increasing interface pressure as shown in the figures. The interface pressure was varied from 0 Kpa to 3448 Kpa in increments of 689 Kpa . For oil cooling in Figure 61 the flow was in the laminar range. Between Re = 22 and Re = 43 the rate of increase of U_c is doubled due to the doubling of the flow rate. Figure 62 shows the variation of the overall heat transfer coefficient for water cooling. The transition of flow from laminar to turbulent occured

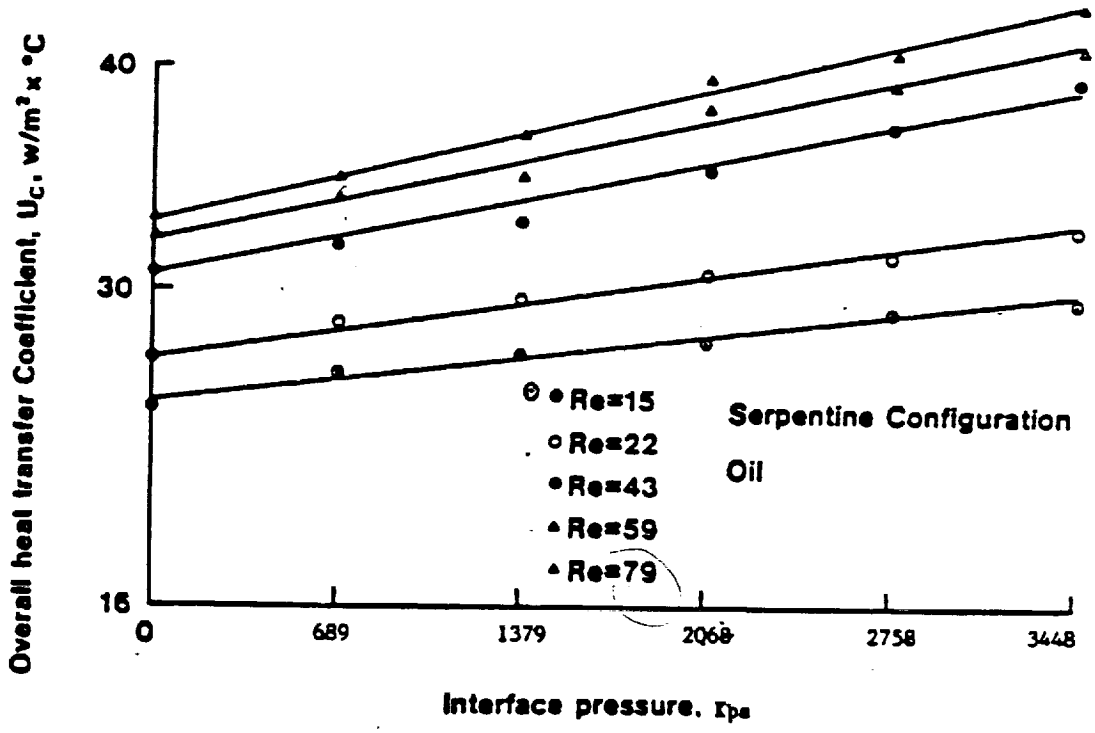

Figure 61 - Variation of the Overall Heat Transfer Coefficient with P and Re for serpentine configuration with oil as coolant

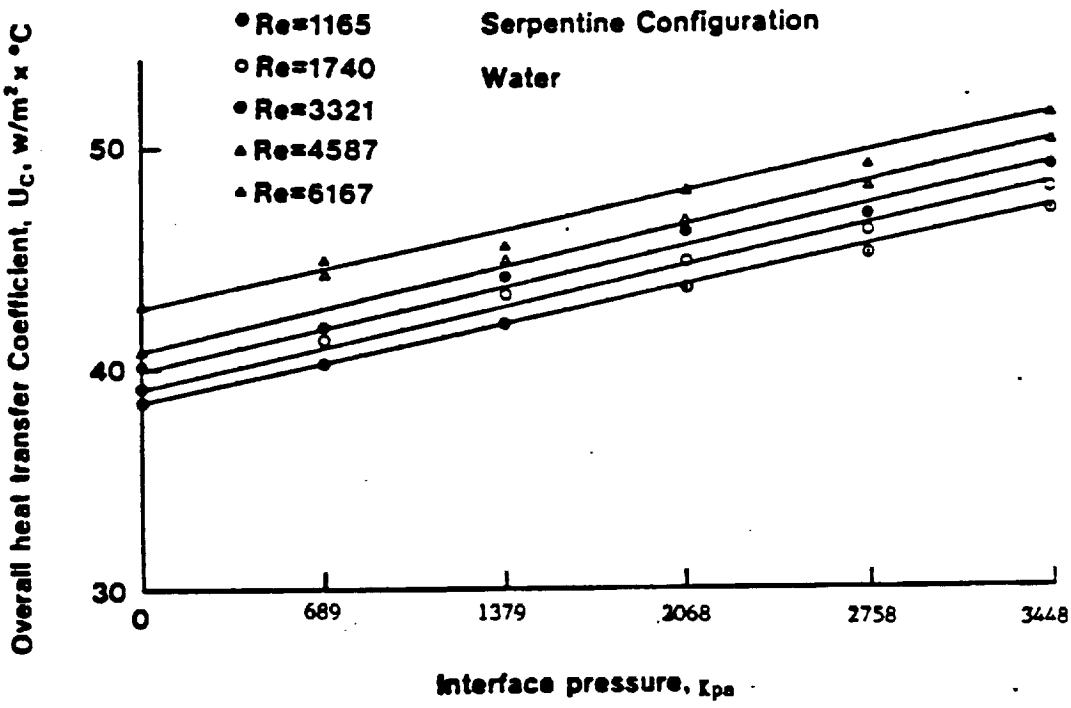

Figure 62 - Variation of the Overall Heat Transfer Coefficient with P and Re for serpentine configuration with water as coolant

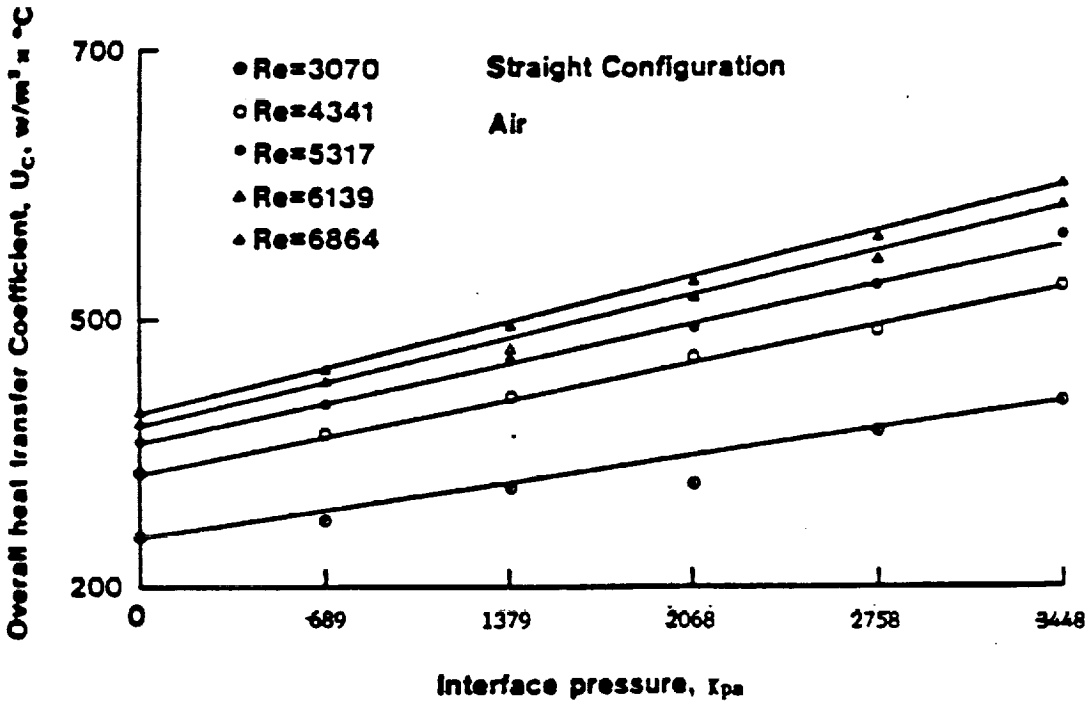

Figure 63 - Variation of the Overall Heat Transfer Coefficient with P and Re for straight configuration with air as coolant

between Re = 1740 and Re = 3321 . In Figure 63 for air cooling, the transition from laminar to turbulent is between 3070 and 4341.

Figure 64 show the relationship of the ratio of the overall heat transfer coefficients without and with the thermal contact resistance term (U/U_c) decreasing as the pressure increases. (U/U_c) varied from 1.15 at P = 0 Kpa to 1.05 at P = 3448 Kpa, for oil and water, while for air it varied from 1.05 to 0.7 at P = 0 Kpa and P = 3448 Kpa respectively.

Two series of test were conducted for measurements of the thermal contact resistance and the data obtained was plotted for both configurations, serpentine and straight. As shown in Figure 25 the thermal contact resistance varies from 0.0016 at 0 Kpa to 0.000812 $m^2.°C/w$ at 3448 Kpa . Figure 65 and 66 show the effect of increasing interface pressure on the thermal contact conductance. As expected, the conductance increases with increasing contact pressure. The values of contact conductance measured during the unloading phase are significantly higher than the values obtained during loading phase. This increase of conductance can be explained by the better conformity of two interfaces after the maximum load has been reached, i.e., a plastic deformation of the surface asperities has resulted in a greater true area of contact.

The effective temperature drop across the interface of the cell/cooling plates for both cooling plate configurations was plotted versus pressure, in Figure 26 ,

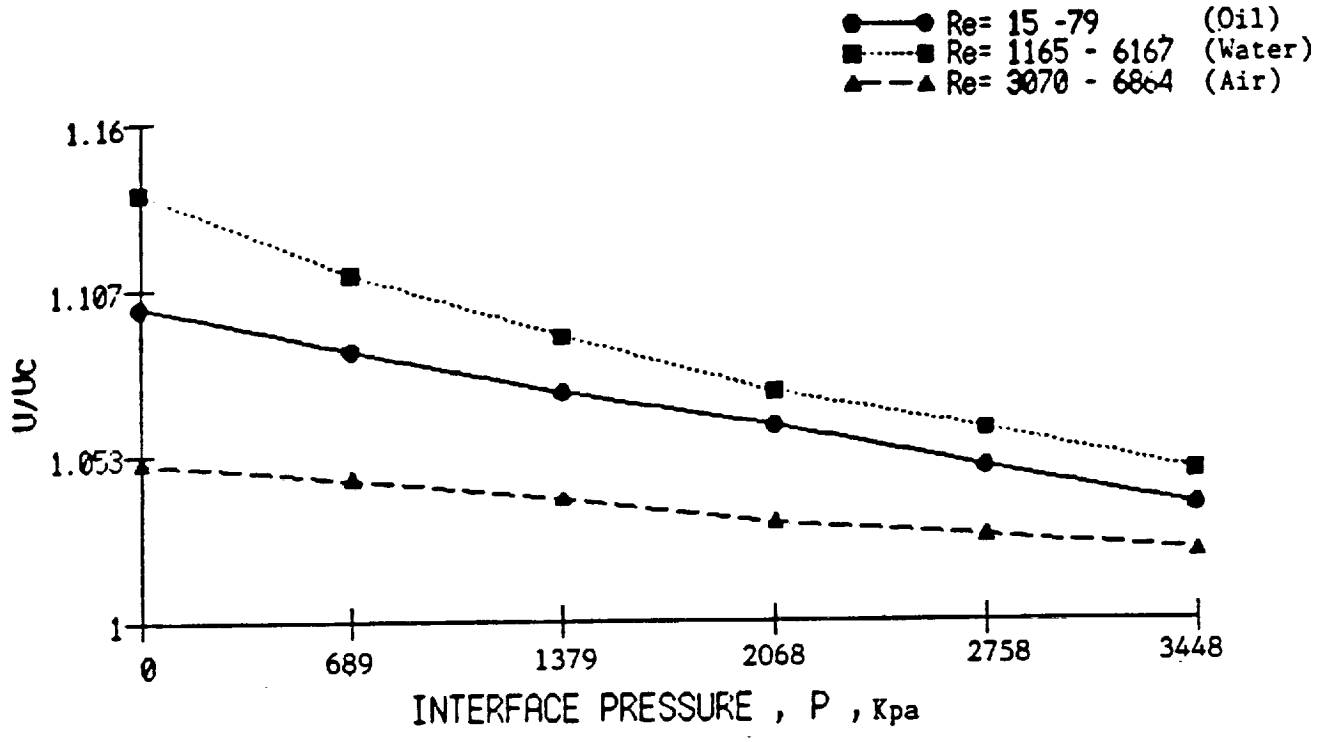

Figure 64 - U/U_c versus Interface Pressure for Serpentine and Straight Configurations with Air, Water and Oil as Coolants.

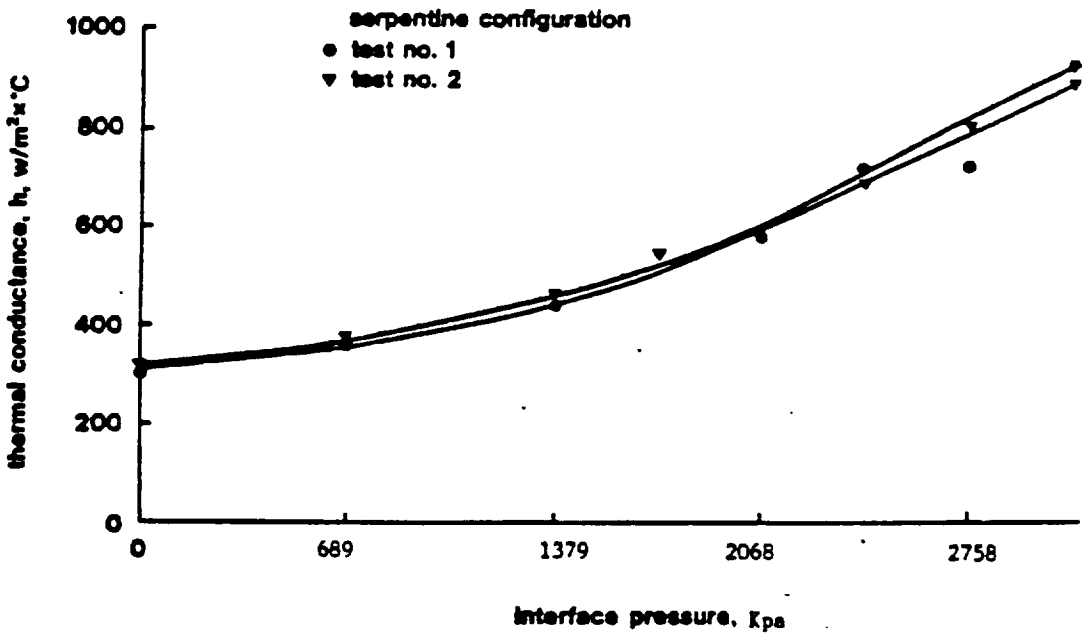

Figure 65- Effects of Contact Pressure on the Thermal Conductance for serpentine configuration

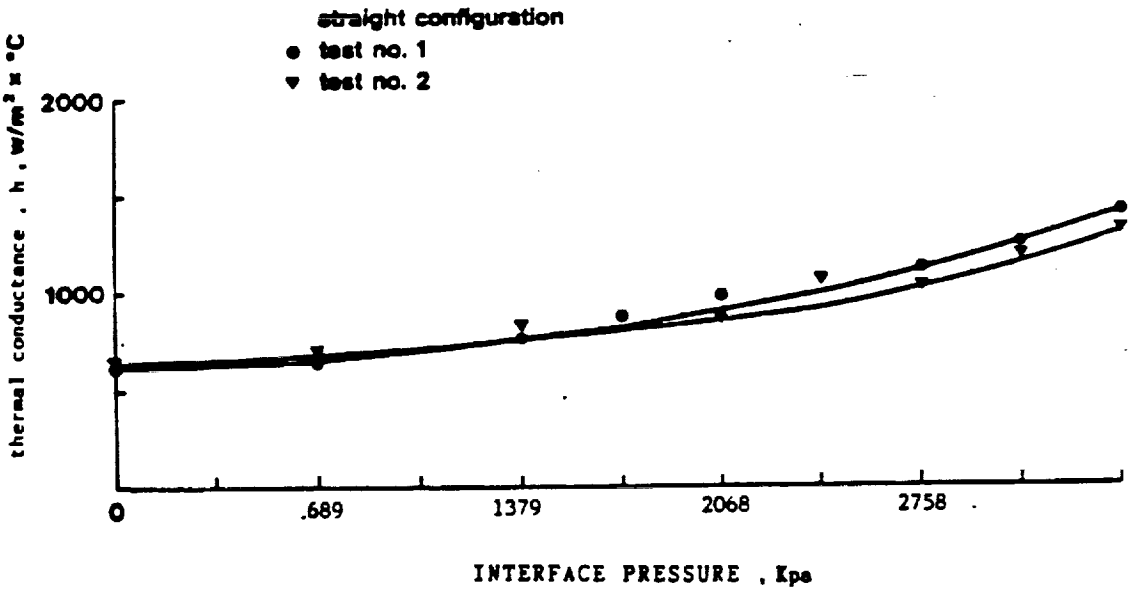

Figure 66 - Effects of Contact Pressure on the Thermal Conductance for straight configuration

the numerical correlation for this data is represented by Eq. (31) . Similarly, Eq. (29) and (30) represent the contact resistance as function of pressure for the two cooling plate configurations.

The experimental heat transfer condition is one of asymmetrical heating since only the curved boundary (i.e. cell plate), transfers energy to the flow. If the average experimental heat transfer coefficient for this condition is used to compare the corresponding experimental temperature data, the nature of the thermal boundary condition is irrelevant. Nusselt number values for all three situations were plotted versus Reynolds number on a log-log scale. For each case, data for three tests were plotted as shown in Figures 67 , 68 and 69 .

The data for the heat transfer measurements such as heat transfer coefficient and Nusselt number shown in Tables 1.1 through 3.6 were correlated into a single relation, which is given by Eq. (22). Consequently, equations representing data for oil, water and air cooling were formed and results obtained by these equations were plotted against the experimental results as shown in Figures 67 , 68 and 69 . Table 2 represents measured measured and calculated data by equations (24), (26) and (28) for all three coolants, oil, water and air.

The experimental error could be reduced by maintaining the largest possible temperature difference between the coolant and the cell plate. Since the heat transfer rates increased with increasing Reynolds numbers, the input power

to the cell plate had to be limited to keep the cell temperatures below 200 °C to prevent damage to the thermocouple adhesive bonds. This condition was used for most of the tests. There was no significant change in the heat transfer rate when the power dissipated in the cell was reduced by one half. This showed that the inaccuracies in the thermocouple measurements did not significantly effect the results.

TABLE 2

Comparison Between Experiment and Correlation

Air Case

Re	3070	4341	5317	6139	6864
NU_{exp}	3.005	4.840	6.872	6.632	7.28
NU_{co}	3.148	4.61	5.744	6.724	7.60

Water Case

Re	1165	1740	3321	4587	6167
NU_{exp}	0.525	0.520	0.545	0.55	0.565
NU_{co}	0.488	0.499	0.517	0.527	0.545

Oil Case

Re	15	22	43	59	79
NU_{exp}	1.34	1.49	1.74	1.86	1.93
NU_{co}	1.373	1.491	1.723	1.842	1.961

where,

NU_{exp} = Nusselt Number (Experimental)

NU_{co} = Nusselt Number (correlation)

Three measurements for the heat transfer coefficients were made for each coolant under the same conditions. No major differences were made for each coolant under the same conditions. No major differences were noticed except that for each coolant a different heat transfer rate was obtained which was expected. The greatest heat transfer rate was obtained with air cooling. The air exit temperature averaged about 60 °C while for oil and water cooling it averaged about 120 and 50 °C respectively. The Reynolds number ranged from 15 to 80 for oil. For air and water it ranged from 1000 to 7000 which is well in the turbulent region for air and both laminar and turbulent for water.

The lowest heat transfer rate was obtained with water cooling. Comparing the oil and water cooling cases, it is noticed that the values of the heat transfer coefficient were nearly equal. As an example of the significance of these results, consider the design of a nuclear reactor cooling system where the heat flux is a known function of length along the tube. Typically the heat flux is low near the entrance and exit reaching a maximum at the midpoint. If the coolant is a liquid metal, considerable error in the predicted surface temperatures can result unless variable heat-flux theory is employed. On the other hand, if the coolant is a gas, or pressurized water, the varying heat flux has little influence, and it is adequate to use a Nusselt number based on constant heat flux theory to calculate the local temperature difference between the fluid and the wall surfaces.

In general terms, the accuracy of the experimental data and the results, is considered good, although some factors such as surface roughness, friction, geometry of the cooling channels and configuration of plates could have effected the results to some extent. The effect of the surface roughness on the heat transfer for flow in tube is essentially the same as that for the external boundary layer. The only differences arise from the fact that for flow in tube the friction coefficient is based on the mean flow velocity and the heat transfer coefficient is based on the mixed mean fluid temperature.

It should also be noted that artificial roughness or turbulence promoters are frequently employed as a means to increase the heat transfer coefficient. A comprehensive review of methods for augmentation of convective heat transfer is given by Bergles (35), (36) . However, differences between the measured average heat transfer coefficient and the predicted by the use of existing correlations do exist. This difference is a result of the effects of asymmetry of heat transfer and the inadequacy of the hydraulic radius concept itself in the case of noncircular cooling channels. The average heat transfer coefficient used in the theoretical prediction was taken from existing correlations, and of course that correlation refered to a particular geometry and thermal boundary conditions.

A tabulation of measured heat transfer coefficients, thermal contact resistance and other parameters are all presented in the appendix.

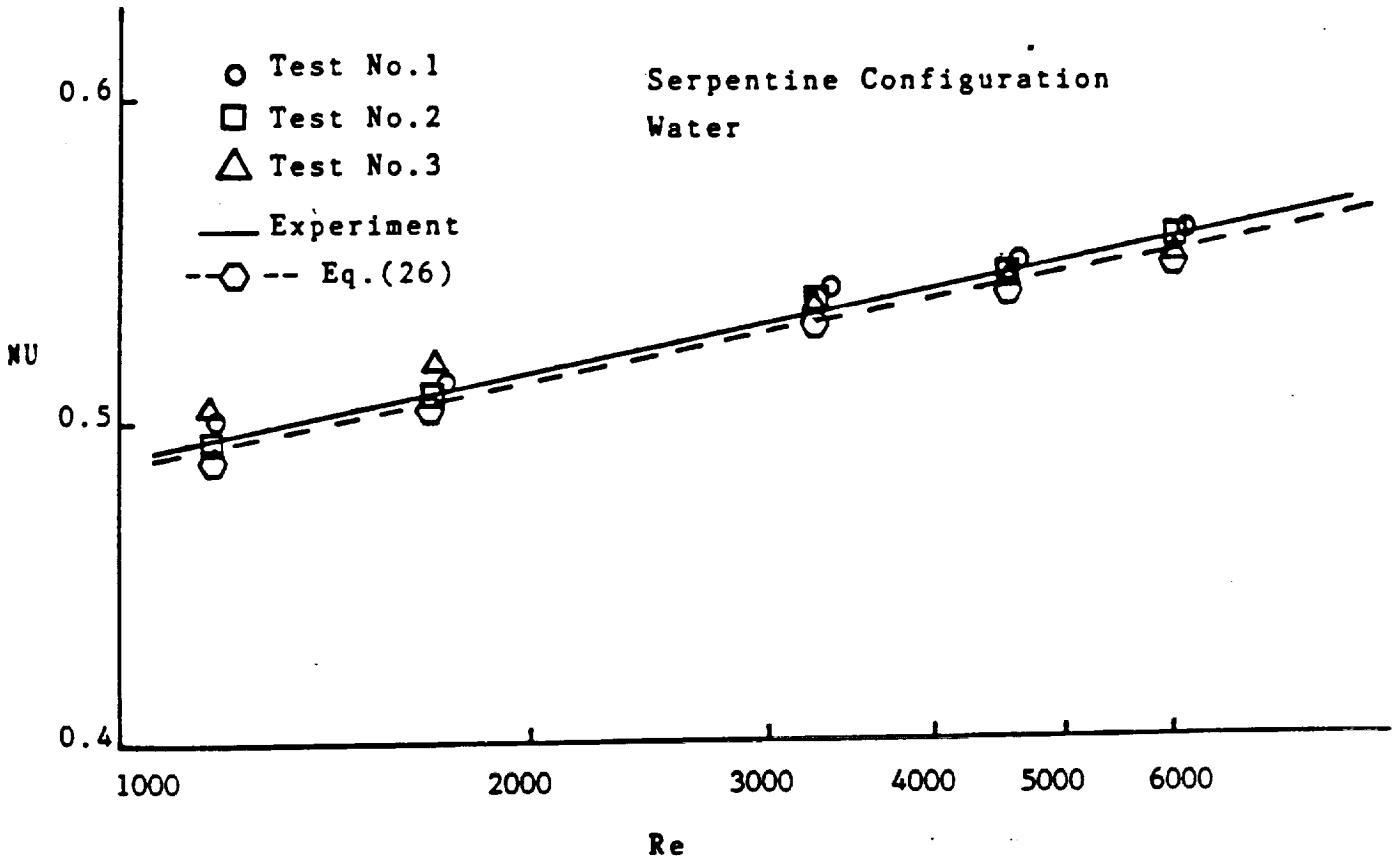

Figure 67 -Nusselt Number versus Reynolds Number for Serpentine Configuration with Water as a Coolant.

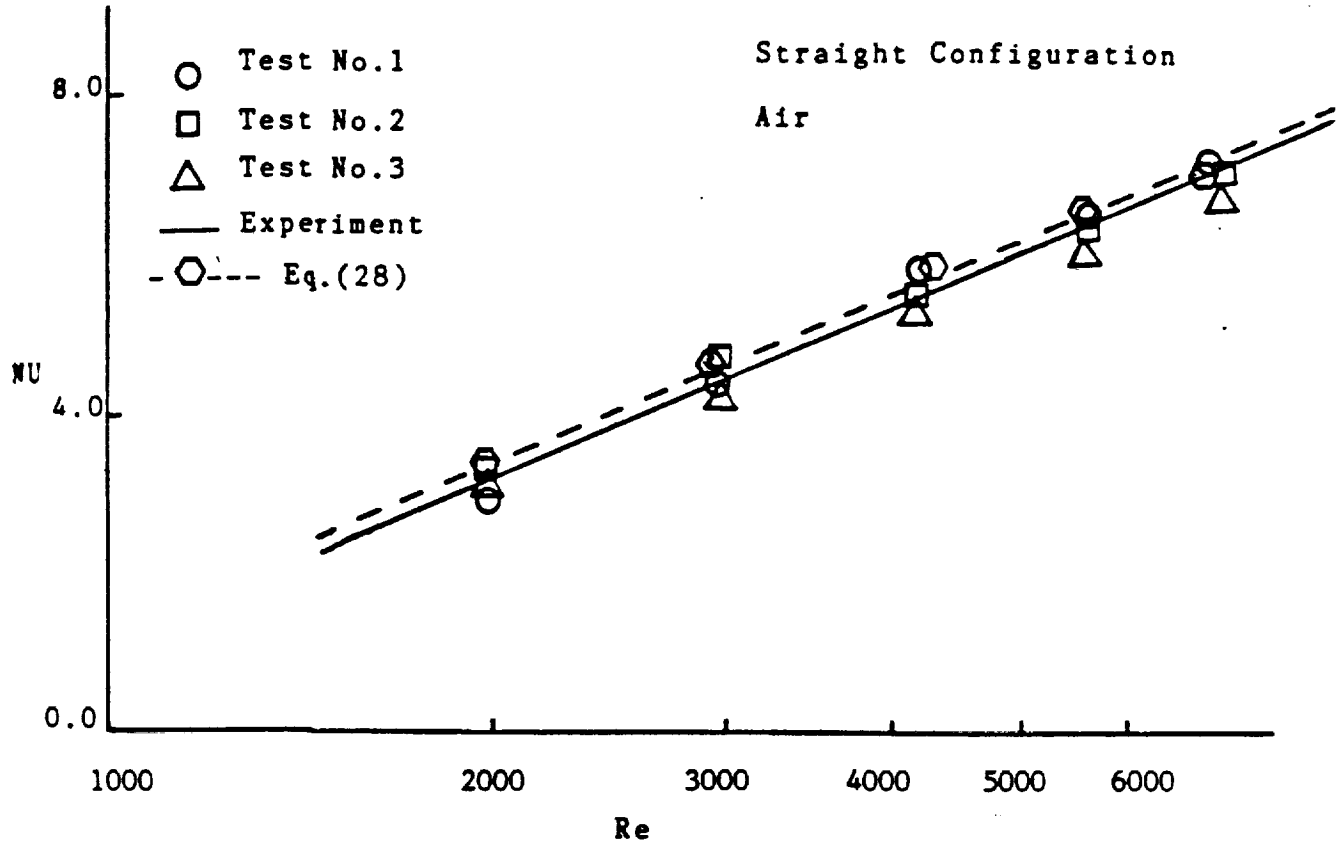

Figure 68 -Nusselt Number versus Reynolds Number for Straight Configuration with Air as a Coolant.

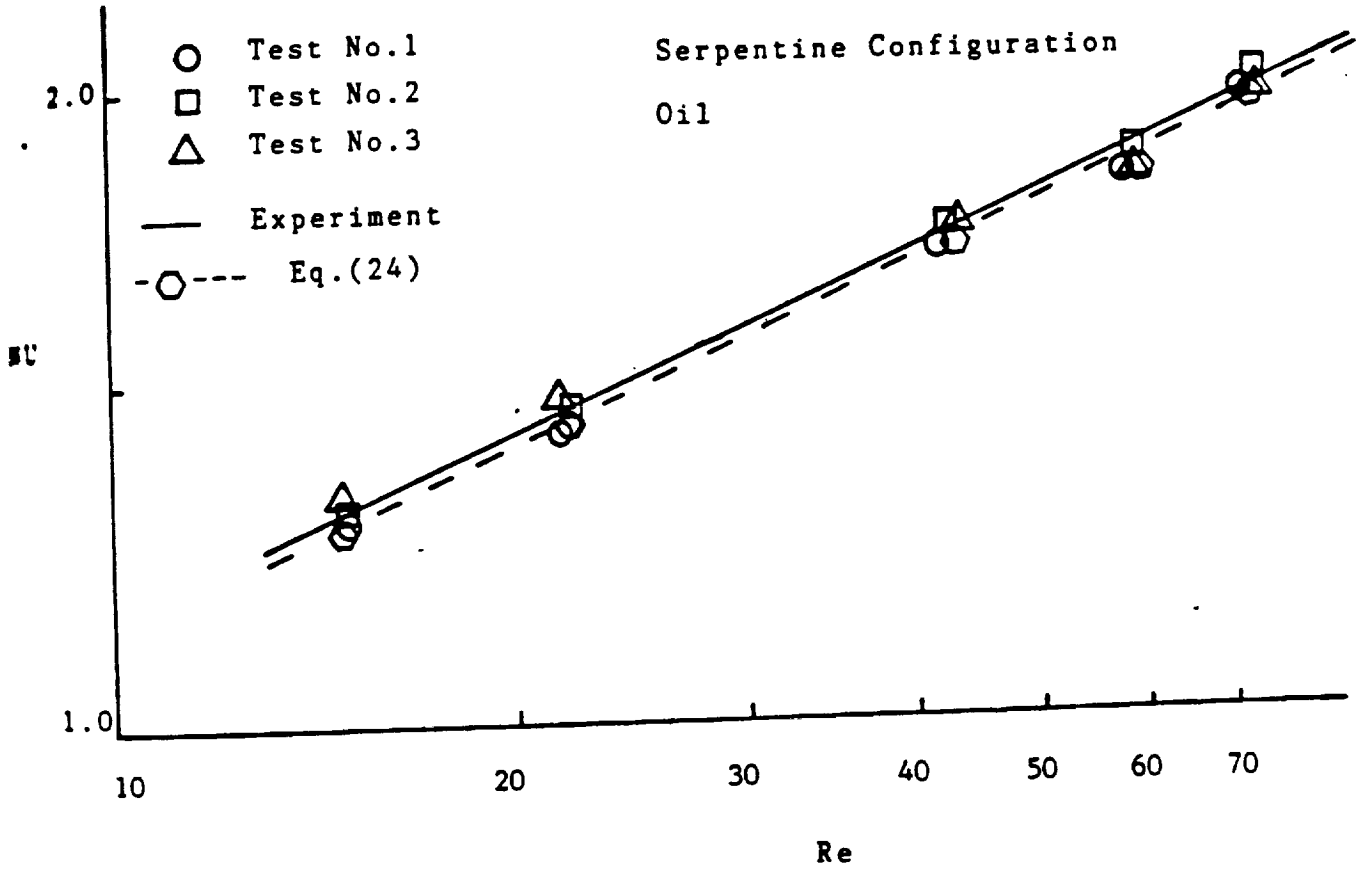

Figure 69 -Nusselt Number versus Reynolds Number for Serpentine Configuration with Oil as a Coolant.

CHAPTER VIII

CONCLUSIONS AND RECOMMENDATIONS

7.1 CONCLUSIONS

A. Based on the experimental results, it may be con. that each of the cooling system used in this experiment ha. its advantages and disadvantages as far as the performance of the cooling system is concerned. Performance characteristics for each of the cooling plate can be listed as follows:

1. The advantages of using the straight channel configuration lies in its special characteristics of having a short flow length, large effective heat transfer area, good temperature uniformity and smaller temperature differential between coolant and cell plate. Also, it has a high reliability and low cost.

However, some disadvantages are summerized by its limitations to the use of gases only which limits the size of the plate since gases have low heat capacity. Besides the difficulties in controling air leakage.

2. The serpentine configuration does not have any limitations towrds the size of the plate (i.e. plate can be large) since

liquids have high heat capacity. Another advantage is the capability of using two phase flow coolant (41).

Nevertheless, the serpentine configuration is costly and complex in construction. Also, it provides less temperature uniformity, high inlet and outlet coolant temperature differential. It has a relatively small heat transfer area, long flow path which makes it not applicable for gases.

B. the cooling system performance and the efficiency of the fuel-cell stack is a strong function of the clamping pressure. The effect of the clamping pressure for the two configurations investigated can be summerized as follows:

1. For both configurations straight and serpentine with water, oil and air cooling, the higher the clamping pressure, the higher the value of the overall heat transfer coefficient, the greater will be the efficiency of the fuel-cell stack.
2. Higher heat transfer coefficient has been obtained for air cooling, while it has been nearly equal for oil and water cooling.

8.2 Recommendations

The present study is the first in correlating heat transfer coefficient for the cooling system in the fuel-cells. Future studies are recommended in the following directions:

1. Studies of the transient effects of the cooling system parameters on the overall heat transfer coefficient and the uniformity of electrode plate temperature distribution.
2. Development of a mathematical relation for the coolant flow rate as a function of electric load, the stack clamping

the mean temperature of the electrode plates, and
physical properties of the coolant.
ting steady state and transient analysis for the
of cooling system parameters on heat transfer in the
using real fuel and air.

r",

r in

vol. 1,

in Fuel

63,

Battery",

ant

Institute

for

rs

angular
80)

11-
s)

ling
of

lm
75)

of a
on

BIBLIOGRAPHY

1. Rosenhow, W.M. and Hartnett, J.P., "Handbook of Heat Transfer", McGraw Hill, 1973

2. Eckhert, E.R.G. and Drake, R.M., "Heat and Mass Transfer", 2nd edition, McGraw Hill, 1959

3. Maru, H.C., CHI, C., patel, D., and Burns, D., "Heat Transfer in Phosphoric Acid Fuel Cell Stacks", proceedings of the 13th Intersociety Energy Conversion Engineering Conference, vol. 1, p. 723-731, San Dile Diego, August 1978.

4. Baker, B.S., Gidaspow, D. and Wasan, D., "Thermal Phenomena in Fuel Cells and Batteries", in Tobias, C.W. (ed.), Advances in Electrochemistry and Electrochemical Engineering, vol. 8, p. 63, Wiley, New York, NY, 1971

5. Gidaspow, D. and Baker, B.S., "Heat Transfer in a Fuel Cell Battery", A.I.C.H.E Journal, vol. 11, No. 5, p. 825, 1965

6. Alkasab, K.A., Lu, C.Y., "Phosphoric Acid Fuel Cell Power Plant Performance Model and Computer Program", NASA CR-174638, 1984

7. Benjamin, T.G. et.al., "Handbook of Fuel Cell Performance", Institute of Gas Technology. Report prepared for Department of Energy Publication, Contract No. EC-77-C003-1545, May 1980

8. Baughn, J.W. "Survey of Heat Transfer Measurement Techniques for Forced Convection Flow in Channels" in NATO Advanced Study Institute Turbulent Forced Convection in Channels and Bundles: Theory and Applications to Heat Exchangers and Nuclear Reactors (Hemisphere, 1979) pp. 1029-1032

9. Davenport, C.J. "Heat Transfer and Fluid Flow in Louvered Triangular ducts", PhD thesis (CNAA-Coventry (Lanchester) Polytechnic 1980)

10. Kim, H.K., Moffat, R.J. and Kays, W.M. "Heat Transfer to a Full-Coverage Surface with Compound-Angle (30 and 45 degree Celsius) Hole Injection", NASA CR3103 (February 1979)

11. Eriksin, V.L. and Goldstein, R.J. "Heat Transfer and Film Cooling Following Injection through Inclined Circular Tubes", Journal of Heat Transfer (May 1974) pp. 239-245

12. Blair, M.F. Private Communication (1974)

13. Blair, M.F. and Lander, R.D. "New Techniques for Measuring Film Cooling Effectiveness", Journal of Heat Transfer (November 1975) pp. 539-543

14. Hippensteele, S.A., Russel, L.M. and Stepka, F.A. "Evaluation of a Method for Heat Transfer Measurements and Thermal Visualisation Using a Composite of a Heater Element and Liquid Crystals"

NASA TM 81639 (1981)

15. Crawford, M.E., Kays, W.M. and Moffat, R.J. "Full-coverage Film Cooling on Flat Isothermal Surfaces: a Summary Report on Data and Predictions" NASA CR 3219 (January 1980)

16. Hay, N. and West, P.D. "Heat Transfer in Free Swirling Flow in a Pipe" Journal of Heat Transfer (August 1975) pp. 416-441

17. Portat, M., Bruere, A., Godefroy, J.C. and Helias, F. "Measurement Possibilities on Turbomachines with Thin Film Transducers" ONERA Report (to be published)

18. J.P. Holman, Heat Transfer (4th edn). McGraw Hill, New York (1976)

19. C.A.C. Altemani and E.M. Sparrow, Turbulent Heat Transfer and Fluid Flow in an Unsymmetrically Heated Triangular Duct, Trans. Am. Soc. Mech. Engrs, J. Heat Transfer 102(4), 590-597 (1980)

20. A.D. Gosman, W.M. Pun, A.K. Runchal, D.B. Spalding and M. Wolfstein, Heat and Mass Transfer in Recirculating Flows. Academic Press, New York (1969)

21. "Thermal Conductance of Metallic Contacts", Jacob, K.B. and Starr, C., Rev. Sci. Instr., vol. 10, April 1939, pp. 140-141

22. "Thermal Contact Resistance of Laminated and Machined Joints", Brunot, A.W. and Bucklani, F.F., Trans. ASME, vol. 71, No. 3, April 1949, pp. 253-256, Discussion p. 257

23. "Thermal Resistance Measurements of Joint Formed Between Stationary Metal Surfaces", Wiells, N.D. and Ryder, E.A., Trans. ASME, vol. 71, No. 3, April 1949, pp. 259-266, Discussion pp. 266-267

24. "Thermal Conductance of Contacts in Aircraft Joints", Barzelay, M.E., Tong, K.N. and Holloway, G.F., NACA T N3167, 1954

25. "Effect of Pressure on Thermal Conductance of Contact Joints", Barzelay, M.E., Tong, K.N. and Holloway, G.F., NACA T N3295, May 1955

26. "Heat TRansfer at the Interface of Dissimilar Materials: Evidence of Thermal-Comparator Experiments", Powell, R.W., Tye, R.P. and Jolleffe, B.W., Int. Journal of Heat and Mass Transfer, vol. 5, 1962, pp. 897-902

27. Moru, H.C., Patel, D., Scozzafava, H., and Abens, S. "Pressurization of Phosphoric Acid Fuel Cell", paper presented at Pittsburgh Electrochemical Society meeting, Pittsburgh, oct. 1978

28. Steele, R.V., et. al., "Comparative Assessment of Residential Energy Supply Systems that use Fuel Cells", SRI Technical Report No. EPA-600/7-70-105b prepared for Industrial Environmental Research Lab, April 1979

29. Mansour, Momtaz, "National Fuel Cell Program Plan", in Fuel Cells:

Technology Status and Applications, Institute of Gas Technology Symposium, Chicago, Ill., Nov. 16-18, 1961

30. Simons, Stephen N.M et.al. "Phosphoric Acid Fuel Cells-Technology Status", ibid.

31. Gillis, Edward A., "Fuel Cells for Electric Utilities", Chem. Engr. Prog., vol. 76, No. 10, pp. 88-93. Oct. '80

32. Kunz, H.R. "The State of Art of Hydrogen-Air Phosphoric Acid Electrolyte Fuel Cells", Electrochemical Society Proceedings, vol. 77-6

33. Hoover, D.Q., "Cell and Stack Design Alternatives" Westinghouse report prepared for Department of Energy, Contract No. ET-78-C-03-2031, February 14, 1979

34. Kays, W.M., "Convective Heat and Mass Transfer", 2nd ed., McGraw Hill Book Company, New York, 1980

35. Bergles, A.E., "In Applied Mechanics Reviews", vol. 26, 1973, pp. 675-682

36. Bergles, A.E., "Report HTL-8, Engineering Research Institute, Iwa State University, Ames, 1975

37. Boyle, R.J., "Heat Transfer in Serpentine Passages with Turbulence Promoters", NASA Lewis Research Center, Cleveland, Ohio, ASME Transactions, 1984

38. Devore, L.J., "Probability and Statistics for Engineers and Science", Brooks/Cole Publishing Company, Monterey, California, 1982

39. Gillis, Edward A. "Fuel Cells for Electric Utilities", Chem. Engr. Prog., vol. 76, No. 10, pp. 88-93, Oct'80

40. Hooie, Diane T. "GRI Program Objective and Plans," in Fuel Cells: Technology Status and Applications, Institute for Gas Technology Symposium, Chicago, Ill., Nov., 16-18, 1981

41. Buggy, J.J., et.al. "Effect of Alternate Fuels on the Performance and Economics of Dispersed Fuel Cells", EPRI-1936, July, 1981. Prepared by the Westinghouse Electric Corp.

42. Henson, L.J., and Jachson, S.B. "Performance and Cost Impacts of Using Coal-Derived Fuels in Phosphoric Acid Fuel Cell Power Plants", TVA/OP/EDT-81/31. Based on study by United Technology Corp.

43. Warshay, M., Prokopius, P. Simons, S., & King, R. Status of Commercial Phosphoric Acid Fuel Cell System Development, NASA TM-81641, 1981. Presented at the 19th Aerospace Sciences Mtng., (Am, Inst. Aeronautics & Astronautics) St. Louis, Jan. 12-15, 1981

44. Alkasab, K.A., A.F. Presler, and C.Y. Lu, "Thermodynamic and Performance Model for Phosphoric Acid Fuel-Cell System", Proceedings

Sixth IASTED International Symposium on Energy '83, San Francisco, May 16-18, 1983

45. Hoover, D.Q., "Cell Module and Fuel Conditioner Development", Final Report of Westinghouse Corp. to NASA, Lewis, Contract No. DEN 3-161, Feb. 1982

46. "Improvement in Fuel Cell Technology Base, Phase II", Final Report to Department of Energy under Contract No. DE-AC-03-79ET11301, April 1977 to March 1980

47. "Improvement in Fuel Cell Technology Base, Phase I", United Technologies Corp., South Windsor, CT, FCR-0735. Final Report to Department of Energy under Contract No. EY-76-C-03-1169, March 31, 1977

48. "Technology Development for Phosphoric Acid Fuel Cell Power Plant, Phase I", Quarterly Reports to NASA under Contract DEN3-67, September, 1979 to November, 1980

49. "Program to Develop and Test Fuel Cell Driven Total Energy System, Phase I - Cell and Stack DEsign Alternatives", Final Report to Department of Energy under Contract No. DE-AC03-78ET11300, September, 1978 to October, 1980

50. "Phosphoric Acid Fuel Cell Stack and System Development", Quarterly Reports to Department of Energy under Contract No. DE-AC01-78ET15366, January, 1978 to November, 1980

51. "Fabrication and Testing of TAA Bonded Carbon Electrodes", Final Report to the Department of Energy under Contract No. DE-78-C-03-1156, March, 1978 to May, 1979

52. "Fuel Cell Catalyst Sintering Studies", Final Report to EPRI on Project 633-1-2, July, 1978

53. "Improved Cathodes for Phosphoric Acid Fuel Cells", Final Report to EPRI Project 634-1, June, 1977

54. Cordier, H., "Experimental Study of Contact Thermal Resistance", Annales de Physique, vol. 6, No. 1-2, January 1961, pp. 5-19

55. Chilton, T.H. and Colburn, A.P. 'Mass Transfer (absortion) Coefficients' Industrial Engineering Chemistry 26 (1943), pp. 1183-1187

56. Sherwood, T.K., Pigford, R.L. and Wilke, C.R. 'Mass Transfer' (McGraw-Hill, 1975) pp. 159-171

57. Hoover, D.Q., et. al., "Cell and Stack Design Alternatives," Westinghouse R+D Center Report, Submitted to Department of Energy under Contract No. DE-AC03-78ET11300, 1980.

58. Johnson, W.H., "Phosphoric Acid Technology Improvement Program." Paper presented at National Fuel Cell Seminar, San Francisco, July 11-13, 1978.

59. Johnson, W.H., "Improvement of Fuel Cell Technology Base," UTC Technical Progress Report FCR-1809, Contract No. ET-76-C003-1169. South Windsor, Connecticut, April, 1978.

APPENDICES

APPENDIX A

FIGURES

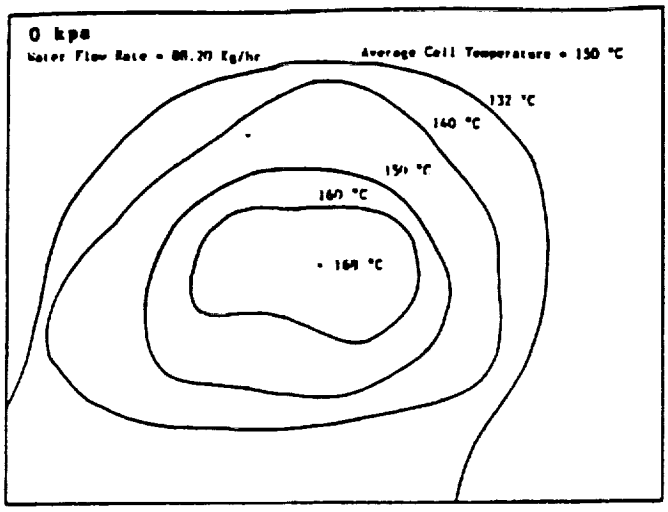

Figure 69-Effects of Coolant Flow Rate and Stack Clamping Pressure on the Temperature Distributions. (Serpentine, Water Cooling)

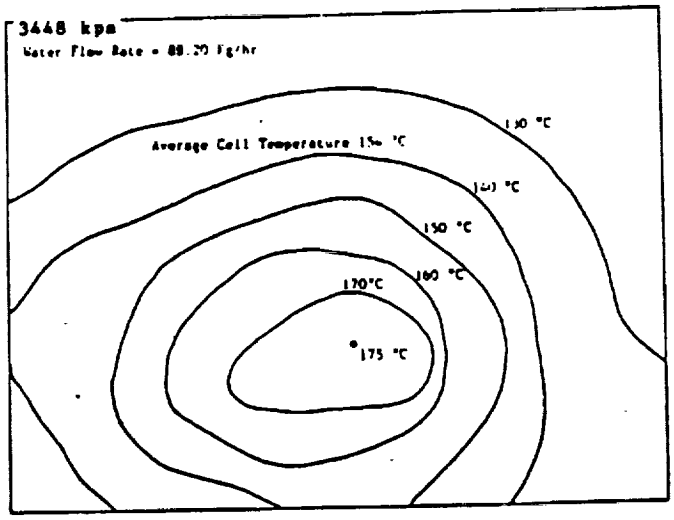

Figure 70-Effects of Coolant Flow Rate and Stack Clamping Pressure on the Temperature Distributions. (Serpentine, Water Cooling)

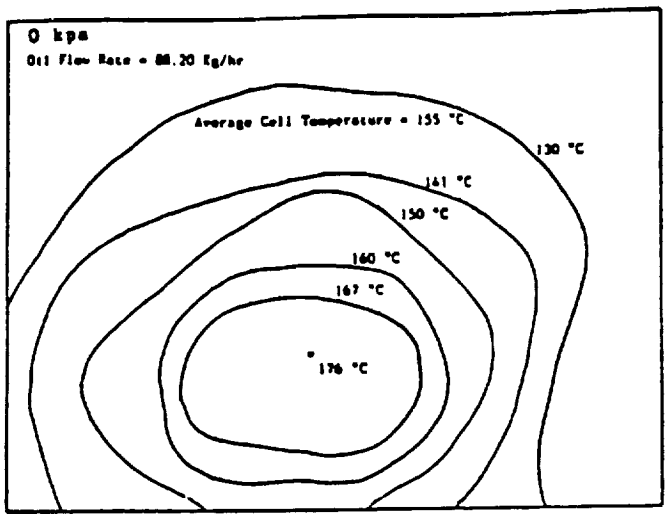

Figure 71 -Effects of Coolant Flow Rate and Stack Clamping Pressure on the Temperature Distributions. (Serpentine, Oil Cooling)

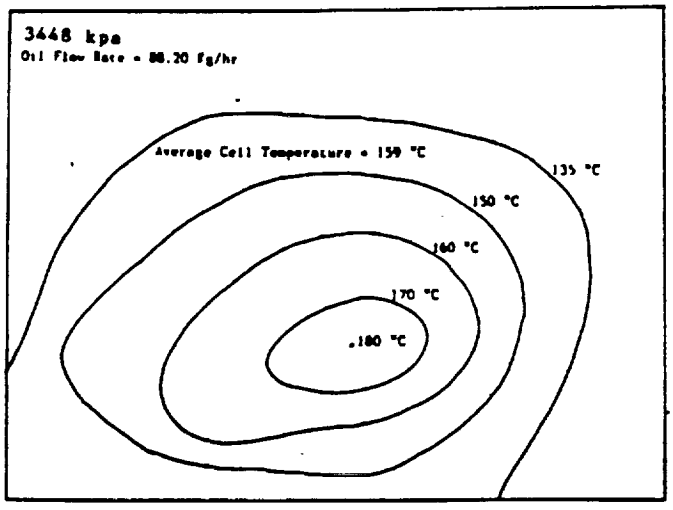

Figure 72-Effects of Coolant Flow Rate and Stack Clamping Pressure on the Temperature Distributions. (Serpentine, Oil Cooling)

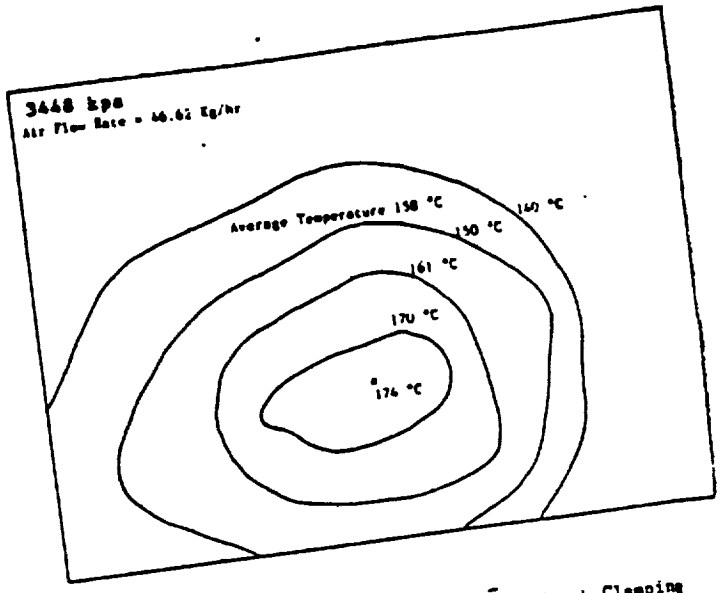

Figure 73-Effects of Coolant Flow Rate and Stack Clamping Pressure on the Temperature Distributions. (Straight, Air Cooling)

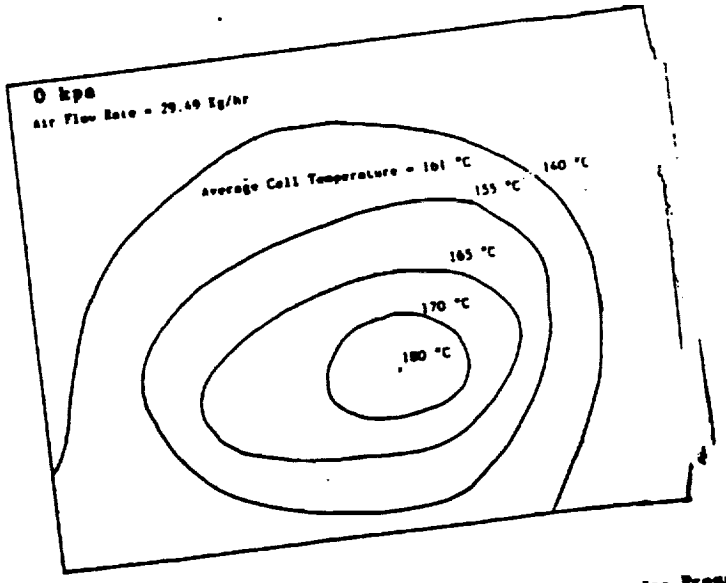

Figure 74 -Effects of Coolant Flow Rate and Stack Clamping Pressure on the Temperature [illegible] (Straight, Air Cooling)

APPENDIX B

TABLES OF DATA AND RESULTS

TABLE 3

Comparison of the Analytical and Experimental Results (Water Case)

Re	T_{out} (Measured)	T_{out} (Calculated)
P = 0 psi (0 Kpa)		
1165	48.40	53.710
1740	47.50	52.366
3321	46.00	47.598
4587	45.20	46.560
6165	44.40	43.923
P = 100 psi (689 Kpa)		
1165	51.10	54.567
1740	49.53	51.278
3321	46.95	47.775
4587	44.75	44.732
6165	43.10	43.553
P = 200 psi (1379 Kpa)		
1165	55.20	55.894
1740	53.76	52.248
3321	48.74	47.735
4587	44.31	45.138
6165	46.29	44.902

TABLE 3 - Continued

*Comparison of the Analytical and Experimental Results (Water Case)

Re	T_{out} (Measured)	T_{out} (Calculated)
P = 300 psi	(2068 Kpa)	
1165	54.20	54.737
1740	52.41	51.079
3321	45.35	45.723
4587	45.79	45.072
6165	43.10	42.832
P = 400 psi	(2758 Kpa)	
1165	55.40	55.849
1740	55.54	52.360
3321	51.76	48.469
4587	53.50	47.757
6165	55.44	47.548
P = 500 psi	(3448 Kpa)	
1165	47.32	49.760
1740	45.52	47.463
3321	39.31	42.106
4587	38.51	40.717
6165	39.93	40.813

TABLE 4

*Comparison of Analytical and Experimental Results (Air Case)

P = 0 psi (0 Kpa)

Re	T_{out} (Measured)	T_{out} (Calculated)
3070	71.40	73.649
4341	66.38	68.131
5317	65.62	64.537
6139	63.96	58.272
6864	61.00	56.791
P = 100 psi	(689 Kpa)	
3070	73.40	75.413
4341	66.38	66.042
5317	58.62	55.924
6139	63.96	56.073
6864	53.50	50.1974
P = 200 psi	(1379 Kpa)	
3070	74.10	70.031
4341	67.38	64.497
5317	65.22	59.943
6139	63.00	54.692
6864	61.34	51.061

TABLE 4 - Continued

*Comparison of Analytical and Experimental Results (Air Case)

Re	T_{out} (Measured)	T_{out} (Calculated)
P = 300 psi (2068 Kpa)		
3070	73.20	75.385
4341	70.40	74.293
5317	66.78	63.787
6139	65.20	59.193
6864	64.55	54.511
P = 400 psi (2758 Kpa)		
3070	73.87	67.146
4341	67.57	69.981
5317	63.04	61.292
6139	55.24	48.929
6864	56.67	48.379
P = 500 psi (3448 Kpa)		
3070	77.00	70.769
4341	68.10	67.467
5317	64.00	60.669
6139	61.81	56.460
6864	63.47	59.924

TABLE 5

•Comparison of the Analytical and Experimental Results (Oil Case)

Re	T_{out} (Measured)	T_{out} (Calculated)
P = 0 psi (0 Kpa)		
15	107.50	107.333
22	106.60	107.369
43	90.70	88.423
59	75.70	77.644
79	65.20	70.298
P = 100 psi (689 Kpa)		
15	108.20	114.830
22	107.90	105.649
43	92.30	88.871
59	82.65	79.678
79	66.85	69.777
P = 200 psi (1379 Kpa)		
15	107.80	113.362
22	111.65	106.820
43	95.60	89.957
59	80.15	77.983
79	67.20	68.738

TABLE 5 -Continued

*Comparison of the Analytical and Experimental Results (Oil Case)

Re	T_{out} (Measured)	T_{out} (Calculated)
P = 300 psi (2068 Kpa)		
15	98.57	107.369
22	102.80	101.085
43	91.00	84.988
59	78.30	75.010
79	75.75	71.819
P = 400 psi (2758 Kpa)		
15	95.10	103.888
22	101.75	99.599
43	90.45	83.245
59	78.40	74.489
79	65.65	66.053
P = 500 psi (3448 Kpa)		
15	90.42	100.48
22	95.32	94.942
43	85.25	80.692
59	74.14	71.295
79	62.639	61.120

TABLE 6

*Contact Resistance Measurement for Straight Channels Cooling Plate

Test #1

Pressure (psi), (Kpa)		T (°C)	r_c · (°C.m²/w)	$h_c = 1/r_c$ (w/°C.m²)
100	689	6.8	0.001499	667.11
200	1379	5.6	0.001234	810.37
250	1724	5.0	0.001102	907.44
300	2068	4.7	0.001036	965.25
400	2758	4.0	0.000882	1133.79
450	3103	3.62	0.000805	1246.88
500	3448	3.51	0.000780	1282.05

Test #2

100	689	6.7	0.001478	676.59
200	1379	5.4	0.001195	836.82
250	1724	3.65	0.000810	1234.57
300	2068	5.1	0.001125	888.89
350	2413	3.9	0.000860	1162.79
400	2758	4.44	0.000980	1020.41
450	3103	3.8	0.000840	1190.48
500	3448	4.0	0.000880	1136.36

TABLE 7

*Contact Resistance Measurements for Serpentine Cooling Plate

Test #1

Pressure (psi), (Kpa)		T (°C)	r_c (°C.m²/w)	$h_c = 1/r_c$ (w/°C.m²)
100	689	8.0	0.00281	355.87
200	1379	6.5	0.00228	438.60
300	2068	4.8	0.00168	595.24
400	2758	4.0	0.00140	714.28
500	3448	3.1	0.00109	917.43

Test #2

100	689	7.8	0.00275	363.64
200	1379	6.1	0.00215	465.12
250	1724	5.3	0.00185	540.54
300	2068	4.75	0.00167	598.80
400	2758	3.55	0.00125	800.00
500	3448	3.3	0.00115	869.56

TABLE 1.1

$\dot{m}$ (Kg/Hr)	Re	h ($w/m^{2}.^{o}C$)	Nu	U ($w/m^{2}.^{o}C$)	Uc ($w/m^{2}.^{o}C$)
16.66	15	26.76	1.22	24.21	22.28
24.87	22	29.84	1.36	26.70	24.38
47.50	43	34.82	1.59	30.62	27.60
65.60	59	36.66	1.67	32.04	28.75
88.20	79	38.03	1.73	33.08	29.58

Test #1, Oil with P= 0 psi (0 kpa)

TABLE 1.1 -Continued

$\dot{m}$ (Kg/Hr)	Tw (^{o}C)	Tc (^{o}C)
16.66	129.97	86.50
24.87	181.10	85.60
47.50	151.53	69.70
65.60	132.43	54.70
88.20	119.13	44.20

TABLE 1.2

$\dot{m}$ (Kg/Hr)	Re	h ($w/m^2.^oC$)	Nu	U ($w/m^2.^oC$)	Uc ($w/m^2.^oC$)
16.66	15	28.30	1.29	25.46	23.76
24.87	22	31.45	1.43	27.98	25.94
47.50	43	35.22	1.60	30.93	28.44
65.60	59	38.17	1.74	33.18	30.34
88.20	79	39.49	1.80	34.18	31.17

Test # 1, Oil with P= 100 psi (689 kpa)

TABLE 1.2 -Continued

$\dot{m}$ (Kg/Hr)	Tw (^oC)	Tc (^oC)
16.66	187.90	87.20
24.87	177.50	86.90
47.50	152.20	71.30
65.60	136.30	61.65
88.20	118.01	45.85

TABLE 1.3

$\dot{m}$ (Kg/Hr)	Re	h ($w/m^2.^oC$)	Nu	U ($w/m^2.^oC$)	Uc ($w/m^2.^oC$)
16.66	15	28.96	1.32	25.99	24.57
24.87	22	32.03	1.46	28.44	26.75
47.50	43	35.76	1.63	31.35	29.29
65.60	59	38.61	1.76	33.51	31.18
88.20	79	40.86	1.86	35.19	32.64

Test #1, Oil with P= 200 psi (1379 kpa)

TABLE 1.3 -Continued

$\dot{m}$ (Kg/Hr)	Tw (^oC)	Tc (^oC)
16.66	185.20	86.80
24.87	179.61	90.65
47.50	154.27	74.60
65.60	132.95	59.15
88.20	115.93	46.20

TABLE 1.4

$\dot{m}$ (Kg/Hr)	Re	h ($w/m^2.^oC$)	Nu	U ($w/m^2.^oC$)	Uc ($w/m^2.^oC$)
16.66	15	29.39	1.34	26.34	25.17
24.87	22	32.67	1.49	28.95	27.54
47.50	43	38.17	1.74	33.18	31.35
65.60	59	40.82	1.86	35.17	33.12
88.20	79	42.34	1.93	36.29	34.11

Test # 1, Oil with P= 300 psi (2068 kpa)

TABLE 1.4 -Continued

$\dot{m}$ (Kg/Hr)	Tw (^oC)	Tc (^oC)
16.66	174.50	77.57
24.87	168.97	81.80
47.50	144.65	70.00
65.60	127.10	57.30
88.20	122.05	54.75

TABLE 1.5

$\dot{m}$ (Kg/Hr)	Re	h ($w/m^2.^oC$)	Nu	U ($w/m^2.^oC$)	Uc ($w/m^2.^oC$)
16.66	15	30.27	1.38	26.34	25.17
24.87	22	33.34	1.52	28.95	27.54
47.50	43	39.67	1.81	33.18	31.35
65.60	59	41.49	1.89	35.17	33.12
88.20	79	43.21	1.97	36.29	34.11

Test #1, Oil with P= 400 psi (2758 kpa)

TABLE 1.5 -Continued

$\dot{m}$ (Kg/Hr)	Tw (^oC)	Tc (^oC)
16.66	168.28	74.10
24.87	166.20	80.75
47.50	141.27	69.45
65.60	126.07	57.40
88.20	110.58	44.65

TABLE 1.6

$\dot{m}$ (Kg/Hr)	Re	h ($w/m^2.^oC$)	Nu	U ($w/m^2.^oC$)	Uc ($w/m^2.^oC$)
16.66	15	30.71	1.40	27.39	26.60
24.87	22	34.22	1.56	30.16	29.19
47.50	43	39.53	1.80	34.21	32.98
65.60	59	43.00	1.96	36.77	35.36
88.20	79	44.75	2.04	38.05	36.53

Test #1, Oil with P= 500 psi (3448 kpa)

TABLE 1.6 -Continued

$\dot{m}$ (Kg/Hr)	$\bar{T}w$ (^oC)	Tc (^oC)
16.66	162.20	69.42
24.87	157.58	74.32
47.50	136.33	64.25
65.60	119.41	53.14
88.20	103.79	40.12

TABLE 2.1

$\dot{m}$ (Kg/Hr)	Re	h ($w/m^2.^oC$)	Nu	U ($w/m^2.^oC$)	Uc ($w/m^2.^oC$)
16.66	1165	44.74	0.462	38.04	33.49
24.87	1740	45.13	0.466	38.32	33.71
47.50	3321	46.87	0.484	39.57	34.67
65.60	4587	47.17	0.487	39.78	34.83
88.20	6167	51.33	0.530	42.70	37.70

Test #1, Water with P= 0 psi (0 kpa)

TABLE 2.1 -Continued

$\dot{m}$ (Kg/Hr)	Tw (^oC)	Tc (^oC)
16.66	91.08	27.40
24.87	92.46	26.50
47.50	85.77	25.00
65.60	84.61	24.20
88.20	78.91	23.40

TABLE 2.2

$\dot{m}$ (Kg/Hr)	Re	h ($w/m^2.^oC$)	Nu	U ($w/m^2.^oC$)	Uc ($w/m^2.^oC$)
16.66	1165	45.52	0.470	38.60	34.81
24.87	1740	46.49	0.480	39.29	35.37
47.50	3321	47.36	0.489	39.92	35.88
65.60	4587	50.65	0.523	42.21	37.72
88.20	6167	51.04	0.527	42.50	37.95

Test #1, Water with P= 100 psi (689 kpa)

TABLE 2.2 -Continued

$\dot{m}$ (Kg/Hr)	Tw (^oC)	Tc (^oC)
16.66	92.69	30.10
24.87	89.82	28.53
47.50	86.11	25.95
65.60	80.00	23.75
88.20	77.93	22.10

TABLE 2.3

$\dot{m}$ (Kg/Hr)	Re	h ($w/m^2.^oC$)	Nu	U ($w/m^2.^oC$)	Uc ($w/m^2.^oC$)
16.66	1165	46.49	0.480	39.29	36.13
24.87	1740	48.10	0.496	40.44	37.09
47.50	3321	48.91	0.505	41.01	37.58
65.60	4587	49.39	0.510	41.35	37.86
88.20	6167	50.85	0.525	42.36	38.71

Test #1, Water with P= 200 psi (1379 kpa)

TABLE 2.3 -Continued

$\dot{m}$ (Kg/Hr)	Tw (^oC)	Tc (^oC)
16.66	95.49	34.20
24.87	92.00	32.76
47.50	86.00	27.74
65.60	81.00	23.31
88.20	81.33	25.29

TABLE 2.4

$\dot{m}$ (Kg/Hr)	Re	h ($w/m^2.^oC$)	Nu	U ($w/m^2.^oC$)	Uc ($w/m^2.^oC$)
16.66	1165	47.65	0.492	40.12	37.47
24.87	1740	49.20	0.508	41.22	38.43
47.50	3321	50.21	0.517	41.92	39.04
65.60	4587	50.85	0.525	42.36	39.43
88.20	6167	52.76	0.544	43.68	40.56

Test #1, Water with P= 300 psi(2068 kpa)

TABLE 2.4 -Continued

$\dot{m}$ (Kg/Hr)	Tw (^oC)	Tc (^oC)
16.66	93.00	33.20
24.87	89.33	31.41
47.50	81.10	24.35
65.60	80.83	24.79
88.20	76.10	22.10

TABLE 2.5

$\dot{m}$ (Kg/Hr)	Re	h ($w/m^2.^oC$)	Nu	U ($w/m^2.^oC$)	Uc ($w/m^2.^oC$)
16.66	1165	48.33	0.499	40.60	38.43
24.87	1740	49.39	0.510	41.35	39.10
47.50	3321	49.98	0.516	41.76	39.45
65.60	4587	51.81	0.535	43.03	40.60
88.20	6167	53.20	0.549	43.99	41.45

Test #1, Water with P= 400 psi (2758 kpa)

TABLE 2.5 -Continued

$\dot{m}$ (Kg/Hr)	Tw (^oC)	Tc (^oC)
16.66	95.36	36.40
24.87	92.23	34.54
47.50	87.77	30.76
65.60	87.50	32.50
88.20	88.00	34.44

TABLE 2.6

$\dot{m}$ (Kg/Hr)	Re	h ($w/m^2.^oC$)	Nu	U ($w/m^2.^oC$)	Uc ($w/m^2.^oC$)
16.66	1165	50.85	0.525	42.37	40.50
24.87	1740	50.36	0.520	42.03	40.19
47.50	3321	52.78	0.545	43.70	41.71
65.60	4587	53.27	0.550	44.03	42.02
88.20	6167	54.72	0.565	45.02	42.91

Test #1, Water with P= 500 psi (3448 kpa)

TABLE 2.6 -Continued

$\dot{m}$ (Kg/Hr)	Tw (^oC)	Tc (^oC)
16.66	82.36	26.32
24.87	81.10	24.52
47.50	72.30	18.31
65.60	70.00	17.51
88.20	71.00	18.93

TABLE 3.1

$\dot{m}$ (Kg/Hr)	Re	h ($w/m^2.^oC$)	Nu	U ($w/m^2.^oC$)	Uc ($w/m^2.^oC$)
0.6950	3070	19.966	3.005	18.51	17.98
0.9829	4341	32.518	4.895	28.83	27.57
1.2038	5317	43.713	6.5799	37.29	35.22
1.3900	6139	43.99	6.622	37.50	35.40
1.5540	6864	48.375	7.2817	40.63	38.18

Test #1, Air with P= 0 psi (0 kpa)

TABLE 3.1 -Continued

$\dot{m}$ (Kg/Hr)	Tc (^oC)	ΔTc (^oC)	ΔTm (^oC)
0.6950	50.10	55.00	74.38
0.9829	48.41	50.19	58.94
1.2038	45.60	45.20	53.70
1.3900	41.22	35.95	44.13
1.5540	39.95	33.70	42.06

TABLE 3.2

$\dot{m}$ (Kg/Hr)	Re	h ($w/m^2.^oC$)	Nu	U ($w/m^2.^oC$)	Uc ($w/m^2.^oC$)
0.6950	3070	20.156	3.034	18.67	18.21
0.9829	4341	34.500	5.193	30.37	29.16
1.2038	5317	41.08	6.1836	35.36	33.72
1.3900	6139	49.48	7.448	41.41	39.18
1.5540	6864	49.175	7.402	41.19	38.99

Test #1, Air with P= 100 psi (689 kpa)

TABLE 3.2 -Continued

$\dot{m}$ (Kg/Hr)	Tc (^oC)	ΔTc (^oC)	ΔTm (^oC)
0.6950	52.40	58.30	78.10
0.9829	45.38	42.20	46.71
1.2038	44.62	39.35	44.80
1.3900	42.96	36.45	39.78
1.554	40.00	28.10	34.50

TABLE 3.3

$\dot{m}$ (Kg/Hr)	Re	h ($w/m^2.^oC$)	Nu	U ($w/m^2.^oC$)	Uc ($w/m^2.^oC$)
0.6950	3070	22.60	3.40	20.75	20.25
0.9829	4341	36.484	5.492	31.89	30.73
1.2038	5317	43.822	6.596	37.37	35.78
1.3900	6139	46.897	7.059	39.59	37.80
1.5540	6864	52.92	7.965	43.79	41.62

Test #1, Air with P= 200 psi (1379 kpa)

TABLE 3.3 -Continued

$\dot{m}$ (Kg/Hr)	Tc (^oC)	ΔTc (^oC)	ΔTm (^oC)
0.6950	53.10	55.70	66.54
0.9829	46.30	41.33	43.26
1.2038	44.20	38.20	40.77
1.3900	42.00	33.26	38.30
1.5540	41.34	31.80	36.28

TABLE 3.4

$\dot{m}$ (Kg/Hr)	Re	h ($w/m^2.^oC$)	Nu	U ($w/m^2.^oC$)	Uc ($w/m^2.^oC$)
0.6950	3070	20.534	3.091	18.99	18.63
0.9829	4341	38.08	5.731	33.11	32.02
1.2038	5317	45.611	6.865	36.67	37.18
1.3900	6139	51.28	7.718	42.67	40.86
1.5540	6864	54.33	8.178	44.76	42.77

Test #1, Air with P= 300 psi (2068 kpa)

TABLE 3.4 -Continued

$\dot{m}$ (Kg/Hr)	Tc (^oC)	ΔTc (^oC)	ΔTm (^oC)
0.6950	52.20	55.82	73.40
0.9829	49.40	51.72	51.87
1.2038	45.79	41.33	42.38
1.3900	44.20	38.00	40.02
1.5540	42.11	34.00	37.78

TABLE 3.5

$\dot{m}$ (Kg/Hr)	Re	h ($w/m^2.^oC$)	Nu	U ($w/m^2.^oC$)	Uc ($w/m^2.^oC$)
0.6950	3070	24.596	3.702	22.42	21.98
0.9829	4341	40.52	6.098	34.94	33.88
1.2038	5317	46.68	7.027	39.43	38.08
1.3900	6139	53.25	8.016	44.02	42.35
1.5400	6864	56.85	8.557	46.45	44.59

Test #1, Air with P= 400 psi (2758 kpa)

TABLE 3.5 -Continued

$\dot{m}$ (Kg/Hr)	Tc (^oC)	ΔTc (^oC)	ΔTm (^oC)
0.6950	48.40	51.82	56.89
0.9829	46.57	51.14	48.20
1.2038	42.04	42.12	42.20
1.3900	39.24	33.25	33.72
1.5540	38.14	32.60	34.62

TABLE 3.6

$\dot{m}$ (Kg/Hr)	Re	h ($w/m^2.^oC$)	Nu	U ($w/m^2.^oC$)	Uc ($w/m^2.^oC$)
0.6950	3070	26.268	3.954	23.81	23.37
0.9829	4341	42.03	6.327	36.06	35.07
1.2038	5317	49.255	7.414	41.25	39.97
1.3900	6139	55.103	8.29	45.98	43.73
1.5540	6864	57.654	8.678	46.98	45.33

Test #1, Air with P= 500 psi (3448 kpa)

TABLE 3.6 -Continued

$\dot{m}$ (Kg/Hr)	Tc (^oC)	ΔTc (^oC)	ΔTm (^oC)
0.6950	49.00	50.12	51.52
0.9829	47.10	48.30	43.88
1.2038	43.00	42.40	40.26
1.3900	40.81	39.61	38.82
1.5540	38.47	34.95	36.60

APPENDIX C

SAMPLE CALCULATIONS

APPENDIX C

SAMPLE CALCULATIONS

I. Heat Transfer Analysis (Oil or Water Case)

Data Available (from page 144)

Re = 22

P = 0 psi

D = 0.00635 m

$q" = 2849.40\ w/m^2$

$K = 13.93 \times 10^{-2} w/m\ .°C$

$T_{in} = 21\ °C$

$T_w = 181.10\ °C$

$T_c = 85.60\ °C$

$\Delta x = 0.00787\ m$

$K_{graphite} = 2\ w/m.°C$

1- Heat Transfer Coefficient

$$h = \frac{q"}{T_w - T_c} = \frac{2849.40}{(181.10 - 85.60)} = 29.84\ w/m^2.°C$$

2- Nusselt Number

$$Nu = \frac{hD}{K} = \frac{(29.84)(0.00635)}{13 \times 10^{-2}} = 1.360$$

3- Thermal Contact Resistance

$$r_c = 0.00357\ e^{(-0.002356\ P)}$$

$$r_c = 0.00357\ °C.m^2/w$$

4- Overall Heat Transfer Coefficient

$$U_c = \frac{1}{\left[\frac{1}{H} + \frac{\Delta x}{K} + r_c\right]} = \frac{1}{\left[\frac{1}{29.84} + 0.003935 + 0.00357\right]}$$

$$U_c = 24.36 \text{ w/m}^2.^\circ\text{C}$$

$$U = \frac{1}{\left[\frac{1}{H} + \frac{\Delta x}{K}\right]} = \frac{1}{\left[\frac{1}{29.84} + 0.003935\right]}$$

$$U = 26.70 \text{ w/m}^2.^\circ\text{C}$$

*Similar procedure is repeated for water except for the use of the properties of water.

II. Heat Transfer Analysis (Air Case)

Data Available (from page 157)

$P = 100$ psi

$Re = 4341$

$m = 0.9829$ Kg/hr

$\Delta T_m = T_w - T_c = 46.71$ °C

$\Delta T_c = T_{out} - T_{in} = 42.20$ °C

$A = 0.007187$ m² ; $D = 0.00558$ m

$C_p = 1.004$ KJ/Kg.°C

$K_A = 0.0371$ w/m .°C

$K_G = 2$ w/m.°C

$\Delta x = 0.00787$

1- Heat Transfer Coefficient

$$h = \frac{(0.9829)(1.004)(42.20)}{(0.007187)(46.71)} [0.278]$$

$$h = 34.50 \ w/m^2.°C$$

2- Nusselt Number

$$NU = \frac{hD}{K} = \frac{(0.00558)(34.50)}{0.0371} = 5.19$$

3- Thermal Contact Resistance

$$r_c = 0.0015812 \ e^{(-0.001413p)}$$

$$r_c = 0.0015812 \ °C.m^2/w$$

4- Overall Heat Transfer Coefficient

$$U_c = \frac{1}{(\frac{1}{h} + \frac{\Delta x}{K} + r_c)} = \frac{1}{(\frac{1}{34.5} + 0.003935 + 0.0015812)}$$

$$U_c = 29.036 \ w/m^2.°C$$

$$U = \frac{1}{(\frac{1}{h} + \frac{\Delta x}{K})} = \frac{1}{(\frac{1}{34.5} + 0.003935)}$$

$$U = 30.37 \ w/m^2.°C$$